Technische Universität München

Fakultät für Medizin

Chirurgische Klinik und Poliklinik-Molekulare Tumorbiologie

Ras-driven mouse models of colorectal cancer:
Interaction of MAPKs with the nuclear receptor PPARγ

Teresa Maria Friedrich

Vollständiger Abdruck der von der Fakultät für Medizin der Technischen Universität München zur Erlangung des akademischen Grades eines

Doktors der Naturwissenschaften

genehmigten Dissertation.

Vorsitzender: Univ.-Prof. Dr. Jürgen Ruland

Prüfer der Dissertation: 1. Priv.-Doz. Dr. Klaus-Peter Janssen
                            2. Univ.-Prof. Dr. Jürgen Scheurle

Die Dissertation wurde am 26.08.2013 bei der Technischen Universität München eingereicht und durch die Fakultät für Medizin am 25.02.2014 angenommen.

Zusammenfassung

Dickdarmkrebs ist die zweithäufigste Krebserkrankung in Europa. Mit fortschreitender Erkrankung sinken die Heilungschancen. Daher konnten im Jahr 2006 etwa 50 % der Patienten nicht mehr erfolgreich therapiert werden. Das Auftreten genetischer Mutationen steht einer effektiven Behandlung entgegen, wobei besonders K-Ras im kolorektalen Karzinom häufig mutiert und aktiviert ist. Die Aktivierung des Ras-Signalweges führt zu einem unkontrollierten Wachstum der Krebszellen. Der Transkriptionsfaktor PPARγ ist im Darm stark exprimiert, verhindert Entzündungen und hemmt dadurch die Entstehung von Krebserkrankungen die durch chronische Entzündung im Darm begünstigt werden.

In dieser Arbeit wurden zwei neue Mausmodelle etabliert und analysiert. Im Fokus stand hierbei besonders der Zusammenhang der Signalwege des aktiven Ras und PPARγ Proteins im Tumor. Genetisch modifizierte Mäuse, denen die Tumorsuppressoren APC und Cav1 fehlten, entwickelten große, vaskularisierte Tumore im Dickdarm mit einer Penetranz von etwa 80 %. Vergleichende genetische Analysen des Tumors mit Normalgewebe zeigten eine Aktivierung der WNT-, N-Ras- und K-Ras-Signalwege, Zielgene von PPARγ waren hingegen herunterreguliert. Allerdings wies PPARγ auf Proteinebene keine Veränderung auf. Weitere Untersuchungen zeigten, dass der aktive Ras-Signalweg zu einer Translokation des PPARγ vom Zellkern in das Cytosol und daher zu dessen Inaktivierung führte. Diese Inaktivierung wurde durch eine Behandlung mit dem PPARγ-Ligand Rosiglitazon aufgehoben und das Tumorwachstum dadurch gehemmt. Der Ras-Signalweg wurde durch die Behandlung unterdrückt, während Zielgene von PPARγ hochreguliert wurden. Eine Aktivierung des PPARγ führte unter anderem zu einer vermehrten Expression der endogenen Ras-Inhibitoren Cav1 und Dok1. In Zelllinien konnte gezeigt werden, dass der Ras-Signalweg PPARγ durch Phosphorylierung oder Export aus dem Zellkern inhibiert. Auf der anderen Seite wurde durch Dok1 der Transport von PPARγ in den Zellkern unterstützt und das Wachstum der Zelle durch Rosiglitazon zusätzlich gehemmt. Um die *in vivo* Interaktion von K-Ras und PPARγ weiter zu untersuchen, wurde ein zweites Mausmodell etabliert, indem K-Ras aktiviert und PPARγ im intestinalen Gewebe ausgeschaltet wurde. Der Verlust von PPARγ verstärkte das Auftreten von Läsionen im Dünndarm.

Zusammenfassend lässt sich sagen, dass durch die Liganden-gesteuerte Aktivierung von PPARγ die inhibitorischen Proteine Cav1 und Dok1 hochreguliert werden, die den Ras-Signalweg hemmen, was wiederum zu einer Abschaltung der Hemmung von PPARγ durch den aktiven mutierten Ras-Signalweg führt. Diese Arbeit zeigte, dass PPARγ eine wichtige Rolle in der Tumorentwicklung hat. Eine pharmakologische Aktivierung von PPARγ würde daher eine alternative Therapie für Darmkrebspatienten darstellen, die auf herkömmliche anti-EGFR Therapien (z.B. Cetuximab) nicht mehr ansprechen.

Summary

Colorectal cancer is the second most frequent tumor disease in Europe. Therapy efficacy decreases with increasing stages of the disease, and therefore almost half of the CRC patients died in the year 2006. Accumulation of mutations exacerbates unresponsiveness to therapies. Especially K-Ras is often mutated and activated in colorectal cancer. Activation of the Ras-signaling pathway *via* the EGFR-Ras-Raf-MEK-ERK-cascade leads to aberrant proliferation of the tumor cell. The nuclear transcription factor PPARγ is highly expressed throughout the GI-tract. PPARγ inhibits inflammation and therefore prevents cancer originating from chronic inflammation.

In this thesis, two new mouse models were established and analyzed. Particularly, the interaction of active Ras- and PPARγ-signaling in the tumor was examined. A new mouse model lacking the tumor suppressors APC and Caveolin-1 was established. Approximately 80 % of these mice developed large, vascularized tumors in the colon. Comparison of the genetic profile from tumor and normal tissue revealed gene signatures for active WNT-, N-Ras- and K-Ras-signaling in the tumor. On the other hand, PPARγ target genes were reduced in the tumor without changing the expression level of PPARγ itself. Further analysis revealed that active Ras-signaling correlated with nuclear export of PPARγ to the cytosol and its inactivation. Treatment of mice with the PPARγ agonist rosiglitazone reactivated PPARγ and reduced tumor growth. Ras-signaling was inhibited, whereas PPARγ target genes were upregulated. Furthermore, PPARγ activation led to upregulation of the endogenous Ras-inhibitors Cav1 and Dok1 (docking protein 1). It was shown *in vitro* that the active Ras-signaling-pathway inhibits PPARγ by its phosphorylation or its nuclear export. On the other hand, Dok1 promotes nuclear import of PPARγ and sensitized the cells to rosiglitazone-treatment. To further study the interaction of K-Ras and PPARγ *in vivo*, a second mouse model was established, where K-Ras is activated and PPARγ is lost in the GI-tract. Loss of PPARγ exacerbated the appearance of hyperplastic lesions in the small intestine.

In sum, a negative "feedback loop" might exist where activation of PPARγ upregulates Ras-inhibitors that then in turn inhibit Ras-signaling which further promotes the PPARγ activity. This thesis may indicate that PPARγ plays an important role in colorectal tumorigenesis. Activation of PPARγ may therefore constitute a potential novel therapy to treat CRC patients that do not respond to common anti-EGFR (e.g. cetuximab) treatment.

Table of contents

Table of contents

1. Introduction

1.1 Colorectal Cancer and staging

Colorectal cancer (CRC) is the second most frequent tumor disease in Europe. In 2006 about 412000 people were diagnosed with colorectal cancer in Europe and approximately half of them died [1]. Until now, most of the patients are diagnosed in an advanced state of the disease where therapy is mostly inefficient. Therefore the detection of colorectal cancer in an early stage of the disease is of particular interest because the survival of CRC patients depends on the stage of the tumor.

In 1932 Cuthbert Dukes described the first model for staging CRC, which was then modified in the year 1973 showing that the survival of the patients decreases with increasing tumor stages. The stages are subdivided into A, B, C and D and define the severity of the tumor, ranging from invasiveness of the tumor (stage B) to spreading of metastases to the lymph nodes (stage C) or other more distant organs (stage D) [2]. This system was replaced by the TNM system, which defines the tumor in more detail. It was first described by the UICC (International Union Against Cancer) and is also used by the AJCC (American Joint Committee on Cancer). It can be applied for all forms of cancer and characterizes the tumors on the basis of three features. "T" (tumor) refers to the size and the invasion of the tumor to the intestinal wall. "N" (nodal) defines the involvement of the disease to nearby lymphatic nodes and "M" (metastases) the existence of metastases (Table 1). The TNM values are the basis for the stage of the tumor, ranging from I to IV (Fig.1).
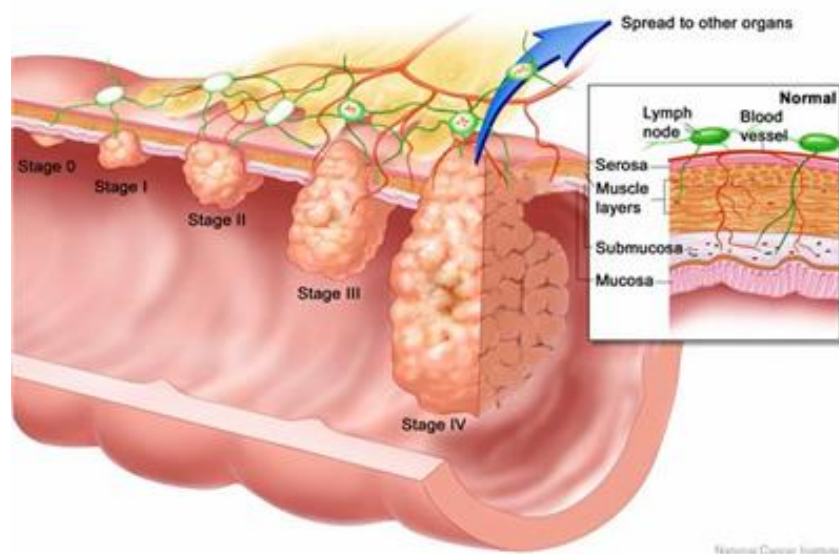
Figure 1 Staging of colorectal cancer and structure of the intestinal wall (courtesy of the National Cancer Institute-http://www.oregonsurgical.com/surgery_coloncancer.htm)

Stages, TNM status, definitions, Dukes' modified staging and the corresponding 5-year-survival are summarized in table 1.

<u>Table 1</u> Colorectal cancer staging correlated to TNM with Definition, Dukes' staging and 5-year survival adapted from Compton [3]

AJCC	TNM	Definition	modified Dukes'	TNM	5-year survival (%)
Stage 0	Tis N0 M0	Tumor *in situ*	-	Tis N0 M0	>90
Stage I	T1 N0 M0	Tumor invades submucosa	A	T1 N0 M0	>90
	T2 N0 M0	Tumor invades muscularis propria		T2 N0 M0	80-85
Stage II	T3 N0 M0	Tumor invades through muscularis propria	B	T3 N0 M0	70-75
	T4 N0 M0	Tumor invades other organs		T4 N0 M0	70-75
Stage III	anyT N1 M0	Metastases in 1-3 lymph nodes	C	T2 N1-3 M0	70-75
	anyT N2 M0	Metastases in > 4 lymph nodes		T3 N1-3 M0	50-65
				T4 N1-3 M0	25-45
Stage IV	anyT any N M1	Distant metastases	D	M1	<3

Further staging parameters are, for example, the grade ("G") that describes the tumor's differentiation status, ranging from well-differentiated (Grade 1) to undifferentiated (Grade 4). The "R" classification provides information about the status (residual tumor/no residual tumor) after surgical resection. Furthermore, "V" has been designated for the invasion into venous vessels and "L" for the invasion into lymphatic vessels. [3, 4]

There is epidemiological evidence that diet, lifestyle or medication can increase the risk for CRC. For example, consumption of a diet that is high in fiber and physical activity decrease the risk for this disease. In contrast excessive consumption of red meat, alcohol and smoking as well as obesity can augment the risk. [5, 6]

Inheritance is also a risk factor for developing CRC, e.g. familial adenomatous polyposis (APC) and hereditary non-polyposis CRC (HNPCC) which are due to mutations in DNA mismatch-repair genes [2].

Inflammatory bowel diseases (IBDs) like ulcerative colitis or Crohn's disease are also supposed to elevate the risk of developing CRC. Chronic inflammation of the intestines often originates from a defective immune response [7]. Alterations in the gut microbiome and the

integrity or permeability of the epithelial barrier in the gastrointestinal tract are presumed to play a causative role in chronic inflammation [8, 9].

1.2 Genetic background of CRC

Sporadic, non-hereditary CRC is the most common form of colorectal cancer with an incidence of about 85 % [10]. This type of cancer develops spontaneously, through mutation of different genes as described in more detail in 1.3. Chromosomal instability (CIN) is responsible for about 85 % of this type of CRC leading to tumor aneuploidy (abnormal number of chromosomes). The other 15 % show microsatellite instability (MSI), that occurs by hypermethylation (increase in methylation) of CpG islands in the promoter region of mismatch repair genes leading to their silencing. These genes such as *MLH1*, *MSH2* and *MSH6* eliminate errors that arise during DNA replication [11-13].

In addition, there are two other types of CRC that develop in patients with hereditary disposition. With an incidence of 5 %, hereditary non-polyposis colon cancer (HNPCC), also called Lynch syndrome (described in 1966 by Lynch *et al.* [14]), is the second most common type of hereditary CRC [10]. This autosomal dominant disease leads to colorectal cancer at a mean age of 44 years. There are two groups of HNPCC, Lynch's syndrome I with tumors limited to the colon and Lynch's syndrome II with tumors in other organs of e.g. the gastrointestinal tract. Tumors of HNPCC often appear in the proximal colon and are due to microsatellite instability (MSI) [15]. Familial adenomatous polyposis (FAP) is the least common type of CRC with 1 out of 12000 cases [10]. It is characterized by the development of hundreds to thousands of adenomas in the large intestine, finally progressing to carcinoma at the age of 35-40 years. It is also an autosomal dominant disease, induced by the mutation of the tumor suppressor gene *APC* (adenomatous polyposis coli) [16].

1.3 Adenoma-Carcinoma-Sequence

The development of an adenoma to a carcinoma is a process of several steps, where different genes lose or gain their function as a consequence of mutations. This model, describing the genetic alterations that occur during the carcinogenesis, was proposed by Fearon and Vogelstein in 1990 [17]. Figure 2 shows the modified adenoma to carcinoma sequence published by Davies in 2005 [2].
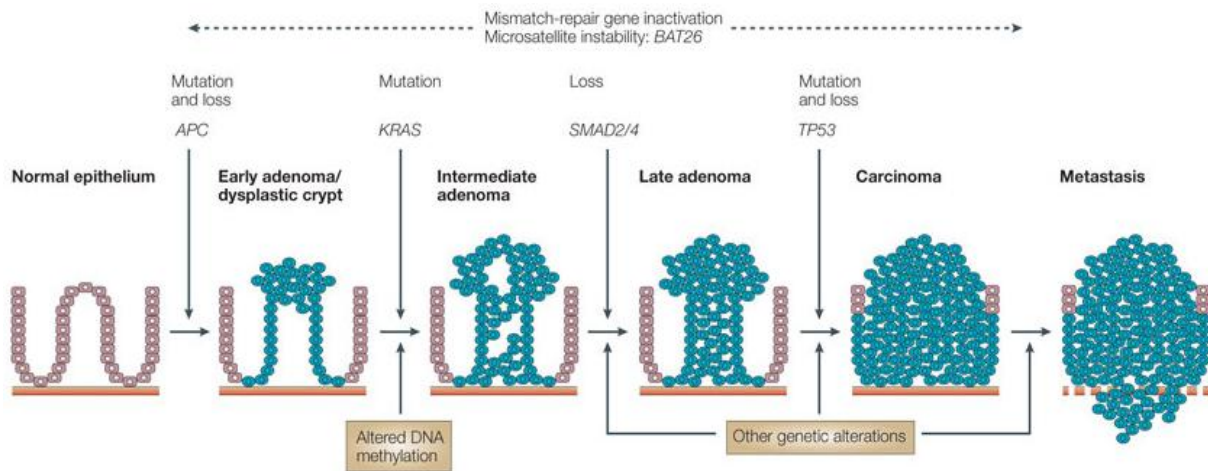
Figure 2 **The Vogelstein adenoma to carcinoma sequence** modified by Davies showing development from normal epithelium to adenoma and carcinoma by accumulation of genetic abnormalities (copied from Davies [2])

During carcinogenesis, a number of genes like *APC*, *KRAS* and *P53* are differentially expressed in different stages of the tumor and genetic alterations accumulated during this process. The first major event in CRC development is the loss of the tumor suppressor gene *APC*. This gene usually inhibits β-catenin, a signaling molecule of the WNT-pathway. In a defective WNT-pathway, c-Myc is active and disturbs the balance between proliferation and apoptosis, so that the epithelium becomes hyperproliferative. An additional prominent modification of genes is the *KRAS* gene, a proto-oncogene. K-Ras gets activated due to mutation and stimulates cell survival. Furthermore, mutation in the tumor suppressor gene *P53* leads to its inactivation. P53 is involved in DNA repair, induction of growth arrest and apoptosis. If p53 function gets lost, cells are predisposed to accumulate genetic mutations. These modifications lead to disruption of the balance between proliferation and apoptosis of epithelial cells resulting in growth of adenomas that finally develop to carcinomas. [17, 18]

1.4 Molecular pathways of CRC

After the publications of Fearon and Vogelstein [17], other findings concerning development of CRC revealed the existence of microsatellite instability (MSI) and the CpG island methylator phenotype (CIMP). Three pathways for CRC have been postulated so far:

Chromosomal instability (CIN) is defined as gain or loss of whole chromosomes or at least of parts of the chromosomes that harbor genes responsible for the development of CRC. CIN is a consequence of aberrant chromosomal segregation leading to aneuploidy (imbalance in chromosomal number), dysfunctional telomeres or a defective DNA damage response. This causes an imbalance in the number of chromosomes, sub-chromosomal genomic amplification and loss of heterozygosity. These aberrations of the chromosomes are often

found in regions harboring genes that are important for cancer development e.g. *VEGF*, *MYC* or *MET*. Linked to these abnormalities is the accumulation of mutations in tumor suppressor genes like *APC* on chromosome 5q21 or *P53* on chromosome 17p, although it is not clear whether CIN has an influence on the accumulation of mutations or *vice versa*. Also single mutations in codon 12 or 13 of the tumor promoter gene *KRAS* in the CIN pathway have been observed.

The second pathway for CRC is the microsatellite instability (MSI) pathway. Microsatellites are short nucleotide repeats that are distributed all over the genome. They are susceptible to mutations which are in turn repaired by DNA mismatch repair (MMR) systems. MSI is therefore an indicator of a defective MMR system. HNPCC is a consequence of germline mutations in the MMR genes. In 15 % of sporadic CRC, MMR genes are silenced by somatic mutations or hypermethylation. In 1997, five microsatellite loci were defined that provide information about the MSI status. Instability of two or more markers is determined as MSI-high, of just one marker as MSI-low and as MSS (microsatellite stable) when there is no instability. MSI-high tumors are less responsive to treatment with the drugs 5-FU (5-Fluorouracil) or cisplatin. Nevertheless, patients that are classified as MSI-high show increased overall survival. Furthermore, MSI-high tumors show less LOH and less mutations in *KRAS* or *P53* but higher incidence of *BRAF*$_{V600E}$ mutations. Genes containing these MSI and which are therefore more prone to accumulate mutations encode for proteins that are necessary for DNA repair like *MSH3* and *MSH6* or *MLH3*, for apoptosis such as *BAX* or *CASP5*, for signal transduction including *TGFβRII* or for cell cycle like *PTEN.*

The third pathway of CRC is the CpG island methylator phenotype (CIMP). Epigenetic modifications are the basis of this pathway. Genetic expression is modified without altering the sequence of the DNA. CIMP is achieved through methylation of the DNA or modifications of the histones. Methylation of the DNA usually takes place at the 5'-CpG-3' dinucleotide (**C**ytosin-**p**hosphatidyl-**G**uanin) and the methylation in an intronic or promoter region usually leads to silencing of the gene. Genes like e.g. *APC* are silenced through hypermethylation in CRC. As for MSI there are five markers that were chosen for defining the CIMP status. Those include *CACNA1G*, *IGF2*, *NEUROG1*, *RUNX3* and *SOCS1*. If at least three markers are methylated this tumor is defined as CIMP positive. These tumors often exhibit MSI and are *BRAF*$_{V600E}$ mutated. [19, 12, 13, 20, 21]
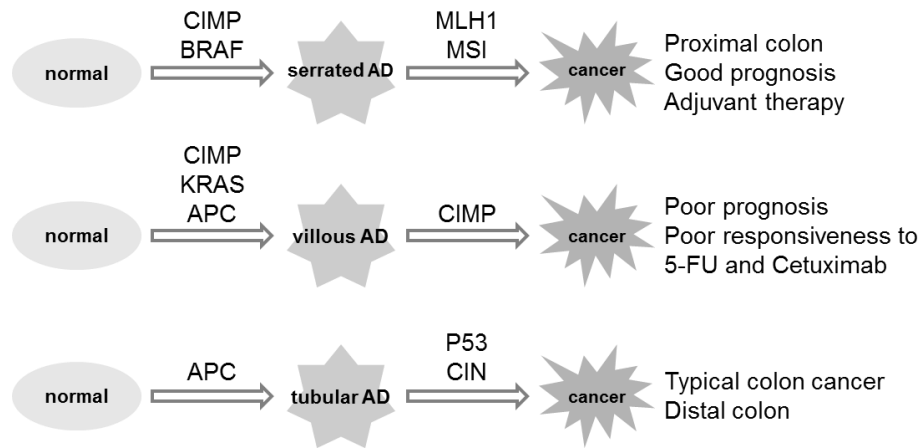
Figure 3 Summary of the three different pathways to colorectal cancer (adapted from Issa[22]). Pathway one and three show better outcome compared to pathway two. The most common pathway is the third one (APC) with 50-70%.

The CIN and the MSI pathways represent the classical pathway of colorectal cancer, saying that *APC* mutation is the initial event leading to ACF (aberrant crypt foci) and hence to development of tumors through accumulation of other mutations (see Vogelstein sequence). The CIMP pathway, however, displays the serrated pathway to colorectal cancer which appears to be independent of *APC*. The lesions like hyperplastic polyps, sessile serrated polyps, serrated adenoma, mixed polyps or sessile/traditional serrated adenomas (SSA/TSA) all show a "sawtooth"-like structure of the epithelium. There is a high frequency of *KRAS* or *BRAF* mutations found in these serrated lesions which leads to the conclusion that the Ras/Raf/MEK/ERK-pathway is a driver of serrated tumorigenesis. [23, 24]

Based on these different pathways of CRC it is now possible to differentiate between tumors with good prognosis (MSI, *BRAF* unmutated) and poor prognosis (CIMP, no MSI). The MSI status provides information about the 5-FU-sensitivity of the tumor, and *KRAS* mutations (CIMP) are very resistant towards cetuximab treatment. Conclusively, the treatment of the individual tumor could be selected on the basis of molecular characterization and hence improve the clinical outcome for a given patient ("personalized medicine") (Fig.3). [22]

1.5 Treatment of CRC

Colorectal cancer can be diagnosed in different ways. The most insensitive method to screen for CRC is the "fecal occult blood test" which detects blood in the stool. Besides other detection methods, colonoscopy is the most effective one to detect CRC. It also has the advantage that polyps, that are supposed to be the first step in colorectal carcinogenesis, can immediately be removed during this procedure [11].

When already in an advanced stage, treatment with chemotherapy is the only option to treat CRC. Metastatic CRC is treated with a combination therapy of 5-fluorouracil with oxaliplatin

(FOLFOX) or irinotecan (FOLFIRI). In addition, monoclonal antibodies like bevacizumab (Avastin®, Roche) that binds VEGF (vascular endothelial growth factor) or cetuximab (Erbitux®, Merck KgaA) targeting EGFR (epidermal growth factor receptor) are in use. By combining drugs like 5-FU and monoclonal antibodies, the efficiency of CRC treatment was improved [25].

The EGFR is located on the cell surface and gets activated by binding signaling molecules like e.g. EGF. This binding leads to activation of the Ras/Raf/MEK/ERK-pathway followed by survival and proliferation of the cell. Mutation and activation of the *KRAS* gene, which is often observed in human tumors results in inefficiency of EGFR antibodies. Thus it is necessary to circumvent the *RAS* mutation, which renders the GTPase locked in a constitutive active state, and target proteins downstream of Ras like Raf, MEK or ERK. Drugs targeting Raf are sorafenib, a weak inhibitor of Raf, and the more selective inhibitor PLX4032 [25].

MEK inhibitors were shown to be effective in melanoma cell lines with mutant *BRAF*. In cell lines with oncogenic Ras, MEK inhibition was found to be less effective and variable relating to its inhibitory effect. Recent studies showed that there is a "compensatory or negative feedback loop" between PI3-Kinase and the Raf-MEK-ERK pathway that compensates the effect of MEK blocking, as has been shown in breast cancer cells. Furthermore, combined inhibition of PI3K and MEK decreased tumor cell growth [25,26].

Due to the different mutations, especially in advanced stages, drug resistance is a major problem. Therefore early diagnostic biomarkers and new treatments need to be developed.

1.6 Proteins involved in CRC

1.6.1 MAPKs

Mitogen-activated protein kinases (MAPKs) are serine/threonine-specific kinases that are activated by extracellular stimuli. They are responsible for various cellular processes like proliferation, differentiation, survival and apoptosis, stress response and oncogenic transformation. The Ras/Raf/MEK/ERK-pathway is the most important one of the four known cascades in human cancers and is responsible for processes like differentiation, development or proliferation [27, 28]. This pathway is activated by growth factors leading to the phosphorylation of Ras-GDP to Ras-GTP that activates Raf-kinases. Raf in turn phosphorylates and activates MEK1/MEK2 which then transmits the signal to ERK1/ERK2 (extracellular signal-regulated kinase 1/2) (p44/42) [29]. There is an interaction between the Ras/Raf/MEK/ERK- and the Ras/PI3K/PTEN/Akt-pathways to control cellular growth or even tumorigenesis [30].

There are four different Ras-proteins known: Ha-Ras (H-Ras), N-Ras, Ki-Ras4A and Ki-Ras4B (K-Ras) with distinct activation potentials [30]. Ras-signaling is of special interest as

KRAS is mutated and activated in human cancers like colorectal cancer [31]. Different *KRAS* mutations have been discovered [32]. Mutations like e.g. G12D (Gly→Asp), G12V (Gly→Val) and G13D (Gly→Asp) were found to have an effect on the patients clinical outcome combined with the MSI and *BRAF*$_{V600E}$ status [33].

1.6.2   PPARγ

Peroxisome proliferator-activated receptor γ is a 50 kDa transcription factor of the nuclear receptor family [34]. There are two different isoforms of PPARγ, PPAR-γ1 and PPAR-γ2, as a result of alternative splicing. PPAR-γ1 is found in tissues like the lower intestine or macrophages. PPAR-γ2, with a 30 amino acid extension at the N-Terminus, is expressed mainly in the white adipose tissue [35]. PPARγ consists of an N-terminal transactivation function 1 (TAF-1) for ligand independent activation, a DNA binding domain, a hinge region and a ligand binding domain containing the C-terminal TAF-2 helix [36].

Ligand-independent activation	DNA binding domain	Hinge region	Ligand-binding domain and receptor dimerization	un-known

Figure 4 **Structure of nuclear receptors like PPAR-gamma adapted from Murphy [36].** From left to right: Ligand-independent activation (TAF-1), DNA binding domain containing a P-Box (interaction with DNA sequences) and a D-Box (selection of the distance between the two DNA binding sites), ligand binding domain for ligand dependent activation (TAF-2). The domain with unknown function is not present in all nuclear receptors.

PPARγ regulates a plethora of genes and is therefore involved in cellular processes like differentiation, immunity and metabolism [34]. Ligand-activated PPARγ forms heterodimers with the 9-cis retinoic X receptor (RXR), another member of the nuclear receptor superfamily. This RXR-PPAR complex enters the nucleus and binds to PPAR responsive elements (PPREs) in the promoter region of target genes. Physiological ligands for PPARγ activation are e.g. polyunsaturated fatty acids, prostaglandin J2 derivatives and nitro-oleic acid, which are all naturally occurring in the diet or in inflammatory lesions. Other ligands for PPARγ are Thiazolidinediones like rosiglitazone and pioglitazone which are synthetic drugs used as insulin sensitizers for the treatment of type II diabetes [35]. PPARγ functions as a transcription factor that can be inhibited by growth factors. This event is mediated by phosphorylation of Ser84/Ser112 by mitogen activated kinases (MAPK)/ extracellular-signal regulated kinases 1 and 2 (ERK1/2). Phosphorylation can also be achieved by other kinases like c-Jun N-terminal kinase or p38MAPK induced by stress stimuli or proinflammatory mediators, which confirms the role of PPARγ as an inhibitor of proliferation and inflammation [37]. Another way to inhibit PPARγ by MAPKs is the nuclear export of PPARγ by direct interaction with MEK

(MAPK/ERK kinase 1/2) [34]. PPARγ is highly expressed in the colon [38] and inhibits the expression of inflammatory cytokines and proliferation [36]. PPARγ as a transcription factor regulates several target genes like cytokeratins or some carcinoembryonic antigens that are important for colon carcinogenesis because of their role in growth and differentiation of intestinal epithelial and immune cells (macrophages, T-cells). Proteins that are responsible for cell cycle inhibition like P21, P18 or P27 are also activated by PPARγ. One gene that is inactivated by PPARγ is *CYCLIND1*, which is necessary for the G1/S transition in the cell cycle. Importantly, PPARγ suppresses matrix metalloproteinase-9 (MMP-9), an important factor in metastasis [39]. In colorectal cancer patients of different tumor stages nuclear PPARγ expression was shown to be associated with good prognosis, higher survival rate and a less aggressive, less metastatic phenotype [40, 41]. Although there are lots of reports that PPARγ acts as a tumor suppressor, there is also evidence that PPARγ agonists can promote tumor growth in mice with an *Apc^{min/+}* mutation alluding at the possibility that PPARγ loses its anti-tumoral effects in presence of active WNT-signaling, a predominant phenotype of the classical route to CRC [42].

1.6.3 Caveolin-1

Caveolin-1 is the essential protein of caveolae, flask-shaped plasma membrane invaginations that are ubiquitously distributed in the tissue. It interacts with glycosphingolipids and cholesterol and is therefore often associated with lipid rafts. Caveolin-1, a 22 kDa scaffold protein of 178 amino acids, is located within a fragile DNA locus (next to the *CMET* gene) which is often deleted or amplified in cancers. Caveolin-1 consists of three exons that are highly conserved.
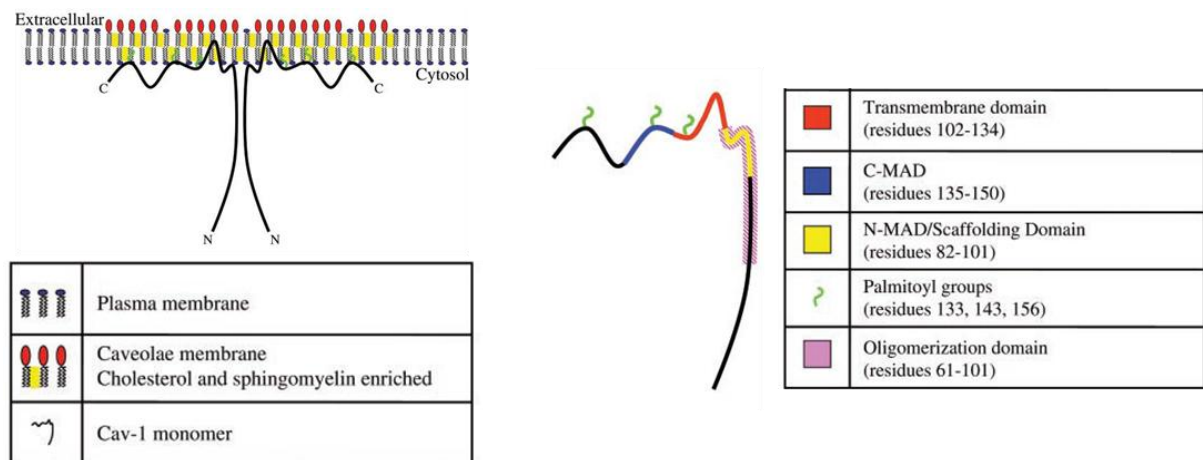
Figure 5 Caveolin-1 associated to the plasma membrane (left) and individual domains of a caveolin-1 monomer (copied from Cohen [43]). COOH-terminal and NH2-terminal membrane attachment domain (C/N-MAD) are fundamental for membrane attachment. The transmembrane

domain inserts Cav-1 into the membrane. The Oligomerization domain allows Cav1 to bind the monomers to each other.

Caveolin-1 can interact with signaling molecules like receptors, kinases, G-proteins or adhesion molecules and controls their distribution and activity. It is therefore involved in cellular processes like transport, signal transduction or endocytosis and regulates proliferation, differentiation, apoptosis and invasion. Because of these properties, caveolin is thought to play a role in the pathogenesis of human diseases like cancer [43, 44]. Thus Caveolin-1 might inhibit tumor progression because it blocks signaling proteins and even oncogenes like Ha-Ras or MAPK by means of its scaffolding motif, kinases which in turn abrogate the activity of PPARγ [44, 45]. In more advanced stages of cancer, Caveolin-1 expression was found to be increased where it switches to a more malignant molecule that promotes chemoresistance, cell survival and metastasis, resulting in decreased overall survival of CRC patients. This malignant shift from a tumor suppressor to a tumor promoter is in part caused by an alteration from a membranal to a soluble form or a change in its interaction partners [43, 44, 46, 47].

1.6.4   APC

The Adenomatous Polyposis Coli (APC) protein is a tumor suppressor that is often found to be mutated in colon cancer. It consists of 2843 amino acids with different domains (Fig. 6) needed for protein-protein interaction with β-catenins, glycogen synthase kinase 3 beta (GSK3β) or microtubules [48]. APC can act as a tumor suppressor by inhibiting the WNT-pathway via downregulation of β-catenin, an activator of proliferative genes like the proto-oncogenes *CMYC* and *CYCLIND1* and also *MMP-7* (matrix metalloproteinase 7) or *CD44*. APC is supposed to interact with Axin and GSK3β to phosphorylate β-catenin. Phosphorylated β-catenin is a target for ubiquitination and proteasomal degradation [49, 50].

Figure 6 Scheme of the adenomatous polyposis coli (APC) protein adapted from Fearon[50] showing the different domains for binding and interaction with other protein partners.

1.7 Mouse models of CRC

1.7.1 APC mouse models

One of the most prominent APC mouse models is the *Apc* min (multiple intestinal metaplasia) mouse with a truncating point mutation at codon 850 of the APC protein. The phenotype is similar to FAP patients that develop up to hundred adenomas in the colon, finally progressing to adenocarcinomas. In contrast, $Apc^{min/+}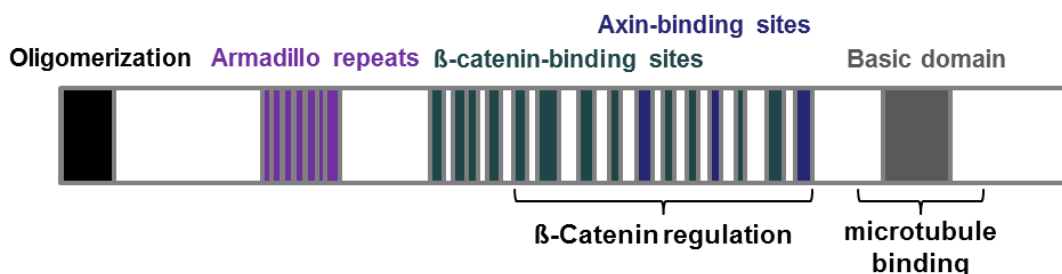$ mice develop about 30 intestinal polyps. This mutation only appears in one allele, homozygosity would lead to lethality of the embryo [51].

Another *Apc*-mutant is the *Apc1638N* mouse, where codon 1638 of the *Apc* gene is mutated. This mutation also occurs in the heterozygous state and mice develop "colonic aberrant crypt foci" and 3-4 adenocarcinomas in the small intestine. Mutation of *Apc* at codon 716 also leads to hundreds of polyps in the small intestine, similar to $Apc^{min/+}$. The deletion of the conditional allele *Apc570* instead results in the development of colon tumors 4 weeks after deletion [10].

All these different *Apc*-mutant mice develop adenomas that do not progress to invasive or metastatic carcinomas. By introduction of other mutant genes or by inbreeding of other backgrounds, this phenotype can change and even carcinomas can arise [52]. The so called "Modifier of *Min*" (MOMs) can change the susceptibility to cancer in these mouse models [53]. For example, crossing of *Apcmin* mice of the B6 background to mice of the BTBR background develop more than 600 tumors and do not live longer than 60 days [54]. On the contrary, upon crossing B6 to the AKR background, mice develop only up to four tumors and live up to one year. The most prominent modifier of min is *Mom1* which is localized on chromosome 4. There are two alleles of *Mom1*: a resistance allele found in AKR mice and a sensitivity allele in B6 mice. This allele was further defined as *Pla2g2a* gene, a secretory phospholipase, which was shown to reduce the tumor number and the tumor size [54, 55]. Another modifier of min is *Mom2*, localized on chromosome 18. One possible gene affected here might be the ATP synthase *Atp5a1*. *Mom3* was detected in *Apcmin* mice that had become strain contaminated resulting in six recombinant lines with varying severity of the disease. *Mom3* was found to be localized on chromosome 18, close to *Apc* and is supposed to alter the number of adenomas by modifying the incidence of the wildtype allele loss. In a similar region to *Mom3* lies *Mom7*. *Mom7* was discovered crossing four different mouse strains. There is one recessive, enhancing allele in BTBR, AKR and A/J leading to an increase in tumor incidence and a dominant, suppressive one in B6 mice. [51, 54] Recently, *Mom12* and *Mom13* were found crossing B6 *Apcmin* with B6 $Cav1^{-/-}$ mice. The offspring showed higher polyp number than the *Apcmin* mice, nevertheless, there was no difference between the different *Cav1*-genotypes indicating the influence of modifier loci. This was

confirmed by the discovery of remaining 129X1/SvJ genomic DNA originating from the *Cav1*^{-/-} mice [56].

1.7.2 K-Ras mouse models

Because of their high mutation rate, *RAS* oncogenes are of special interest in cancer biology. Approximately one third of all human tumors show deregulated Ras-signaling. *KRAS* is the one which is most frequently mutated and which is found in 50 % of all CRCs.

Several distinct mouse models for K-Ras-driven CRC have been developed. One mouse model regarding K-Ras used the spontaneous recombination principle. The *KRAS* G12D mutation leads to Ras-activation in the whole animal causing tumors especially in the lung but also of the thymus and the skin. The colon showed aberrant crypt foci (ACF). Furthermore there are also inducible mouse models for active K-Ras obtained by the Cre/loxP strategy that enables to study tumor progression. In these models, the *KRAS* G12V transgene and the endogenous *KRAS* G12D both generated lung tumors. To further study the role of active K-Ras limited to the intestines another mouse model was developed that limits oncogenic K-Ras (G12V) expression to the epithelial cells of the intestines. This is achieved by using a Cre recombinase which is under control of the murine villin promoter that is only expressed in enterocytes. This tissue specific expression resulted in adenomas or adenocarcinomas of the small intestine through activation of ERK1/2. [31]

1.8 Aim and purpose of this thesis

CRC is the second most frequent tumor disease in Europe [1] and overall survival decreases with increasing progression of the tumor [3]. It is known that WNT/APC- and Ras-signaling are involved in tumor initiation and progression in CRC, but therapy often fails because of activating mutations of proto-oncogenes like e.g. *KRAS* or *BRAF*. Mouse models harboring mutations in *Kras* show tumor growth in the GI-tract [31]. By generation of new mouse models for CRC, further insight into the mechanism of tumorigenesis and the genes involved should be gained to identify possible new therapeutic targets to treat CRC.

PPARγ, a nuclear transcription factor, is highly expressed in the colon [38] and inhibits proliferation and inflammation [36, 37]. Thus, PPARγ plays a role in prevention of colon cancer and inflammatory bowel diseases [38]. On the other hand, activating mutations of the Ras-signaling pathway are common in colon cancer [33] and lead to phosphorylation or nuclear export resulting in inhibition of PPARγ [37].

This thesis aimed to analyze the interaction of PPARγ and Ras-signaling *in vivo* and *in vitro* to further characterize the role of PPARγ in colorectal tumorigenesis. For this purpose, a novel mouse model with deficiency in the tumor suppressors Caveolin-1 and APC was established to determine the effect of Caveolin-1, a Ras-inhibitor, on colorectal tumorigenesis. Furthermore, expression and localization of PPARγ in tumor tissue compared to normal colon tissue was analyzed with regard to active Ras-signaling. Related to this, therapeutic PPARγ activation was tested for its efficiency to inhibit tumorigenesis.

In a second mouse model, knockdown of PPARγ and activation of K-Ras were combined to define the influence of PPARγ on K-Ras driven intestinal tumorigenesis.

The major hypothesis followed in this thesis is that: (i) activity of Ras-signaling in tumorigenesis leads to inhibition of PPARγ and (ii) PPARγ can be reactivated by inhibition of the Ras-pathway and activation by ligand. Reactivation of PPARγ might therefore be a possible new treatment for CRC to circumvent anti-EGFR therapy in non-responsive CRC patients.

2. Materials & Methods

2.1 Materials

Table 2 General chemicals, reagents and solutions

1,4-Dithiothreitol (DTT)	Roth GmbH, Karlsruhe, Germany
Gene Ruler™ 50 bp DNA Ladder	Fermentas GmbH, St. Leon-Rot, Germany
Gene Ruler™ 1 kb DNA Ladder	Fermentas GmbH, St. Leon-Rot, Germany
2-Mercaptoethanol	Sigma-Aldrich Chemie GmbH, Steinheim, Germany
2-Propanol	Merck KGaA, Darmstadt, Germany
6x Orange DNA Loading Dye	Fermentas GmbH, St. Leon-Rot, Germany
Albumin Fraktion V	Roth GmbH, Karlsruhe, Germany
Ammoniumperoxodisulfat	Roth GmbH, Karlsruhe, Germany
Ampicillin >99%	Roth GmbH, Karlsruhe, Germany
Antigen unmasking solution	Vector Laboratories, Inc., Burlingame, USA
Aqua Irrigation Solution	DeltaSelect GmbH, Dreieich, Germany
Biozym LE Agarose	Biozym Scientific GmbH Hess. Oldendorf, Germany
Boric acid	Sigma-Aldrich Chemie GmbH, Steinheim, Germany
Bromophenol Blue	Sigma-Aldrich Chemie GmbH, Steinheim, Germany
Chloroform	Merck KgaA, Darmstadt, Germany
Complete Mini Protease inhibitor cocktail tablets	Roche Diagnostics GmbH, Mannheim, Germany
Dual-Luciferase® Reporter Assay System	Promega Corporation, Madison, USA
DH5 alpha Competent Cells	Invitrogen GmbH, Karlsruhe, Germany
ECL Detection Reagents	GE Healthcare UK Limited, Little Chalfont Buckinghamshire, UK
Ethanol 96% (v/v) technical	Roth GmbH, Karlsruhe, Germany
Ethanol absolute for analysis	Merck KgaA, Darmstadt, Germany
Ethidium bromide (10 mg/ml)	Sigma-Aldrich Chemie GmbH, Steinheim, Germany
Ethylendiaminetetraacetic acid	Sigma-Aldrich Chemie GmbH, Steinheim, Germany
Fluorescent mounting medium	Dako North America, Inc., Carpinteria, USA
Geneticin (G418)	Invitrogen GmbH, Karlsruhe, Germany
Glycerin	Roth GmbH, Karlsruhe, Germany
Glutathione Agarose	Santa Cruz Biotechnology, Inc., Heidelberg, Germany
Hämalaunlösung nach Mayer	Roth GmbH, Karlsruhe, Germany
HEPES	Sigma-Aldrich Chemie GmbH, Steinheim, Germany
Histoclear	Roth GmbH, Karlsruhe, Germany
Hydrochloric acid (1N)	Merck KgaA, Darmstadt, Germany
LB-Agar (Lennox)	Roth GmbH, Karlsruhe, Germany
LB-Medium (Lennox)	Roth GmbH, Karlsruhe, Germany
Magnesiumchlorid	Merck KgaA, Darmstadt, Germany
MES	Sigma-Aldrich Chemie GmbH, Steinheim, Germany
Methanol	Roth GmbH, Karlsruhe, Germany
Sodiumhydroxid pro analysis	Merck KgaA, Darmstadt, Germany
Nonidet P40	Roche Diagnostics GmbH, Mannheim, Germany
PageRuler™ Plus Prestained Protein Ladder	Fermentas GmbH, St. Leon-Rot, Germany
Paraformaldehyd	Merck KgaA, Darmstadt, Germany
Pertex® mounting medium	Medite GmbH, Burgdorf, Germany
Protein A/G PLUS-Agarose sc-2003	Santa Cruz Biotechnology, Inc., Heidelberg, Germany
Proteinase K	Roche Diagnostics GmbH, Mannheim, Germany
Rotiphorese® Gel 30	Roth GmbH, Karlsruhe, Germany
SDS ultra pure	Roth GmbH, Karlsruhe, Germany
Skim milk powder	Sigma-Aldrich Chemie GmbH, Steinheim, Germany
Sodium chloride	Sigma-Aldrich Chemie GmbH, Steinheim, Germany

Sodium orthovanadate (Na$_3$VO$_4$)	Sigma-Aldrich Chemie GmbH, Steinheim, Germany
TEMED	Roth GmbH, Karlsruhe, Germany
Top10 One Shot competent cell	Invitrogen GmbH, Karlsruhe, Germany
TRIS Ultra Qualität	Roth GmbH, Karlsruhe, Germany
Triton® X-100	Sigma-Aldrich Chemie GmbH, Steinheim, Germany
Tween® 20	Roth GmbH, Karlsruhe, Germany

Table 3 Equipment

1 ml Dounce Tissue Grinder "tight"	NeoLab Migge Laborbedarf-Vertriebs GmbH, Heidelberg, Germany
Centrifuge 5415R	Eppendorf AG, Hamburg, Germany
Centrifuge 5810R	Eppendorf AG, Hamburg, Germany
HERAcell® 240 Incubator	Heraeus Holding GmbH, Hanau, Germany
NanoDrop® Spectrophotometer ND-1000	PEQLAB Biotechnologie GmbH, Erlangen, Germany
LightCycler®480	Roche Diagnostics GmbH, Mannheim, Germany
LightCycler®480 Software 1.5	Roche Diagnostics GmbH, Mannheim, Germany
Light Cycler®480 Multiwell Plate 96	Roche Diagnostics GmbH, Mannheim, Germany
Axiovert 40 CFL Microscope	Carl Zeiss MicroImaging GmbH, Göttingen, Germany
Hyper processor SRX-101A X-ray film developing machine	Amersham Biosciences Europe GmbH, Freiburg, Germany
LAS 1000 CCD-Camera & Intelligent Dark Box	FUJIFILM Europe GmbH, Düsseldorf, Germany
Mini-PROTEAN® 3 Cell	Bio-Rad Laboratories GmbH, Munich, Germany
Mini-Sub® Cell GT	Bio-Rad Laboratories GmbH, Munich, Germany
Mini Trans-Blot® Electrophoretic Transfer Cell	Bio-Rad Laboratories GmbH, Munich, Germany
Tecan Infinite M200 microplate reader	TECAN Group Ltd., Männedorf, Switzerland
PowerPac Basic	Bio-Rad Laboratories GmbH, Munich, Germany
ApoTome	Carl Zeiss MicroImaging GmbH, Göttingen, Germany
Axio Imager A.1	Carl Zeiss MicroImaging GmbH, Göttingen, Germany
AxioVision Rel. 4.4	Carl Zeiss MicroImaging GmbH, Göttingen, Germany
Pipettes	Eppendorf AG, Hamburg, Germany
1.5 / 2.0 ml microcentrifuge tubes	Eppendorf AG, Hamburg, Germany
200µl PCR Tubes "Multiply®-µStrip Pro 8-strip"	Sarstedt AG & Co., Nümbrecht, Germany
15 / 50 ml Falcon tubes	BD Biosciences, Heidelberg, Germany
25 cm^2 and 75 cm^2 Tissue Culture Flask	BD Biosciences, Heidelberg, Germany
6-, 12-, 24- and 96- well Tissue Culture Plate	BD Biosciences, Heidelberg, Germany
60 mm, 100 mm and 150 mm Tissue Culture Dish	BD Biosciences, Heidelberg, Germany
Petri dish	BD Biosciences, Heidelberg, Germany
Countess™ cell counter & counting chamber slides	Invitrogen GmbH, Karlsruhe, Germany
Coverslips	Roth GmbH, Karlsruhe, Germany
Superfrost® Plus microscope slides	Menzel GmbH & Co. KG, Braunschweig, Germany
X-Gal (5-bromo-4-chloro-indolyl-β-D-galactopyranoside)	Sigma-Aldrich Chemie GmbH, Steinheim, Germany

Table 4 Cell culture reagents and solutions

0.25% Trypsin-EDTA	Invitrogen GmbH, Karlsruhe, Germany
Dimethyl sulfoxide, minimum 99,5% GC	Sigma-Aldrich Chemie GmbH, Steinheim, Germany
Dulbecco's Modified Eagle Medium (1x) -GlutaMAX™	Invitrogen GmbH, Karlsruhe, Germany
Fetal Bovine Serum	Invitrogen GmbH, Karlsruhe, Germany
PBS Phosphate Buffered Saline pH 7.4	Invitrogen GmbH, Karlsruhe, Germany
Penicillin-Streptomycin	Invitrogen GmbH, Karlsruhe, Germany
Thiazolyl Blue Tetrazolium Bromide (MTT)	Sigma-Aldrich Chemie GmbH, Steinheim, Germany
Trypan Blue stain 0.4%	Invitrogen GmbH, Karlsruhe, Germany
TurboFect™ *in vitro* Transfection Reagent	Fermentas GmbH, St. Leon-Rot, Germany

Materials & Methods

Table 5 Cell lines

SW480	Human colorectal adenocarcinoma	American Type Culture Collection, Manassas, USA
HCT-116	Human colorectal carcinoma	American Type Culture Collection, Manassas, USA
HT-29	Human colorectal adenocarcinoma	American Type Culture Collection, Manassas, USA
Caco-2	Human colorectal adenocarcinoma	American Type Culture Collection, Manassas, USA
Hek-293T	Human embryonic kidney	American Type Culture Collection, Manassas, USA

Table 6 Enzymes

BamHI restriction enzyme 20 u/µl	New England Biolabs GmbH, Frankfurt, Germany
DpnI restriction enzyme 10 u/µl	Promega Corporation, Madison, USA
EcoRI restriction enzyme 20 u/µl	New England Biolabs GmbH, Frankfurt, Germany
HindIII restriction enzyme 20 u/µl	New England Biolabs GmbH, Frankfurt, Germany
NotI restriction enzyme 10 u/µl	Promega Corporation, Madison, USA
T4 Ligase 5 u/µl	Fermentas GmbH, St. Leon-Rot, Germany
GoTaq® Green Master Mix	Promega Corporation, Madison, USA
JumpStart™ RedTaq Ready Mix™ PCR Reaction Mix	Sigma-Aldrich Chemie GmbH, Steinheim, Germany
LightCycler®480 SYBRGreen I Master (2x)	Roche Diagnostics GmbH, Mannheim, Germany
Proteinase K, recombinant PCR grade	Roche Diagnostics GmbH, Mannheim, Germany
RNase-free DNase Set	QIAGEN GmbH, Hilden, Germany

Table 7 Kits

BCA™ Protein Assay Kit	Thermo Fisher Scientific, Inc., Surrey, UK
DAB Peroxidase Substrate Kit	Vector Laboratories, Inc., Burlingame, USA
Duolink® In Situ	OLINK Bioscience, Uppsala, Sweden
HiSpeed® Plasmid Midi Kit	QIAGEN GmbH, Hilden, Germany
QIAshredder™	QIAGEN GmbH, Hilden, Germany
QIAquick Gel Extraction Kit	QIAGEN GmbH, Hilden, Germany
PureYield™ Plasmid MiniPrep System	Promega Corporation, Madison, USA
RNeasy® Mini Kit	QIAGEN GmbH, Hilden, Germany
Vectastain® ABC kit peroxidase Rabbit/Mouse IgG	Vector Laboratories, Inc., Burlingame, USA
Verso™ cDNA Kit	Thermo Fisher Scientific, Inc., Surrey, UK

Table 8 Stimulants

Erlotinib Monohydrochloride	LKT Laboratories, Inc., Minnesota, USA
hEGF, lyophilized	Roche Diagnostics GmbH, Mannheim, Germany
Rosiglitazone	Cayman Chemical, Michigan, USA
U-0126	Cayman Chemical, Michigan, USA

Table 9 Antibodies

β-Catenin (C-18) sc-1496	Santa Cruz Biotechnology, Inc., Heidelberg, Germany
Caveolin-1 (N29) sc-894	Santa Cruz Biotechnology, Inc., Heidelberg, Germany
Cleaved Caspase 3 (Asp175) #9663	Cell Signaling Technology, Inc., Massachusetts, USA
Dok1 (A3) sc-6929	Santa Cruz Biotechnology, Inc., Heidelberg, Germany
Dok1 (M19) sc-6277	Santa Cruz Biotechnology, Inc., Heidelberg, Germany
Ki-67 (Anti-Mouse) Clone TEC-3	DakoCytomation Denmark A/S, Glostrup, Denmark
Lamin A/C (N20) sc-20681	Santa Cruz Biotechnology, Inc., Heidelberg, Germany
Ras, pan, N, H, K	United States Biological, Massachusetts, USA
p38 MAPK #9282	Cell Signaling Technology, Inc., Massachusetts, USA
Phospho-p38 MAPK (Thr180/Tyr182) (D3F9) #4511	Cell Signaling Technology, Inc., Massachusetts, USA
Phospho-Akt (Ser473) (193H12) #4058	Cell Signaling Technology, Inc., Massachusetts, USA
Phospho-GSK-3β (Ser9) (D3A4) #9322	Cell Signaling Technology, Inc., Massachusetts, USA
Phospho-c-Raf (Ser259) # 9421	Cell Signaling Technology, Inc., Massachusetts, USA

Phospho-p44/42 MAPK (Erk1/2) (Thr202/Tyr204) #9101	Cell Signaling Technology, Inc., Massachusetts, USA
Phospho-MEK1/2 (Ser217/221) #9121	Cell Signaling Technology, Inc., Massachusetts, USA
Phospho-SAPK/JNK (Thr183/Tyr185) (81E11) #4668	Cell Signaling Technology, Inc., Massachusetts, USA
PPARγ (E-8) sc-7273	Santa Cruz Biotechnology, Inc., Heidelberg, Germany
PPARγ (H-100) sc-7196	Santa Cruz Biotechnology, Inc., Heidelberg, Germany
PPARγ (C26H12) #2435	Cell Signaling Technology, Inc., Massachusetts, USA
Phospho-PTEN (Ser380) #9551	Cell Signaling Technology, Inc., Massachusetts, USA
SAPK/JNK (56G8) #9258	Cell Signaling Technology, Inc., Massachusetts, USA
Alexa Fluor® 488 goat anti-mouse IgM (µ chain)	Invitrogen GmbH, Karlsruhe, Germany
Alexa Fluor® 594 donkey anti-rabbit IgG (H+L)	Invitrogen GmbH, Karlsruhe, Germany
Alexa Fluor® 488 phalloidin	Invitrogen GmbH, Karlsruhe, Germany
DAPI p.a. 4',6-Diamidino-2-phenylindol Dihydrochlorid	Roth GmbH, Karlsruhe, Germany
Donkey-anti goat IgG-HRP sc-2020	Santa Cruz Biotechnology, Inc., Heidelberg, Germany
ECL™ Peroxidase labelled anti-mouse antibody NA931VS	Amersham Biosciences Europe GmbH, Freiburg, Germany
ECL™ Peroxidase labelled anti-rabbit antibody NA934VS	Amersham Biosciences Europe GmbH, Freiburg, Germany

Table 10 Oligonucleotides

RT-qPCR mouse		
Gene	**Sense**	**Antisense**
Aco	caggaagagcaaggaagtgg	cctttctggctgatcccata
B2m	atgggaagccgaacatactg	cagtctcagtgggggtgaat
Cav1	agccgcgtctactccatcta	tctctttctgcgtgctgatg
Cdx2	tctccgagaggcaggttaaa	gcaaggaggtcacaggactc
Cox2	agaaggaaatggctgcagaa	gctcggcttccagtattgag
Cyclind1	gcgtaccctgacaccaatct	atctccttctgcacgcactt
Dok1	ttttctgccttggagatgct	tctcagcttccaccctcagt
Hmgcs2	ggctgtcaaaacagtgctca	gcaatgtcaccacagaccac
Inos	caccttggagttcacccagt	accactcgtacttgggatgc
Kras	tgcaatgagggaccagtaca	ccaggaccataggcacatct
Lgr5	aacggtcctgtgagtcaacc	agtcatggggtaagctggtg
Lyz1	ctgtgggatcaattgcagtg	cggttttgacattgtgttcg
Met	cgatcagcagtctgtgcatt	acagccggaagagtttctca
Mmp7	agctatgcagctcaccctgt	gagcctgttcccactgatgt
Mmp13	agttgacaggctccgagaaa	ggcactccacatcttggttt
Myc	caacgtcttggaacgtcaga	tcgtctgcttgaatggacag
Nras	tgacttgccaacaaggacag	aaaaggcatcctccacacc
Pepck	ctggcacctcagtgaagaca	tcgatgccttcccagtaaac
Pparγ	ttttcaagggtgccagtttc	aatccttggccctctgagat
Tff1	tggagcacaaggtgatctgt	ggggaagccacaatttatcc
Tff2	tgctttgatcttggatgctg	ggaaaagcagcagtttcgac
Tnfa	acggcatggatctcaaagac	gtgggtgaggagcacgtagt
Wnt6	ttcggggatgagaagtcaag	aaagcccatggcacttacac
RT-qPCR human		
B2M	tgctgtctccatgtttgatgtatct	tctctgctccccacctctaagt
CYCLIND1	gatcaagtgtgacccggact	tcctcctcttcctcctcctc
TFF3	ctccagctctgctgaggagt	gcttgaaacaccaaggcact
DOK1 1-3 (C-terminal)	cctacaaccctgccactgat	tgagttgtggcttttgatgc
DOK1 1-1 (N-terminal)	gaccaagaggtggaggaaga	actcagccagacggatcact
K-Ras codon 12/13 sequencing mouse		
Gene	**Sense**	**Antisense**
Kras	gctccgcggcgcggagagag	ctagaaggcaaatcacacttattccc

Cloning and mutagenesis		
Gene	**Sense**	**Antisense**
humanDOK1p62	taga<u>aatt</u>ctcagctagagccctctgacttg	atga<u>aatt</u>catggacggagcagtgatggaag
humanDOK1p44	atga<u>aatt</u>catgctggagaactccttgtacag	taga<u>aatt</u>ctcaggtagagccctctgacttg
humanDOK1p44Flag	atga<u>aatt</u>**atggactacaaagacgatgacgataaa**atgctggaga	taga<u>aatt</u>ctcaggtagagccctctgacttg
humanDOK1p33Flag	atga<u>aatt</u>**atggactacaaagacgatgacgataaa**atggacggagcagtgatggaag	taga<u>aatt</u>ctcaaggcaacttcccctctgccac
R207A(mutagenesis)	gccctacactctgttg<u>gctgc</u>ctatggccgggacaagg	
R222A(mutagenesis)	tctttcgaggccggc<u>gccgcct</u>gcccctcaggccct	
NES(mutagenesis)	gcagcagcag<u>gcggc</u>gaaggccaag<u>gc</u>gacagacccc	
T7(sequencing)	taatacgactcactataggg	
seqRR222Ahdok1(sequencing)	cagatactggagccactcctgtc	cagtctcaactgcctggaagatg
seqNEShdok1(sequencing)	gcacgtctgctcaggcaggagag	gcttggcaccaccatgcatccttg
Genotyping		
Gene	**Sense**	**Antisense**
Apc	tctcgttctgagaaagacagaagct	tgatacttcttccaaagctttggctat
Cav1-WT	gtgtatgacgcgcacaccaag	cttgagttctgttagcccag
Cav1-KO	ctagtgagacgtgctacttcc	cttgagttctgttagcccag
VillCre	caagcctggctcgacggcc	cgcgaacatcttcaggttct
VillRas	caagcctggctcgacggcc	atttgcggccgctttacataattacacact
Pparγ	ctagtgaagtatactatactctgtgcagcc	gtgtcataataaaacatgggagcatagaagc

2.2   Cell culture

2.2.1   Cell growth conditions

HEK293T, SW480, HCT116, HT-29 and Caco-2 cells were grown in Dulbecco's Modified Eagle's Medium supplemented with 1 % penicillin/streptomycin and 10 % (v/v) fetal calf serum (FCS; all from Gibco/Invitrogen, Carlsbad, CA) at 37°C and 5 % CO_2.

SW480 stable Caveolin-1-transfected clones were grown in Dulbecco`s Modified Eagle's Medium with 1 % penicillin/streptomycin, G418 (200 µg/ml) and 10 % (v/v) fetal calf serum at 37°C and 5 % CO_2.

2.2.2   Stimulation of cells

Table 11 Stimulants and concentrations

Stimulant	Stock concentration	Working concentration	Effect
Rosiglitazone	50 mM in DMSO	0,01-100 µM	PPARγ agonist
hEGF (human epidermal growth factor)	15 µM or 50 µg/ml in dH_2O	12,5-50 ng/ml	stimulates proliferation and differentiation by activation of EGFR
U-0126	10 mM in DMSO	1 µM	MAP Kinase Kinase inhibitor
Erlotinib	5 mM in DMSO	1 µM	EGF-Receptor inhibitor

2.2.2.1 Dose response

Cells were seeded in 96-well plates (2000 cells/well) and incubated overnight for complete adherence. Cells were then stimulated with medium containing rosiglitazone in a range from 0-50 µM (0, 0.01, 0.1, 0.3, 1, 3, 10, 50 µM) and incubated for 2 days. The experiment was analyzed by MTT assay.

2.2.2.2 Kinetics

Cells were seeded in 96-well plates (2000/well) and incubated overnight for complete adherence. The next day, medium containing the designated stimulant was added and cell growth was stopped after 0-8 days by MTT.

2.2.2.3 Rapid signaling assay

Cells were grown to 90 % confluency in 12- or 6-well-plates and starved in medium without serum overnight.

For Ras-inhibition, medium without FCS containing 1 µM U0126 or erlotinib was added and the cells were incubated for 30 min at 37°C. Cells were then stimulated with hEGF to a final concentration of 15 µM for 15 min.

For PPARγ- or Ras-stimulation, 10 µM rosiglitazone or 15 µM EGF were added for the designated time in serum-free medium.

After stimulation cells were washed once with ice-cold PBS and the plates were put on ice and processed either for subcellular fractionation or total cell lysis.

2.2.3 MTT Assay

The MTT Assay is a method to measure the proliferation and vitality of cells. The basic principle of this assay is that thiazolyl blue tetrazolium bromide is metabolized only by living cells to a blue dye (formazan), which can be measured and which is an indicator of the cell viability.

Cells were seeded in 96-well plates in 100 µl medium and treated as required. 10 µl of MTT reagent (5 mg/ml in 1 x PBS) were added to one well and incubated at 37°C for 3 h. The reaction was then stopped by adding 100 µl MTT lysis buffer (10 % (w/v) SDS + 0.01 N HCl) to one well. The plate was incubated overnight at 37°C to achieve complete lysis of the cells. The release of the dye was then measured at 570-650 nm in a 96-well plate reader.

2.2.4 Transient-transfection of cells

Cells were grown to 70 % confluency in 6-well plates. The cells were then transiently cotransfected in DMEM medium with 2 µg DNA/well using TurboFect™ (Fermentas) or 10 nM siRNA with INTERFERin™ (Polyplus) according to the manufacturer`s instructions.

For negative control cells were equally transfected with either empty vector control or Cy3 siRNA (Ambion). Cells were transfected for 8 hours (DNA) or overnight (siRNA).

2.3   Protein preparation and analysis

2.3.1   Preparation of total cell lysate

Cells were washed once with PBS and SDS lysis buffer (50 mM Tris-HCl, pH 7.4, 1 % SDS, 1 mM sodium orthovanadate, 1 mM dithiothreitol, Protease Inhibitor Complete®) was added. Cells were scraped, lysed on ice for 20 min and transferred into 1.5 ml tubes. Cells were then sonicated twice (10 sec, 35 %), centrifuged at 13200 rpm for 10 min at 4°C and the supernatant was collected.

2.3.2   Preparation of total tissue lysate

For protein extraction, 2-3 mm^3 of frozen mouse tissue was added to 800 µl of ice-cold lysis buffer (20 mM HEPES, pH 7.4, 1 mM EDTA, 50 mM ß-glycerophosphate, 10 % (v/v) Glycerol, 1 % (v/v) Triton X-100, 1 mM sodium orthovanadate, 1 mM dithiothreitol, Protease Inhibitor Complete®). The tissue was then homogenized and incubated on ice for at least 60 min. After centrifugation at 10000 rpm at 4°C for 10 min the supernatant containing the proteins was collected and the protein concentration was measured.

2.3.3   Subcellular fractionation of cells

To separate the different compartments of the cell, cytosol, nucleus and insoluble membrane/matrix fraction, subcellular fractionation (SCF) was performed.

Cells were seeded in 6-well plates and stimulated as required for the individual experiment. To terminate the stimulation, cells were washed once with ice-cold PBS and 1 ml of HL buffer (20 mM Tris-HCl, pH 7.4, 2 mM EDTA, 2 mM MgCl$_2$, 1 mM sodium orthovanadate, 1 mM dithiothreitol, Protease Inhibitor Complete®) was added for hypotonic lysis. Cells were scraped and lysed on ice for 20 min, transferred to 2 ml tubes and homogenized with 20 strokes of a blue tip until foaming. After centrifugation at 7000 rpm for 5 min at 4°C, the supernatant with the soluble cytosolic fraction was collected and the nuclear pellet was washed once with ice-cold HL buffer. The nuclei were extracted in 100-150 µl of HS (high salt) buffer (HL buffer supplemented with 450 mM NaCl) on ice for 30 min with frequent vortexing for complete lysis. Upon centrifugation at full speed for 10 min at 4°C, the supernatant containing the nuclear extract was collected. The remaining pellet containing all kinds of membranes (ER, plasmamembrane, nuclearmembrane) was washed once with buffer HS and subjected to extraction in 100 µl SDS lysis buffer (50 mM Tris HCl, pH 7.6,

2 % SDS (w/v)) for 5 min, sonication (10 sec, 35 %, Soniplus, Bandelin, Berlin, Germany) and centrifugation for 10 min at full speed at 4°C.

2.3.4   Subcellular fractionation of tissue

Subcellular fractionation of mouse tissue was done as described for cells with a few modifications. Approximately 3 mm^3 of tissue were added to 500 µl HL-buffer and homogenized using a Dounce homogenizer. Tissue was incubated on ice for 10 min and centrifuged at full speed for 15 min at 4°C. Supernatant containing the cytosolic fraction was collected, pellet was washed once with HL-buffer and nuclear fraction was extracted in 150 µl HS-buffer (supplemented with 25 % glycerol). The fractionation was continued according to the SCF protocol for cells.

2.3.5   Co-Immunoprecipitation

To study protein-protein-interaction CoIP was performed. To this end, cells were grown to 90 % confluency on a 150 mm dish. For hypotonic lysis, 3 ml of Tris-buffer (10 mM Tris-HCl, pH 7.4, 2 mM EDTA, 2 mM MgCl$_2$, 1 mM sodium orthovanadate, 1 mM dithiothreitol, Protease Inhibitor Complete®) were added to the cells. Cells were then scraped, transferred to an Eppendorf tube and homogenized with 20 strokes of a blue tip until foaming. The cells were lysed on ice for 20 min and followed by a centrifugation for 5 min at 13200 rpm at 4°C. 100 µl were separated as input control. 400 µl of the supernatant were mixed with 20 µl of the polyclonal primary antibody. 400 µl were left without antibody as negative control. Tubes were then incubated overnight on a rotator at 4°C. The next day, 20 µl of protein A/G-agarose (Santa Cruz Biotechnology, Inc.) were added to each tube and rotated for additional 2 h at 4°C. Beads were then centrifuged for 1 min at 1000 rpm at 4°C followed by three washing steps with 1 ml wash buffer (Tris-buffer supplemented with 150 mM NaCl). For elution, supernatant was completely removed from the beads and 50 µl of 100 mM glycin (pH 2.2) were added, and the reaction was incubated for 2 min on ice and then stopped by adding 10 µl 1.5 mM Tris-HCl, pH 8.8. After centrifugation for 1 min at 13200 rpm at 4°C, the eluate was collected and the precipitate was supplemented with 30 µl of Tris-buffer. Finally, 20 µl of SDS-loading buffer were added to the eluate, the precipitate and 80 µl of the input collected before and all reactants were boiled for 10 min at 99°C and analyzed by Western Blot.

For MES-lysis (25 mM MES, 140 mM NaCl, 1 % (v/v) Triton X-100) CoIP was performed at RT. Cells were scraped and lysed for 15 min. After centrifugation, all steps were performed on ice. Cells were washed with MES-buffer containing 0.1 % (v/v) Triton X-100. All steps were performed as described for hypotonic lysis.

2.3.6 Mass spectrometry (MS)

Mass spectrometry was done as previously published [57].

2.3.7 Ras Pulldown Assay

To determine active K-Ras in cells or mouse tissue, GTP-Ras Pulldown Assay was performed as described by Janssen *et al.* [58]. Shortly, 1.4 ml of bacterial lysate (provided by KP Janssen, Chirurgische Klinik und Poliklinik, Klinikum rechts der Isar) comprising glutathion-S-transferase-RalGDS (GST-RalGDS) fusion protein were incubated with 200 µl of glutathione agarose (Santa Cruz Biotechnology, Inc.) for 1 h at 4°C. After centrifugation, the pellet was washed with 500 µl of lysis buffer (50 mM Tris-HCl, pH 7.4, 150 mM NaCl, 20 mM $MgCl_2$, 5 mM EDTA, 1 % Triton-X100, 1 % NP-40, 1 mM sodium orthovanadate, 1 mM dithiothreitol, Protease Inhibitor Complete®).

Cells were grown to 90 % confluency on a 16 cm dish, washed once with cold PBS and 2 ml lysis buffer were added directly to the dish. Cells were scrapped with a cell scraper and the lysate was transferred to a 2 ml Eppendorf tube, resuspended and incubated for 20 min on ice. Thereafter, cells were centrifuged for 10 min at full speed and equal volumes of the supernatant were distributed to two Eppendorf tubes. For detection of active Ras in mouse tissue, approximately 10 mg of the tissue were homogenized with a dounce homogenizer in 100 µl lysis buffer. Tissue was incubated for 15 min at 4°C under rotation. The lysate was then centrifuged at 13000 rpm for 10 min at 4°C and the protein concentration was determined. 1.5-2.0 mg of the proteins were used and lysis buffer was added to a final volume of 600 µl. 30 µl of glutathione-beads coupled to GST-RalGDS were then added to the lysates as positive control. As negative control, 30 µl of pure glutathione-beads were added. Lysates were then incubated for 2 hours with rotation. After centrifugation, the pellet was washed 3 times with lysis buffer, resuspended in 5 x SDS loading buffer and analyzed by Western Blot using pan-Ras antibody.

2.3.8 Western Blot

2.3.8.1 Preparation of samples

Protein concentration was measured using the BCA™ Protein Assay Kit (Thermo Fisher Scientific, Inc.) according to the manufacturer`s protocol. The Protein samples were then diluted in dH_2O to a similar concentration and boiled in 5 x SDS loading buffer (62,5 mM Tris-base, pH 10, 10 % (w/v) SDS, 5 % (v/v) ß-Mercaptoethanol, 50 % (v/v) glycerol, bromphenolblue) for 10 min at 99°C. Samples were then briefly centrifuged and further analyzed or, if necessary, stored at -20°C.

2.3.8.2 SDS-polyacrylamide gel electrophoresis

To separate the proteins according to their molecular weight SDS-polyacrylamide gel electrophoresis (SDS-PAGE) was used. Either 10 % or 15 % acrylamide gels were prepared. SDS polyacrylamide gel components were

Component	Separating gel		Stacking gel
	10 %	15 %	
H_2O	3,29 ml	1,89 ml	1,53 ml
Acrylamide (30 %)	2,8 ml	4,2 ml	333 µl
1.5 M Tris-HCl, pH 8.8	2,1 ml	2,1 ml	-
0.5 M Tris-HCl, pH 6.8	-	-	625 µl
SDS (10 %)	83 µl	83 µl	25 µl
APS (10 %)	42 µl	42 µl	12,5 µl
TEMED	2,8 µl	2,8 µl	2,5 µl

Equal amounts of proteins were loaded and the gels were run using the Mini-PROTEAN® 3 Cell system (Bio-Rad Laboratories GmbH) at constant 25 mA in running buffer (192 mM glycine, 25 mM TRIS-base, 0.1 % (w/v) SDS).

2.3.8.3 Protein transfer and detection

Proteins were then transferred to a nitrocellulose membrane (Whatman) using the Mini Trans-Blot® Electrophoretic Transfer Cell (Bio-Rad Laboratories GmbH) by electrophoresis for 1 h at 100 V in transfer buffer (192 mM glycine, 25 mM Tris-base, 20 % (v/v) Methanol).

After blotting, the membrane was blocked for 1 h in 5 % (w/v) BSA or milk in T-PBS on a shaker at RT. The membrane was then incubated overnight with primary antibody at 4°C with gentle shaking. The membrane was washed 4 x 15 min in T-PBS, peroxidase-labelled secondary antibody (Amersham Bioscience Europe GmbH) was added 1:5000 for 1-2 h in 5 % BSA or milk in T-PBS and the membrane was washed again 4 x 15 min. Immunodetection was performed using ECL Detection Reagent (GE Healthcare UK Ltd.) according to the manufacturer`s protocol. The X-Ray film was placed on the membrane for the respective exposure time and developed in a film processor (Hyperprocessor, Amersham Biosciences Europe GmbH).

2.4   Luciferase Assay

The Luciferase enzyme catalyzes luciferin oxidation under generation of light. The "Relative Light Units" (RLU) can be measured with a luminometer. By linking promoter and/or

enhancer region and luciferase gene in one plasmid, luciferase expression is under control of this promoter and the promoter activity can be quantified by measuring RLUs.

Cells were transiently transfected with either 3xPPRE-TK-luc (for PPARγ activity) (from Fa. Hoffmann-La Roche AG) or SRE-luc (for RAS activity) (from Stratagene) and stimulated with rosiglitazone (0, 0.1, 1 and 10 µM) or 15 µM hEGF for 24 h. Medium was aspirated, 100 µl of 1 x passive lysis buffer (Promega) was added and cells were incubated for 10 min at room temperature on a shaker. Thereafter cells were transferred in tubes and centrifuged at 13200 rpm for 10 min at 4°C to remove cell debris. Luciferase activity was measured by the Steady Glo luciferase assay system (Promega, Madison, WI). 35 µl of "Luciferase Assay Reagent" were mixed with 10 µl lysate and the light emission was measured using a luminometer (GLOMAX). For determination of the transfection rate renilla-luciferase activity was measured adding 35 µl Stop&Glo buffer (Promega) to each sample. For stimulated cells, cells were normalized according to their protein concentration.

2.5 Nucleic acid preparation and analysis

2.5.1 RNA extraction and purification of cells

Cells were seeded in 6-well plates and transfected or stimulated as required. Medium was removed and 350 µl of buffer RLT with 3.5 µl of ß-mercaptoethanol was added, the cell lysates were mixed with 350 µl of 70 % Ethanol and transferred to a silica membrane from the RNeasy Mini Kit (Qiagen GmbH). RNA was extracted according to the manufacturer`s protocol. Free DNA was digested by adding DNase I (QIAGEN) for 15 min and pure RNA was eluted in RNase-free water at RT.

2.5.2 RNA extraction of tissue

2-3 mm^3 of frozen mouse tissue was added to 600 µl buffer RLT supplemented with 6 µl β-mercaptoethanol. Tissue was the homogenized and transferred to a QIAshredder homogenizer (QIAshredder^{TM}, QIAGEN) and the lysate was centrifuged at 13200 rpm for 2 min at RT. The tissue homogenate was then mixed with 600 µl 70 % EtOH and transferred to a silica membrane from the RNeasy^{TM} Mini Kit. The RNA was extracted as described before.

2.5.3 cDNA synthesis

1 µg RNA was used for reverse transcription into cDNA using the Verso^{TM}cDNA Kit (Thermo Fisher Scientific, Inc.) according to the manufacturer`s protocol. After synthesis H$_2$O was added to a final volume of 50 µl.

2.5.4 Genotyping

2.5.4.1 DNA extraction from mouse tails

The tip of a mouse tail was incubated overnight in 750 µl lysis buffer (50 mM Tris-HCl, pH 8.0, 100 mM EDTA, 100 mM NaCl, 1 % SDS, 0.5 mg/ml Proteinase K) at 55°C in a thermoblock under constant and gentle rotation. The next day 300 µl of 5 M NaCl were added, the lysates were vortexed and centrifuged for 30 min at 10000 rpm at 4°C. 200 µl were collected from the middle of the solution and mixed with 175 µl Isopropanol until precipitation of DNA. After centrifugation for 10 min at 13000 rpm at 4°C the DNA pellet was washed 2 x 15 min with ice-cold 75 % EtOH and the pellet was air-dried at RT. When EtOH had completely evaporated DNA was dissolved in 50 µl elution buffer and incubated for 2 h at 37°C.

2.5.4.2 Regular PCR

DNA was diluted to a concentration of 20 ng/µl. For genotyping of *VillCre*, *VillRas*, *Pparγ* and *Cav1*, PCR was performed using GoTag®Green Master Mix (Promega). The reaction setup was as follows:

GoTaq®Green Master Mix (2x)	12,5 µl
Reverse Primer	1,25 µl
Forward Primer	1,25 µl
dH$_2$O	7,5 µl
DNA (20 ng/µl)	2,5 µl

For genotyping of *Apc,* PCR was performed with colorless GoTaq®. The reaction was prepared as follows:

Colorless GoTaq® buffer (5x)	5 µl
100 mM dNTP mix (25 mM each)	0,5 µl
Reverse Primer	1 µl
Forward Primer	1 µl
Taq Polymerase	0,5 µl
dH$_2$O	14,5 µl
DNA (20 ng/µl)	2,5 µl

The PCR-product was amplified using the following program:

95°C   5 min   1 cycle

95°C   1 min

60°C   1 min   40 cycles

72°C   1 min

72°C   5 min   1 cycle

 4°C   ∞   1 cycle

The amplification product was digested using the *HindIII* enzyme. To this end 8 µl of PCR were mixed with 1 µl *HindIII* and 1 µl buffer 2 (both from NEB), and the reaction was incubated for 60 min at 37°C followed by inactivation at 65°C for 20 min. 10 µl were then mixed with 6 x DNA loading buffer (Fermentas).

The digested DNA was loaded on 1 % agarose gels which were run at 100 V for 30 min. *Ppar*γ and *Apc* were analyzed using native gels run for 2-3 h at 100 V.

2.5.5   qPCR

To analyze the expression of genes, quantitative real-time PCR was used. One reaction mix was setup as follows:

Light Cycler® 480 SYBR I Green Master (2x)   10 µl

Forward Primer (10 µM)   1 µl

Reverse Primer (10 µM)   1 µl

dH$_2$O   6 µl

18 µl were added to each well of a 96-well white plate and mixed with 2 µl of the cDNA. For each reaction duplicates were performed. The plate was centrifuged for 1 min at 1000 rpm and the PCR reactions were quantified in a LightCycler® 480 (Roche Diagnostics GmbH) using the following program:

Step	Temperature	Holds	Number of cycles
Pre-Incubation	95°C	5 min	1
	95°C	10 sec	
Amplification	55°C	10 sec	45
	72°C	5 sec	
Final	72°C	2 min	1
Cooling	37°C	10 min	1

The qPCR results were analyzed using the LightCycler® 480 software 1.5.0 (Roche Diagnostics GmbH). During amplification, the SYBR Green binds to double strand DNA and produces a fluorescence signal. An increase in the DNA thus leads to an increase in fluorescence which is measured for each cycle. For the quantification of the DNA a threshold was set on the exponential phase of the amplification, the cycle threshold (Ct). The lower the Ct value, the higher is the amount of DNA and therefore the expression of the gene. The mean value of the Ct was calculated for the duplicates and the Ct of the housekeeping gene (β2M) was subtracted leading to ΔCt. The "calibrator" was then calculated meaning the mean value of all ΔCt values for one gene under different conditions of stimulation or for different individuals (patients, mice). This value was subtracted from the ΔCt resulting in $\Delta\Delta$Ct. Fold induction was calculated using the formula $2^{-\Delta\Delta Ct}$.

2.5.6 Agarose gel electrophoresis

Amplified PCR products were analyzed on 1 % (w/v) agarose gels. Agarose (Biozym) was added to 1 x TAE buffer (40 mM Tris-base, 1 mM EDTA pH 8.0, 20 mM acetic acid), boiled for a few seconds and 0.25 µg/ml ethidiumbromide were added. Gels were run using the Sub®Cell GT (Bio-Rad Laboratories GmbH) equipment for at least 30 min at 100 V. The DNA was detected using a gel documentation device (Bio-Rad Laboratories GmbH) and the software QuantityOne.

2.5.7 Native poly acrylamide gel electrophoresis

Native PAGE separates small DNA fragments better than agarose gels and was used for genotyping of *Pparγ* and *Apc*.

One 12 % native gel contained the following components:

10 x TBE	1 ml
30 % acrylamide	4 ml
80 % glycerol	1 ml
10 % APS	25 µl
TEMED	5 µl
dH$_2$O	4 ml

The gels were run using the Mini-PROTEAN® 3 Cell system (Bio-Rad Laboratories GmbH) at constant 100 V for 1 h. After loading DNA, the gels were run for additional 2-3 h at 100 V in 1 x TBE. Thereafter gels were stained with ethidiumbromide in 1 x TBE for 1 h and DNA was visualized using UV light.

2.6   Molecular cloning

For overexpression of huDok1 in cells, the p62, p44 and p33 isoforms of Dok1 were cloned into the pTarget vector (Promega). Human Dok1 isoforms were amplified from cDNA of SW480 colon cancer cells by PCR setup as follows:

JumpStart™ RedTaq®Ready Mix (Sigma)	12,5 µl
Forward Primer	1,25 µl
Reverse Primer	1,25 µl
dH$_2$O	7,5 µl

The product was amplified using the following program:

95°C	2 min	1 cycle
95°C	30 sec	
55°C	30 sec	35 cycles
72°C	2 min	
72°C	7 min	1 cycle
4°C	∞	1 cycle

The PCR-products were purified on a 1 % agarose gel and the generated 1400 bp, 1030 bp or 840 bp products were excised with a clean scalpel, followed by extraction using the gelextraction kit (QIAGEN) according to the manufacturer`s protocol. Purified PCR products were used for TOPO TA Cloning® (Invitrogen) according to the manufacturer`s protocol for chemical transformation. Reaction was setup as follows:

PCR product	4 µl
salt solution	1 µl
dH$_2$O	-
TOPO® vector	1 µl

The reaction was incubated for 15 min at RT and 2 µl of the TOPO Cloning reaction were added to one vial of OneShot® *E.coli* and mixed gently. Bacteria were incubated for 30 min on ice followed by 30 sec heat-shock at 42°C. 1 ml SOC-Medium was added and the bacteria were incubated for 1 h at 37°C gently shaking at 300 g. Bacteria were then plated on LB agar plates containing 100 µg/ml ampicillin supplemented with 1 mg X-Gal (5-Brom-4-chlor-3-indoxyl-β-D-galactopyranosid, Sigma). The next day white colonies (white color indicates the positive insertion of the PCR product in TOPO vector) were picked and colony

PCR was performed. To this end one colony was picked with a white tip of pipette, transferred to another LB agar plate and the tip was then incubated in 100 µl LB medium for 1 h at 37°C under gentle shaking. The PCR reaction was setup as described before using 5 µl of the bacteria suspension. The PCR was loaded on a 1 % agarose gel. If a positive band was detected, clones were incubated overnight in 5 ml LB containing 100 µg/ml ampicillin and the plasmid was prepared using the MiniPrep Kit (Promega) according to the manufacturer`s protocol. The product was sequenced by the service of the GATC Biotech AG. Clones with the correct Dok1 sequence were then used for overexpression in pTarget vector. Digestion was performed using the *EcoRI* enzyme (Promega) for pTarget and Dok_Topo. Digestion-reaction was setup as follows:

pTarget/Topo plasmid	2 µg
EcoRI	1 µl
EcoRI buffer	1 µl
dH$_2$O	ad 10 µl

The Digestion-reaction was loaded on a 1 % agarose gel. Insert and pTarget vector were then excised and purified as described before. Insert and vector were subjected to ligation in a ratio 3 to 1.

T4 ligase	1 µl
T4 buffer	1 µl
insert	30 ng
vector	10 ng

} 8µl

The reaction was setup and incubated overnight at 11°C in a PCR cycler. 1 µl of the ligation mix was then added to 50 µl of *E.coli* DH5α. The reaction was incubated on ice for 1 h, heat-shocked for 90 sec at 42°C and put back on ice for 2 min. 500 µl of LB medium were added, incubated for 1 h at 37°C and the bacterial suspension was plated on LB agar plates supplemented with ampicillin. Colonies were picked, resuspended in 100 µl LB medium and colony-orientation-PCR was performed using forward primer in pTarget vector and reverse primer in insert. Positive clones were picked and sequenced by GATC service.

2.7 Mutagenesis

Mutations of the cloned huDokp62 isoform were done using QuikChange Site-Directed Mutagenesis Kit (Agilent Technologies) and huDok1_pTarget plasmid according to protocol with the appropriate primers listed in table 10.

2.8 Immunochemical methods

2.8.1 Preparation of mouse tissue

For paraffin embedding, mouse tissue (Ileum, Colon and Cecum) was inserted in embedding cassettes and fixed overnight in 4 % (w/v) paraformaldehyde in PBS at 4°C. Tissue was dehydrated in an autotechnicon and embedded in paraffin. Blocks were stored at room temperature and transferred to -20°C freezer for 1 h before being cut to 3 µm slices with a microtome (Leica RM 2145).

For Cryopreservation, tissue was snap-frozen in liquid nitrogen using cryotubes (Sarstedt) and stored at -80°C. For analysis, frozen tissue was cut with a microtome-cryostat (Leica) at -20°C.

2.8.2 Immunofluorescence staining of cells

Immunofluorescence was used to determine the localization of a protein in the cells.

Cells were grown on slides placed in 6-well plates to 50 % confluency, washed once with PBS and fixed with fixative (4 % PFA (w/v) in PBS) for 20 min at room temperature. Cells were then washed three times for 5 min with PBS followed by blocking with 100 % FCS for 30 min. Permeabilisation was achieved using permeabilisation buffer (0.1 % Triton-X 100 (v/v) in PBS) for 10 min. Cells were washed once again with PBS and incubated with primary antibody diluted 1:500 in AB dilution buffer (1 % FCS (v/v) in PBS) overnight at 4°C. After incubation cells were washed three times for 5 min and incubated with secondary antibody (1:500) or phalloidin (all Invitrogen) in AB dilution buffer followed by washing and incubation with DAPI (1:2000 in PBS) (Roth GmbH) for 10 min to stain the nuclei. All steps were carried out in the dark. Cells were washed again and one drop of mounting medium (Dako) was added and the cover slips were placed on the microscope slides (SuperFrost Plus, Thermo Scientific Inc.). Slides were dried overnight and stored at 4°C in the dark. Fluorescence was analyzed using a fluorescent microscope and the software AxioVision 4.8 (all Carl Zeiss GmbH).

2.8.3 Proximity ligation assay

Besides CoIP, this assay is another method to detect protein interactions in the cell. The two antibodies of the proteins of interest bind the antigens in the cell. The secondary antibodies are labeled with oligonucleotides ("PLA probes") and bind the primary antibodies. If the probes are in close proximity, the oligonucleotides are ligated and amplified via rolling circle amplification using fluorescently labeled oligonucleotides. The fluorescent oligonucleotides are then visible as a red fluorescent spot.

PLA was performed according to the manufacturer's protocol. Hek293 cells were grown on 18 mm^2 slides placed in 24-well plates. The cells were then washed once with PBS and fixed for 20 min in 4 % formaldehyde in PBS at RT. Cells were then washed three times for 5 min with PBS followed by blocking with blocking solution (all solutions are provided from Olink) for 30 min at 37°C (dry incubator) in a humidity chamber. Cells were then permeabilized with 0.1 % Triton-X 100 (v/v) in PBS for 10 min, washed once with PBS and incubated with primary antibodies 1:250 in antibody diluent at 4°C overnight. Slides were washed twice in 1 x Wash Buffer A for 5 min and were then incubated with the PLA probe solution for 1 h at 37°C. Slides were washed again for 2 x 5 min in 1 x Wash Buffer A and incubated with Ligation-Ligase solution for 30 min at 37°C. After ligation, slides were washed 2 x 2 min in 1 x Wash Buffer A and incubated with Amplification-Polymerase solution for 100 min at 37°C in the dark. After washing in 1 x Wash Buffer B for 10 min slides were incubated with Phalloidin diluted 1:500 in 1 x Wash Buffer B for another 10 min. After washing with 1 x Wash Buffer B for additional 10 min, slides were washed with 0.01 x Wash Buffer B for 2 min. Cover slips were dried at RT in the dark and put on slides together with Duolink in Situ Mounting Medium with DAPI.

2.8.4 Immunofluorescence staining for TRITC-UEA in mouse tissue

Paraffin sections were deparaffinized, rehydrated and unmasked according to the protocol for Immunohistochemistry. The tissue was then blocked for 60 min in 1 % BSA in PBS. Antibody for TRITC-UEA was added 1:200 in 1 % BSA in PBS supplemented with 0.3 % Triton X-100 (antibody dilution buffer) and the tissue slides were incubated overnight at 4°C. After washing for 3 x 5 min, the tissue was incubated with Phalloidin (1:500) and DAPI (1:2000) in antibody dilution buffer and incubated for 10 min at RT. After washing for 3 x 5 min in PBS, cover slips were put on the slides together with Dako mounting medium.

2.8.5 H&E staining of tissue sections

For histologic examinations paraffin slices were stained with Haematoxilin (Nuclei, blue) and Eosin (Cytoplasm, red). Slices were deparaffinized twice for 5 min in Histoclear (Roth) and rehydrated twice for 3 min in 100 % EtOH, 96 % EtOH and 70 % EtOH. Slices were then stained for 5 min in "Hämalaun nach Mayer" (Roth), rinsed in tapwater for 10 min and stained for 5 min in Eosin, and were then dehydrated for 25 sec in 96 % Ethanol and Isopropanol and twice for 1.5 min in Histoclear. One drop of PERTEX mounting medium (Medite GmbH) was added and the slide was covered with a coverslip.

Cryosections were fixed in 4 % (w/v) PFA in PBS for 15 min, washed three times in PBS and stained for max. 1 min in "Hämalaun nach Mayer" (Roth). Sections were rinsed under tapwater for 10 min and dehydrated for 1 min in 96 % EtOH and Isopropanol followed by

immersion in Histoclear for 2 x 3 min. Slides were covered with coverslips using PERTEX mounting medium.

2.8.6 Immunohistochemistry

Paraffin sections were deparaffinized in Histoclear, rehydrated 2 x 3 min in 100 % EtOH, 96 % EtOH, 70 % EtOH and dH_2O. The sections were then subjected to high temperature antigen retrieval in Vectastain antigen unmasking solution (10 mmol/L citrate buffer, pH 6.0) (Vector Laboratories, Inc.) and were then heated in a microwave for 10 min without boiling. After cooling to RT for 30 min sections were washed 3 x 2 min in PBS and the endogenous peroxidase activity was quenched with 3 % (v/v) H_2O_2 in PBS for 20 min. After washing steps of 3 x 2 min in PBS, slides were put in a humid chamber and blocked with 5 % (v/v) normal goat or rabbit serum (depending on species the secondary antibody was made in) in 1 % (w/v) BSA in PBS for 1 h. Primary antibody diluted 1:25-1:100 in 1 % (w/v) BSA in PBS was spotted on the slides and the slides were incubated overnight at 4°C.

After washing, slides were incubated with biotinylated secondary mouse (Vector® M.O.M^{TM} Immunodetection Kit) or rabbit (Vectastain® ABC Kit peroxidase rabbit IgG) (both from Vectastain Laboratories, Inc.) antibody diluted 1:500 in 1 % (w/v) BSA in PBS or M.O.M diluent for 1 h at room temperature in a humid chamber. Slides were washed again and ABC-Mixture (Vectastain Laboratories, prepared according to manufacturer`s instructions) was added and the slides were incubated for 30 min. Slides were washed, DAB-mixture from DAB peroxidase substrate Kit (Vectastain Laboratories, Inc., prepared according to manufacturer`s instructions) was dropped on the tissue sections and the slides were incubated for 1-5 min until the tissue turned brown. The reaction was stopped by washing three times in dH_2O for 1 min and slides were counterstained in "Hämalaun nach Mayer" for 5 min. Excessive color was washed out under tap water for 10 min and slices were dehydrated and mounted as described before.

For frozen cryosections slices were fixed in 4 % PFA, washed in PBS and incubated in 3 % H_2O_2. The procedure was continued as described for paraffin slices.

2.9 Breeding of mice

2.9.1 *Apc^{min/+}//Cav1*-KO mice

Caveolin-1 knockout (Cav1-KO) mice (strain Cav1tm1Mls/J; stock number 004585) and control wildtype (WT) mice (strain B6129SF2/J; stock number 101045) were obtained from Jackson Laboratory (Bar Harbor, Maine). *Apc^{min/+}* mice (Charles River Laboratories, Wilmington, MA) were maintained on a pure C57BL/6J background. To generate the colorectal cancer tumor model, male *Apc^{min/+}* mice were interbred with female Cav1-KO mice.

The F1 littermates were then intercrossed for at least 8 generations to get the *Apc*-wildtype genotypes (*Apc^{+/+}//Cav1^{+/+}, Apc^{+/+}//Cav1^{+/-}, Apc^{+/+}//Cav1^{-/-}*) and the *Apc*-mutated mice (*Apc^{min/+}//Cav1^{+/+}, Apc^{min/+}//Cav1^{+/-}, Apc^{min/+}//Cav1^{-/-}*).

Mice received a chow diet or a chow diet (from Altromin, Lage, Germany) supplemented with 0.02 % (w/w) rosiglitazone maleate (Chemos GmbH, Regenstauf, Germany), a dose which corresponds to approximately 25 mg/kg per day for 4 months. [59]

2.9.2 PPARγ//RAS mice

Transgenic mice expressing the human *KRAS* G12V mutant and mice expressing the Cre recombinase under the murine villin promoter in enterocytes were obtained from S. Robine, Institute Curie, Paris [58]. Homozygous floxed PPARγ (PPARγ-FL/FL) (strain B6.129-Ppargtm2Rev/J; stock 004584) and control wildtype strain C57BL/6J mice were obtained from the Jackson Laboratory, Bar Harbor, Maine. Female hemizygous K-RasG12V+/CRE+ mice were intercrossed with male PPARγ-FL/FL mice. The obtained F1 littermates were K-RasG12V+/CRE+/PPARγ-FL/+. There were no homozygous K-RasG12V+/CRE+/PPARγ-FL/FL born, indicating potential lethality of absence of PPARγ in the intestine. Animal studies were conducted in agreement with the ethical guidelines of the TU München and approved by the appropriate government authorities.

2.10 Statistics

Results are means ± standard errors (S.E.) from at least three independent experiments or three animals per genotype. The software Graphpad Prism (version 4.0) was used to describe the survival distribution of the different genotypes *via* Kaplan-Meier-method. Survival was analyzed using the Log Rank test. The software SAS (version 9.3) was used for analysis of the *in vivo* data. For simple comparison of two means, significance was analyzed using Student's *t*-test (Microsoft Excel), which is explained in more detail in the Appendices. *P*-values of 0.05 or less were considered significant.

3. Results

3.1 The *Apcmin//Cav1*-KO mouse model

3.1.1 Establishment of *the Apcmin//Cav1*-KO mouse model

For generation of the *Apcmin/+//Cav1*-KO colorectal cancer mouse model, male *Apc$^{min/+}$* mice were first interbred with female *Cav1$^{-/-}$* mice. The F1 littermates were then intercrossed leading to the following genoptypes: *Apc$^{min/+}$//Cav1$^{+/+}$, Apc$^{min/+}$//Cav1$^{+/-}$* and *Apc$^{min/+}$//Cav1$^{-/-}$* as well as the corresponding *Apc*-WT strains *Apc$^{+/+}$//Cav1$^{+/+}$, Apc$^{+/+}$//Cav1$^{+/-}$* and *Apc$^{+/+}$//Cav1$^{-/-}$*. These genotypes should elucidate whether absent Caveolin-1 (Cav1) influences tumor formation in the colon *in vivo*. The obtained mice indeed developed CRC and were first analyzed by means of Cav1 expression on the mRNA as well as on the protein level. Caveolin-1 expression was found to be already reduced to 16 % in *Apc$^{min/+}$//Cav1$^{+/-}$* mice compared to *Apc$^{min/+}$//Cav1$^{+/+}$* in normal colon tissue. Furthermore, compared to normal colon tissue, *Cav1* expression was also reduced in tumor tissue to 55 % in *Apc$^{min/+}$//Cav1$^{+/+}$* mice. Nevertheless, significant reduction of *Cav1* was observed only in the homozygous (*Apc$^{min/+}$//Cav$^{-/-}$*) mice. These findings were corroborated by analysis of Cav1 on the protein level, comparing normal ileum, normal colon and colon tumor (Fig.7).
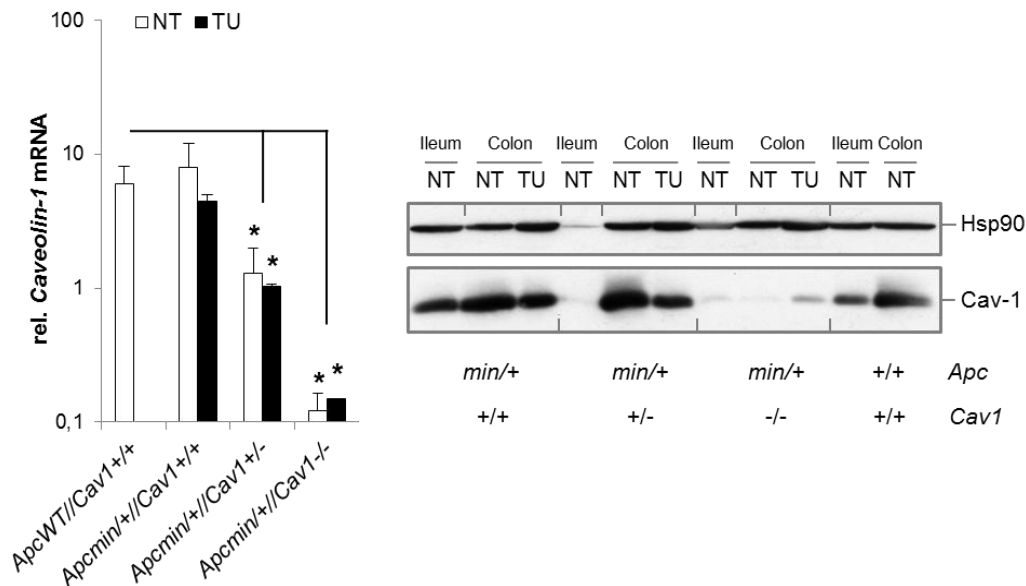
<u>Figure 7</u> Expression of Caveolin-1 in the three different mouse genotypes. Left panel: Caveolin-1 mRNA determined by RT-qPCR for WT, *Apc$^{min/+}$//Cav1$^{+/+}$, Apc$^{min/+}$//Cav1$^{+/-}$* and *Apc$^{min/+}$//Cav1$^{-/-}$* mice comparing TU and NT. CT-values were normalised to β2-microglobulin and calculated as –fold ± S.E. (n=3 per genotype for NT and TU), *t-test $p<0.05$. Right panel: WB of Cav1 protein from WT, *Apc$^{min/+}$//Cav1$^{+/+}$, Apc$^{min/+}$//Cav1$^{+/-}$* and *Apc$^{min/+}$//Cav1$^{-/-}$* mice TU versus NT in Ileum and Colon compared to Hsp90. Caveolin-1 bands in the *Cav1$^{-/-}$* mice might be due to a spill-over from the next lane.

3.1.2 Survival advantage of Caveolin-1 wildtype mice

To investigate if Cav1 has an impact on the survival of the $Apc^{min/+}$ mice, all moribund (sick) mice were analyzed according to their survival. Looking at the mean lifespan of the mice, $Apc^{min/+}//Cav1^{-/-}$ (n=8) lived approximately 155 days (±15) compared to $Apc^{min/+}//Cav1^{+/-}$ (n=54) with 186 days (±5) and $Apc^{min/+}//Cav1^{+/+}$ (n=16) mice with 180 days (±10). The mean lifespan of homozygous mice ($Apc^{min/+}//Cav1^{-/-}$) is therefore reduced by 30 days, probably because of anemia or obstruction in the colon and rectal bleeding induced by the tumor (*t-test p=0.015, $Apc^{min/+}//Cav1^{-/-}$ versus $Apc^{min/+}//Cav1^{+/-}$). Surprisingly, $Apc^{min/+}//Cav1^{+/+}$ mice showed a slight reduction in survival compared to $Cav1^{+/-}$ mice looking at Kaplan-Meier analysis (Fig. 8). The median survival was reduced to 171 days for $Apc^{min/+}//Cav1^{+/+}$ and to 155 days for $Apc^{min/+}//Cav1^{-/-}$ compared to 191 days for $Apc^{min/+}//Cav1^{+/-}$ (*Log Rank test p=0.0367 for $Apc^{min/+}//Cav1^{-/-}$ versus $Apc^{min/+}//Cav1^{+/-}$).
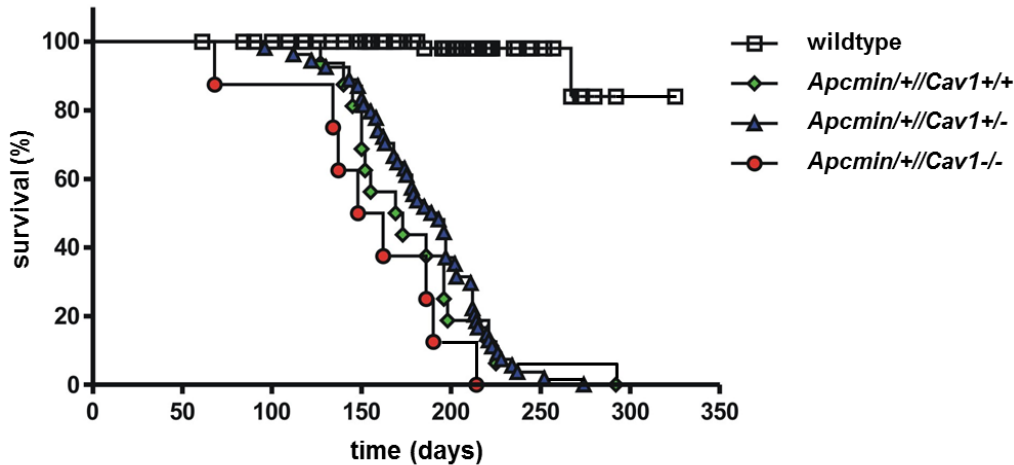
Figure 8 Kaplan-Meier-survival of the different mouse genotypes. Kaplan-Meier-analysis of survival showing earlier death of $Apc^{min/+}//Cav1^{-/-}$ (n=8) compared to $Apc^{min/+}//Cav1^{+/-}$ (n=54) and $Apc^{min/+}//Cav1^{+/+}$ mice (n=16). Wildtype mice (n=84) are shown as a control with only two mice showing signs of illness.

3.1.3 Genetic profile of different genotypes

Analysing the different genotypes in relation to their genetic profile using RT-qPCR, *Cyclind1* was found to be increased 6-fold (*t-test p=0.03) in $Apc^{min/+}//Cav1^{-/-}$ mice TU tissue compared to wildtype NT tissue. *Cyclind1* was only upregulated 2.5- and 2-fold in $Apc^{min/+}//Cav1^{+/+}$ and $Apc^{min/+}//Cav1^{+/-}$ TU tissue compared with colon tissue from the wildtype. Furthermore, compared to wildtype NT tissue, *Wnt6* mRNA was increased 242-fold (*t-test p=0.03) in $Apc^{min/+}//Cav1^{-/-}$ mice, 67-fold (*t-test p=0.004) in $Apc^{min/+}//Cav1^{+/-}$ mice as well as 20-fold in $Apc^{min/+}//Cav1^{+/+}$ TU tissue (Fig. 9). Interestingly, *Cyclind1* and *Wnt6* expression is higher in homozygous $Cav1^{+/+}$ mice than in heterozygous $Cav1^{+/-}$ mice, which may explain the survival

disadvantage mentioned in 3.1.2. This leads to the assumption that Cav1 decelerates tumor development in the colon.
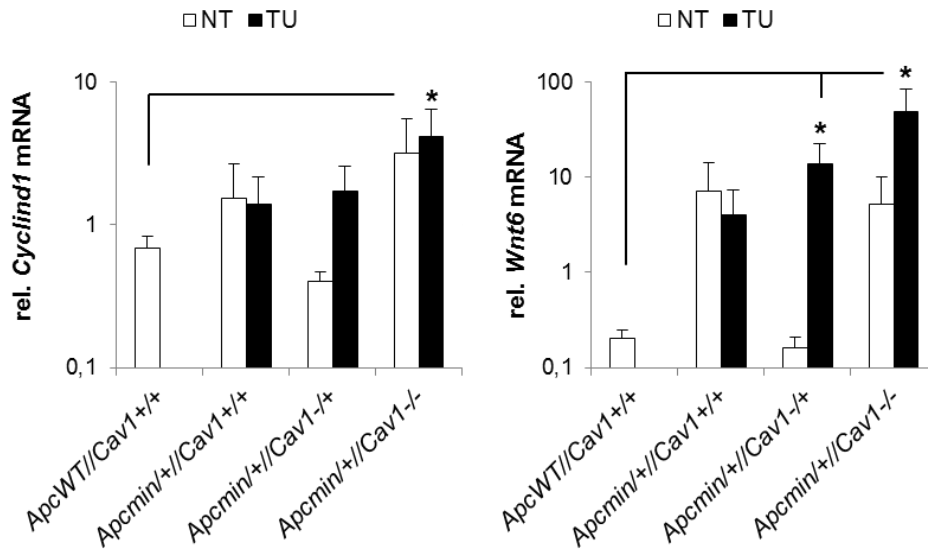

<u>Figure 9</u> Relative expression of *Cyclind1* and *Wnt6* in three different mouse genotypes. Left panel: *Cyclind1* mRNA. Right panel: *Wnt6* mRNA. mRNA was determined by RT-qPCR for WT, *Apc*$^{min/+}$*//Cav1*$^{+/+}$, *Apc*$^{min/+}$*//Cav1*$^{+/-}$ and *Apc*$^{min/+}$*//Cav1*$^{-/-}$ mice comparing TU and NT. CT-values were normalised to β2-microglobulin and calculated as –fold ± S.E. (n=3 per genotype for NT and TU, *t-test $p<0.05$).

3.1.4 Macroscopic analysis

Mice were sacrificed and ileum and colon were analyzed for tumor appearance. One example of this macroscopic analysis showed that *Apc*$^{min/+}$*//Cav1*$^{-/-}$ mostly developed distal colorectal tumors that are often highly vascularized. Figure 10 shows two vascularized tumors with approximately 10 mm length that were observed in the very distal end of the colon. Furthermore, 3-4 very small white tumors were found in the proximal end of the colon.
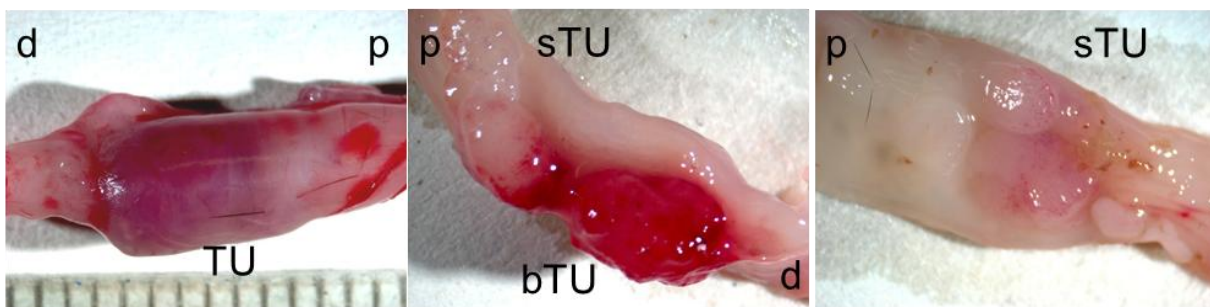
<u>Figure 10</u> Example of colorectal tumors in an *Apc*$^{min+/-}$*//Cav1*$^{-/-}$ mouse. Legend: p-proximal, d-distal, sTU-small tumor, bTU-big tumor. Pictures show a highly vascularized, distal, approximately 10 mm big tumor. Furthermore, small, not vascularized tumors appeared in the proximal colon.

Further macroscopic analysis of n=86 mice in total revealed that 100 % of the $Apc^{min/+}//Cav1^{-/-}$ mice (n=8) developed colorectal tumors shown in figure 10, whereas incidence of tumor development in $Cav1^{+/-}$ (n=59) and $Cav1^{+/+}$ (n=19) mice was only 78 % or 74 %, respectively. To describe these findings in more detail, tumors were divided into two subgroups according to their size, larger (<3 mm) or smaller (>3 mm) than 3 mm. 88 % of the $Apc^{min/+}//Cav1^{-/-}$ mice developed larger tumors in contrast to only 27 % of $Apc^{min/+}//Cav1^{+/-}$ and 42 % of $Apc^{min/+}//Cav1^{+/+}$ mice (Fig. 11).
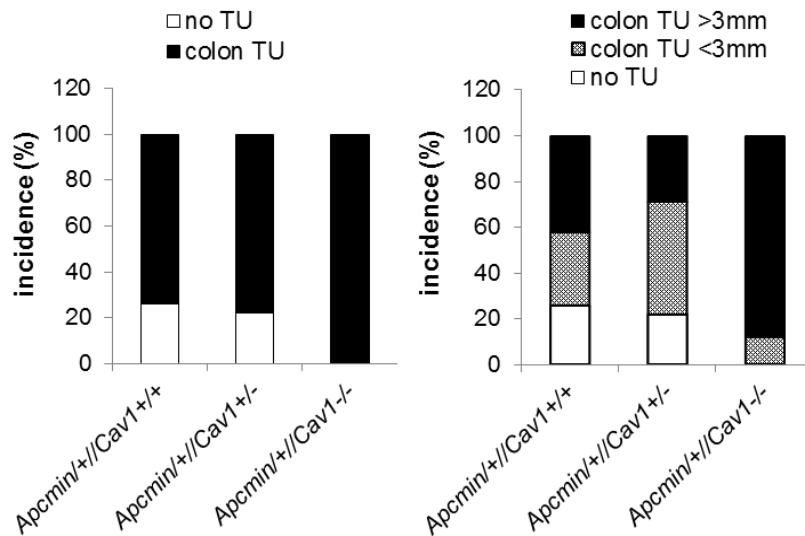
Figure 11 Incidence of colon tumors and colon TU size. Left panel: Mice were analyzed macroscopically for colon TUs. Right panel: Mice were analyzed macroscopically for colon TUs smaller or bigger than 3 mm in the different mouse genotypes; *Cochran-Mantel-Hänzel test p = 0.0168 -/- *versus* +/- and +/+ for TU >3 mm.

3.1.5 Microscopic analysis of CRC mouse model

For histopathological (microscopic) studies, colon (with tumors), cecum and ileum were embedded in paraffin and slices were stained using H&E. Pathological examination (done by T. Gaiser, Institute of Pathology, Universitätsmedizin Mannheim) showed that the tumors are high-grade dysplastic adenomas [60]. In some cases even microinvasion into the lamina muscularis mucosae was observed, but no serrated lesions or predominant inflammatory infiltrate was detected.

As an example for microscopic analysis, colon tumors found in $Apc^{min/+}//Cav1^{-/-}$ (Fig. 12), together with ileum and cecum, were embedded in paraffin, cut into 3 µm sections and stained for H&E. On the basis of these pictures, mice were examined for incidence of colon and cecum tumors, size and number of colon tumors was determined and tumors were analyzed for cysts. Presence of ileal adenoma confirmed the $Apc^{min/+}$-genotype (detailed

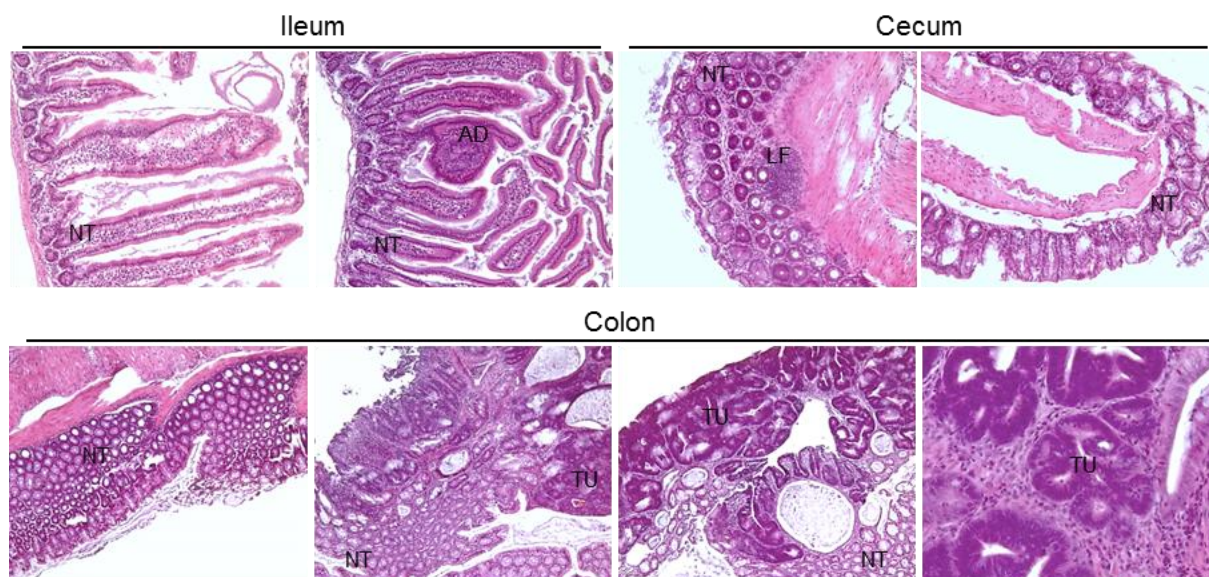microscopic analysis was done by B. Richter-doctoral thesis, Universitätsklinikum Mannheim; as published in [59]).

Figure 12 **Microscopic analysis from *Apc^min+/-^//Cav1^-/-^* mouse tissue.** Picture shows H&E stained paraffin sections from ileum, cecum and colon tissue. Normal tissue (NT), ileal adenoma (AD), colon tumor (TU) and lymphatic follicle (LF) are shown. Nuclei are stained in blue. Other structures like cytoplasm appear in red. Magnification x 200 and x 400

3.1.6 cDNA microarray of colon *versus* tumor tissue

To identify the different gene expression profiles of NT versus TU, cDNA microarray was done (service of TUM microbiology) and analyzed by GSEA (done by H. Einwächter, Department of medicine II, Klinikum rechts der Isar). This analysis revealed that genes associated with the PPARγ transcription factor were downregulated in the tumor tissue compared to normal tissue. Amongst others, downregulated genes were lipoprotein lipase (*Lp1*), fatty acid binding protein 2 (*Fabp2*), phosphoenolpyruvate carboxykinase (*Pck1*), acyl-Coenzyme A oxidase 1 (*Acox1*) and 3-hydroxy-3-methylglutaryl-Coenzyme A synthase 2 (*Hmgcs2*), that are all somehow related to PPARγ. Furthermore, genes related to the Ras-signature were elevated in the tumor, e.g. v-Ki-ras2 Kirsten rat sarcoma viral oncogene homolog (*Kras*) and neuroblastoma ras oncogene (*Nras*). Additionally, RAS-related C3 botulinum substrate (*Rac1*), E26 avian leukemia oncogene 2 (*Ets2*), epidermal growth factor receptor (*Egfr*), ELK3 (*Elk3*), RAS (*Rasd1*) and src homolog 2 domain-containing transforming protein C1 (*Shc1*) were elevated in the tumor tissue compared to normal tissue. Nevertheless, genes involved in proteolytic processes were upregulated in the tumor compared to normal colon tissue, for example, matrix metallopeptidase 2 (*Mmp2*), matrix metallopeptidase 10 (*Mmp10*), matrix metallopeptidase 14 (*Mmp14*), matrix metallopeptidase

13 (*Mmp13*), matrix metallopeptidase 7 (*Mmp7*), met proto-oncogene (*Met*) and cathepsin E (*Ctse*). Further genes that were elevated in the tumor were hypoxia inducible factor 1 (*Hif1α*) and leucine rich repeat containing G protein coupled receptor 5 (*Lgr5*), a stem cell marker (Complete table of the microarray data is available online in [59]).

3.1.7 Validation of microarray results

Genes related to PPARγ and Ras with at least 2-fold change in expression were then validated by qPCR. RNA was isolated from colon and tumor tissue of all mouse genotypes and analyzed separately. There was no significant difference in gene expression between the different genotypes meaning that the tumors had the same genetic characteristics regardless of their genotype. As a consequence, all three genotypes were summarized leading to comparison of NT and TU.

First, genes related to the WNT-pathway were analyzed. *C-Myc and Wnt6* were found to be elevated in the tumor tissue. Furthermore, *Cyclind1* was upregulated in TU. Ras-related genes like *Nras* and *Kras* could also be confirmed to be upregulated in the tumor (Fig. 13).
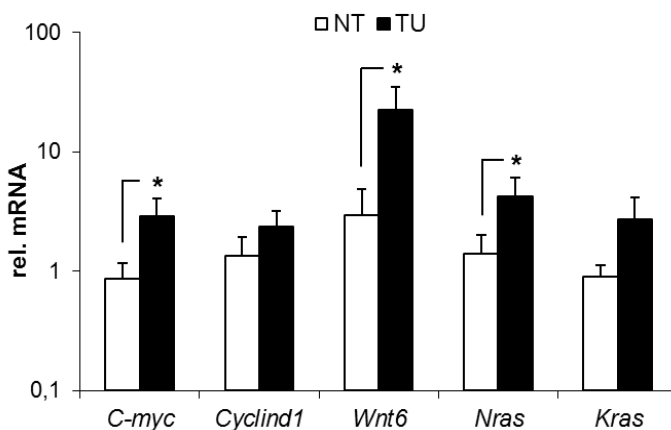

Figure 13 Validation of microarray results for WNT- and Ras-signaling. Expression of *c-Myc, Cyclind1, Wnt6, Nras* and *Kras* mRNA was determined by RT-qPCR and normalized to β2-microglobulin comparing NT and TU of all genotypes (n=13 NT, n=9 TU, *t-test $p<0.05$ NT *versus* TU).

Furthermore, sequencing (service of GATC) of *Kras* cDNA that was isolated from colon and tumor tissue showed no mutation in codon G12 or in G13.

To further validate the microarray results, genes related to PPARγ were analyzed by qPCR. *Pparγ* was not found to be reduced on the mRNA level, but for all that acyl-CoA oxidase (*Aco*) and phosphoenol-pyruvat carboxykinase (*Pepck*), two major PPARγ target genes, were reduced in tumor tissue. Another PPARγ target gene, *Hmgcs2*, was also downregulated in TU compared to NT (Fig. 14).
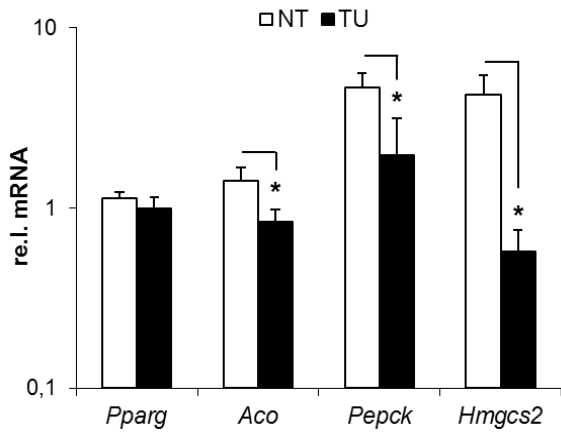
Figure 14 Validation of microarray results for PPARγ target genes. Expression of *Pparγ, Aco, Pepck* and *Hmgcs2*. mRNA was determined by RT-qPCR and normalized to β2-microglobulin comparing NT and TU of all genotypes (n=13 NT, n=9 TU, *t-test p<0.05 NT *versus* TU).

Other validated genes which were decreased in their expression in the tumor were the Ras-inhibitor Caveolin-1 (*Cav1*) itself and homeobox protein Cdx-2 (*Cdx2*), a marker for gastrointestinal differentiation. Genes which were confirmed to be increased in TU were Cyclooxygenase 2 (*Cox2*), trefoil factor 1 and 2 (*Tff1* and *Tff2*), *Lgr5, Lyz1* (*Lgr5* and *Lyz1* are related to paneth/stem cell markers), *MMP7, MMP13, Met*, inducible nitric oxide synthase (*iNOS*) and tumor necrosis factor α (*Tnfα*) (Fig. 15).
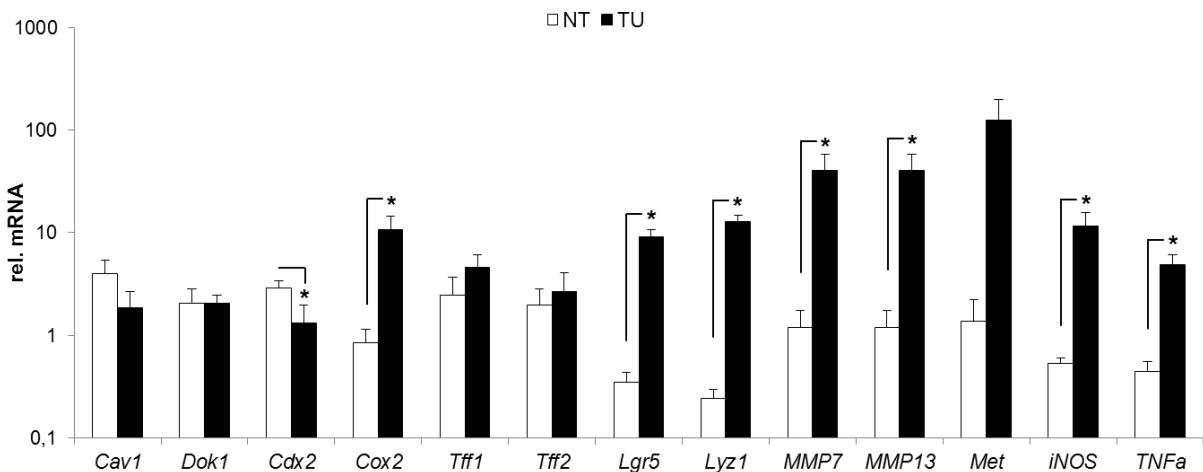

Figure 15 Validation of microarray results. mRNA expression in normal tissue (NT) *versus* colon tumor (TU) was determined by RT-qPCR, normalized to β2-microglobulin and calculated as –fold ± S.E. (n=13 NT, n=9 TU, *t-test p<0.05 NT *versus* TU). *Cav1* and *Cdx2* were downregulated. Genes related to invasion or hypoxia as well as paneth/stem cell markers were upregulated. Because of the high standard error of mean (SEM), *Met* was not found to be significant.

3.1.8 Immunohistochemical analysis

To further characterize the tumor tissue, immunohistochemical (IHC) staining for Ki67, Cleaved Caspase 3, β-Catenin and *Ulex europaeus* agglutinin (UEA) lectin was done (Fig. 16). Positive Ki67 staining showed that the tumor is highly proliferative, contrary to weak staining for Cleaved (active) Caspase 3 revealing less apoptosis. High staining level of β-Catenin corroborated active WNT-signaling and positive immunofluorescence staining for UEA lectin showed a paneth cell signature in the tumor compared to normal colon tissue (negative).
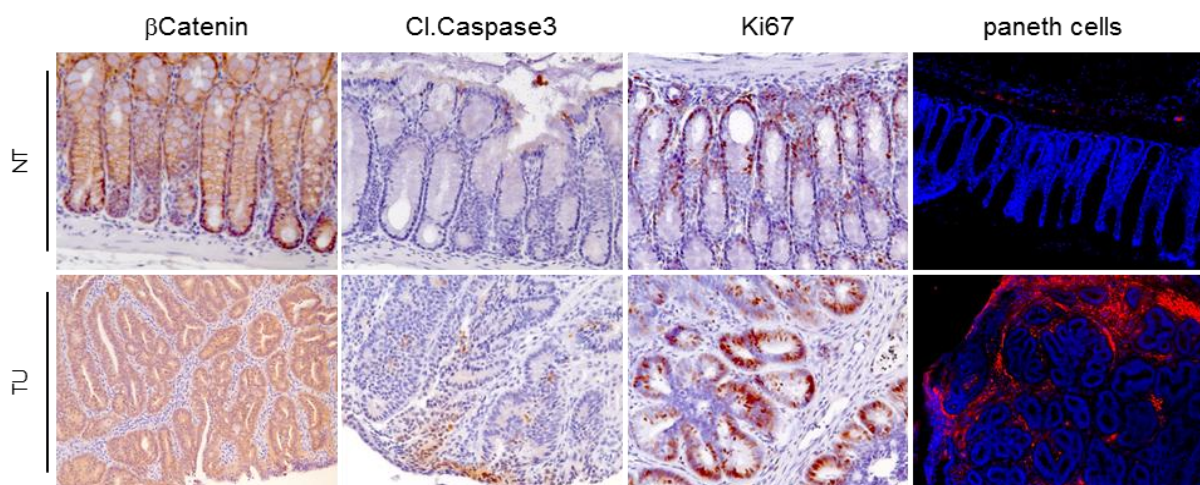

Figure 16 Characterization of colon tumor tissue in *Apc^min/+^//Cav1*-knockout mice. IHC staining of *Apc^min/+^//Cav1^-/-^* normal (NT) and tumor tissue (TU) for β-Catenin (WNT-signaling), Cleaved Caspase3 (apoptosis), Ki67 (proliferation) in brown, immunofluorescence staining for TRITC-UEA in red (paneth cells); blue=nuclei. Magnification IHC x 200, IF x 100

3.1.9 Loss of PPARγ in the nucleus in tumor tissue

As there is no change on the *Pparγ* mRNA level, protein expression was analyzed by WB and bands were quantified, but also revealed no change of PPARγ expression comparing NT *versus* TU. Nevertheless, β-Catenin was upregulated to 150 % (± S.E., n=3, *t-test p=6.4 x 10^{-5}) and GSK-3β was dephosphorylated and activated by 45 % (± S.E., n=3, *t-test p=0.009) confirming active WNT-signaling in the tumor. Activation (dephosphorylation at an inhibitory site) of c-Raf by 53 % (± S.E., n=3, *t-test p=0.0017) and MEK1/2 (phosphorylated at an activating site) to 350 % (± S.E., n=3, *t-test p=0.05) again revealed increased Ras-signaling in the tumor tissue (Fig. 17).
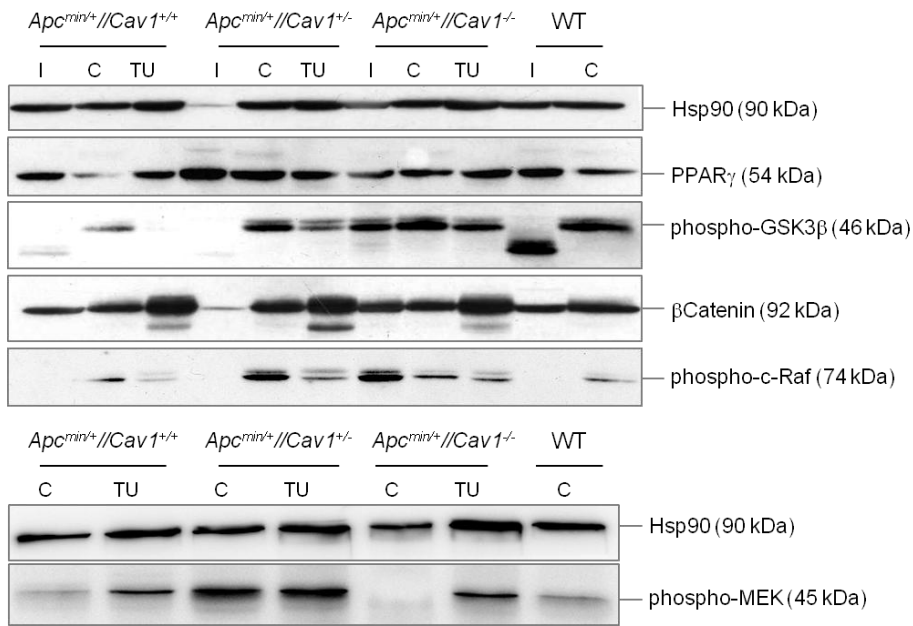
Figure 17 Representative Western Blot from PPARγ, phospho-GSK3β, β-Catenin, phospho-c-Raf and phospho-MEK of all mouse genotypes comparing ileum (I), colon (C) and tumor (TU) tissue. Hsp90 is used as a control to confirm equal protein content.

In addition, inactivation of SAPK/JNK to 30 % (± S.E., n=3, *t-test p=0.0005) and P38 to 30 % (± S.E., n=3, *t-test p=8.7 x 10^{-5}) corroborated absent apoptosis in tumor tissue (Fig. 18).
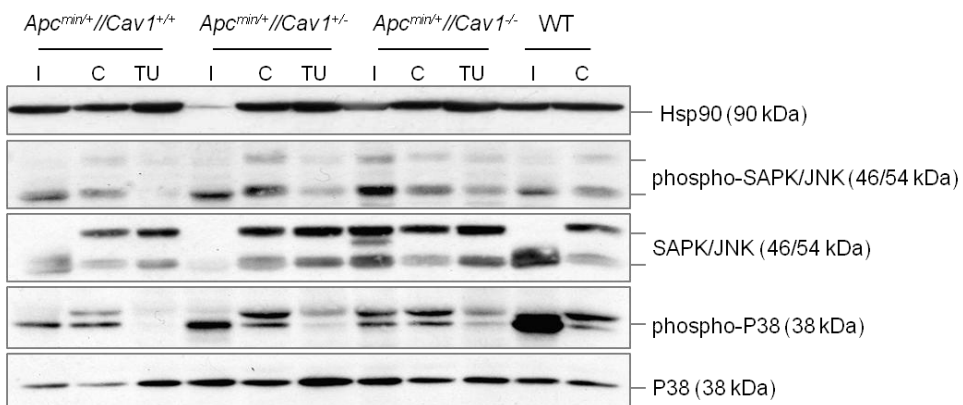

Figure 18 Representative Western Blot from phospho- and general SAPK/JNK as well as phospho- and general P38 of all mouse genotypes comparing ileum (I), colon (C) and tumor (TU) tissue. Hsp90 is used as a control.
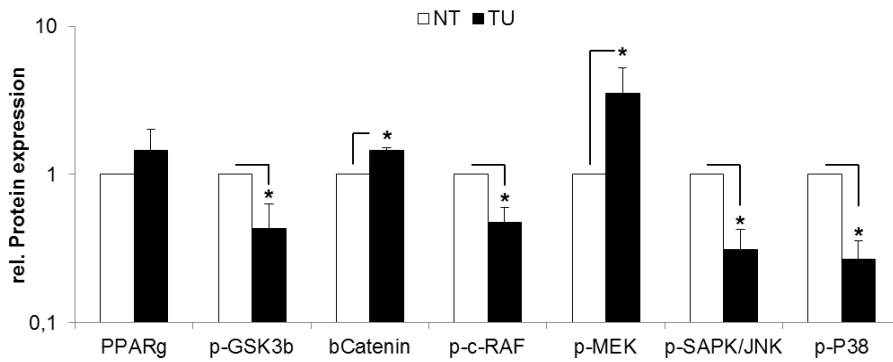
Figure 19 Quantification of PPARγ, phospho-GSK3β, β-Catenin, phospho-c-Raf, phospho-MEK, phospho-SAPK/JNK and phospho-P38 expression in NT *versus* TU. O.D. values were determined from WB bands shown in Fig. 17 and Fig. 18 and normalized to Hsp90. Values were calculated as –fold ± S.E. (n=3, *t-test $p < 0.05$, NT *versus* TU)

To study the localization of PPARγ in TU and NT, immunohistochemistry staining was done. In the colon crypts and the villi of normal tissue, nuclear PPARγ was detected contrary to tumor tissue, where nuclear PPARγ was absent. Furthermore, PPARγ was distributed to the cytosol. Looking at small tumors, cytosolic as well as nuclear staining was detected, concluding that PPARγ changes its localization and therefore its function during NT to TU progression (Fig. 20).
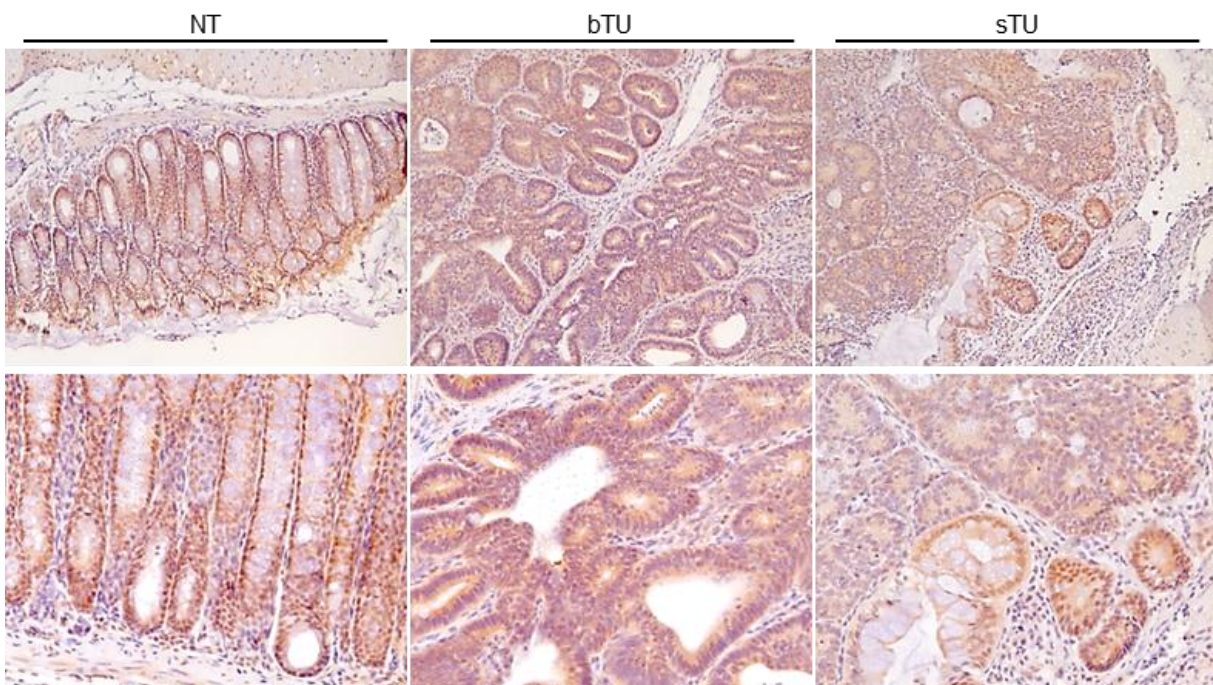

Figure 20 Loss of PPARγ nuclear staining in tumor tissue. IHC staining for PPARγ in an *Apc*[min/+]*//Cav1*^{-/-} mouse; Left: normal colon tissue showing nuclear staining of PPARγ. Middle: big tumor (bTU >3mm) showing cytosolic staining of PPARγ and right: smaller tumor (sTU <3mm) showing cytosolic and nuclear staining of PPARγ.

To corroborate the results of the IHC, TU and NT were subjected to subcellular fractionation (SCF) and analyzed by WB. Decreased PPARγ protein levels were found in the tumor tissue compared to normal tissue in membrane and nuclear fraction. Quantification of the WB bands revealed reduction of PPARγ to 25 % (± S.E., n=3, *p=3.6 x 10^{-5}) in the membrane and to 4 % (± S.E., n=3, 1.4 x 10^{-9}) in the nucleus. In the cytosol, however, PPARγ protein expression did not change in TU compared to NT (Fig. 21). Again, there was no difference between the three *Cav1* genotypes.
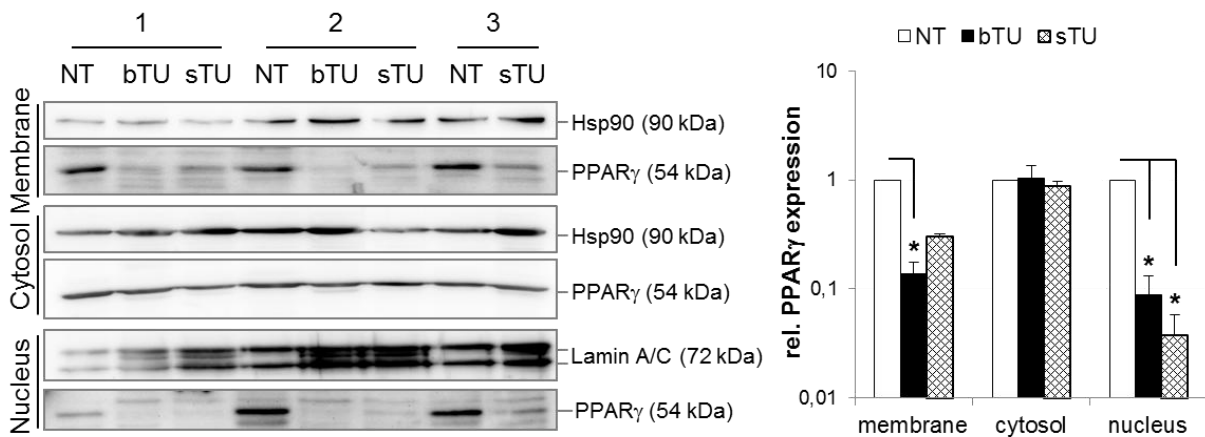

Figure 21 Subcellular fractionation of colon and tumor tissue in three different *Apc$^{min/+}$//Cav1$^{+/-}$* mice. Legend: bTU-tumor bigger than 3 mm, sTU-tumor smaller than 3 mm. Left: Representative Western Blots are shown from nuclear, cytosolic and membrane fraction. Right: Quantification of WB. O.D. values from bands were normalized to Hsp90 or Lamin A/C and calculated as –fold ± S.E. (n=3, *t-test p<0.05 NT *versus* bTU and sTU).

3.1.10 Prevention of CRC formation by the PPARγ ligand rosiglitazone

As shown before, PPARγ gets lost in the tumor tissue compared to colon tissue. To test whether preventive ligand activation of PPARγ can inhibit CRC development, *Apc$^{+/+}$* and *Apc$^{min/+}$* mice (*Cav1$^{+/+}$*, *Cav1$^{+/-}$* and *Cav1$^{-/-}$*) received a chow diet that was supplemented with 0.02 % (w/w) rosiglitazone (~25 mg/kg*day) for 4 months. At 7 months of age, mice were analyzed for tumor formation. Due to low case numbers, all *Apc$^{min/+}$* mice treated with rosiglitazone (n=11) were summarized and compared to all untreated *Apc$^{min/+}$* mice (n=84). First of all, analysis of H&E stained tissue of rosiglitazone-treated *Apc$^{+/+}$* mice (n=12) showed no aberration or tumor formation of colon tissue (data not shown). Furthermore, *Apc$^{min/+}$* mice which received the PPARγ-ligand seemed to be healthier than untreated mice at the same age. Macroscopic evaluation confirmed reduced tumor formation in treated mice. In detail, 21 % of untreated *Apc$^{min/+}$* mice did not develop colon tumors compared to 45 % of the rosiglitazone-treated mice. Furthermore, 42 % of the untreated mice developed small tumors

(< 3 mm) compared with 55 % of the treated mice. Big tumors (> 3 mm) were found in 37 % of the untreated mice. Not one mouse of the rosiglitazone-treated group developed tumors that were bigger than 3 mm (*Fisher Exact test p=0.0097, untreated *versus* rosiglitazone for TU bigger than 3 mm) (Fig. 22).
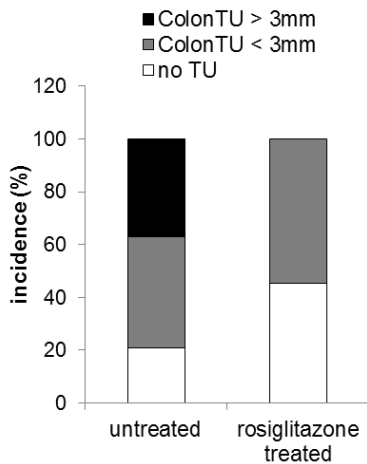

Figure 22 **Incidence of colon tumors in untreated and rosiglitazone-treated mice.** Mice were analyzed macroscopically for colon TUs smaller or bigger than 3 mm in all mouse genotypes (untreated n=86, rosiglitazone-treated n=11, *Fisher Exact test p=0.0097 untreated *versus* rosiglitazone-treated for TU > 3 mm).

Normal colon from untreated and rosiglitazone-treated mice (n=5 for untreated and n=5 for rosiglitazone-treated mice) was then analyzed by RT-qPCR. In rosiglitazone-treated mice, the PPARγ-target genes *Aco* and *Pepck* were found to be re-expressed compared to untreated mice (9- and 2- fold ± S.E., *t-test p<0.05), showing that the ligand was also efficient *in vivo*. Furthermore, the Ras-inhibitors *Cav1* and *Dok1* (docking protein 1) were upregulated by rosiglitazone (2.5- and 1.5- fold ± S.E., *t-test p<0.05). In line with the upregulated Ras-inhibitors was a slight decrease of *Kras* mRNA expression to approximately 80 % (± S.E.), which did not reach significance, probably due to already low *Kras* expression in normal tissue. *Pparγ* expression itself was not significantly upregulated (Fig. 23).
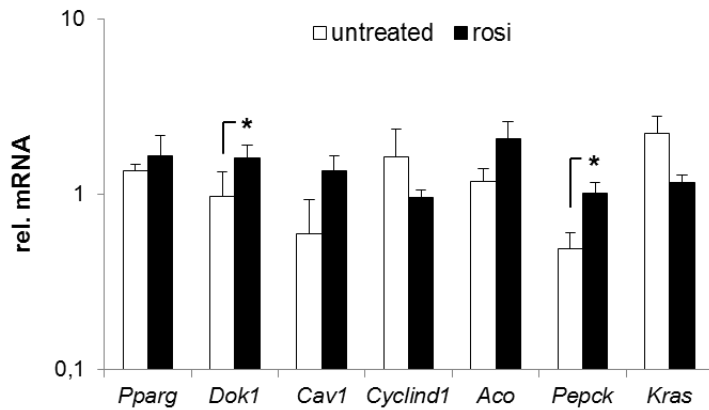
Figure 23 Effect of the rosiglitazone-diet *in vivo* on PPARγ target genes. *Ppary, Dok1, Cav1, Cyclind1, Aco, Pepck* and *Kras* mRNA was quantified using RT-qPCR in normal colon tissue of rosiglitazone-treated and untreated mice. CT-values were normalized to β2-microglobulin and calculated as –fold ± S.E. (n=12 rosiglitazone-treated *versus* n=12 untreated mice, *t-test p<0.05)

These data showed that tumor development with high WNT- and Ras-signaling can be prevented by activation of PPARγ *in vivo.* This inhibition may be due to reactivation of the Ras-inhibitors *Cav1* and *Dok1* through activation of PPARγ. Additionally, efficiency was independent of Caveolin-1 expression.

3.2 Characterization of colorectal cancer cell lines

There are some data already known from the literature about the colorectal cancer cell lines used in this study [61, 62]. Cav1 expression was corroborated during this thesis. The data are summarized in table 12.

Table 12 Summary of characteristics of colorectal cancer cell lines used in this thesis

	HCT116	**SW480**	**HT-29**	**Caco-2**
KRAS	G13D	G12V	WT	WT
BRAF	WT	WT	V600E	WT
Cav1	+++	-	+/- (inducible)	-
WNT pathway	*APC* WT, β-Catenin mut	*APC* mut	*APC* mut	*APC* mut

All cell lines harbor mutations and show activation of the WNT-pathway either by mutation of *APC* or β-Catenin, as common for colorectal cancer. They differ in the *KRAS* and *BRAF* mutation status and their expression level of Cav1.

3.2.1 Influence of Caveolin-1 on proliferation of colorectal cancer cells *in vitro*

We observed in the *Apc^{min/+}//Cav1*-KO mouse model that mice lacking Caveolin-1 developed tumors at an earlier stage than Caveolin-1 wildtype mice. To assess whether Cav1 expression influences cellular proliferation, colorectal cancer cell lines were transfected either with Cav1-shRNA plasmid for knockdown of Cav1 in HCT116 or with pcdna3-Cav1 expression plasmid for overexpression in SW480 cells. Overexpression and knockdown were determined by Western Blot analysis and confirmed that Cav1 expression was reduced to 65 % in HCT116 cells by *shRNA* and overexpressed 133-fold in SW480 cells compared to the respective controls (Fig. 24).
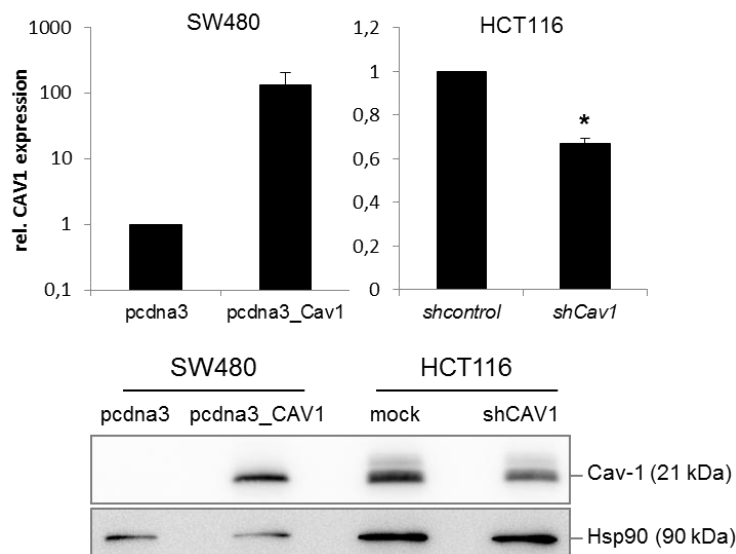

Figure 24 Verification of Caveolin-1 overexpression and knockdown in CRC cells. SW480 and HCT116 cells were transiently transfected with pcdna3_Cav1 plasmid or *shCav1* shRNA. Quantification (top panel) of Western Blot (lower panel) from transfected cells after 48 h. O.D. values were determined from WB bands, normalized to Hsp90 and calculated as -fold ± S.E. (n=3, *t-test p=7.9 x 10^{-5}).

Proliferation was measured using MTT assay after 0, 1, 2, 5, 6 and 7 days. Cav1 expression resulted in inhibition of proliferation in SW480 cells by 5-15 % compared to EV control. On the contrary, knockdown of Cav1 in HCT116 cells led to higher proliferation by 30-40 % compared to scrambled shRNA control (Fig. 25).
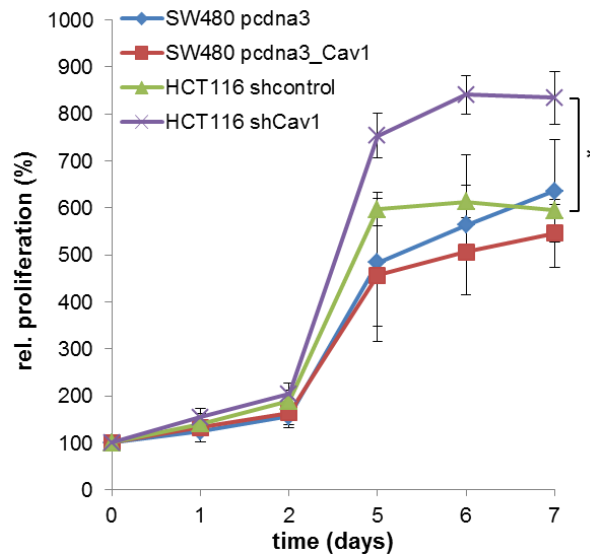
Figure 25 Effect of Caveolin-1 on proliferation of CRC cells. Viability of transiently transfected cells was measured after 0, 1, 2, 5, 6 and 7 days. O.D. values were calculated as % ± S.E. (n=3, *t-test p<0.05 for day 5, 6 and 7 HCT116 *shcontrol* compared to HCT116 *shCav1*).

These results showed that Cav1 regulates the proliferation rate of colorectal cancer cells.

3.2.2 Effects of the PPARγ activator rosiglitazone on colorectal cancer cells

The *Apc^{min/+}* mouse model showed that rosiglitazone reduced colorectal cancer development. To determine if PPARγ activation affects growth of the colorectal cancer cell lines also *in vitro*, sensitivity to the PPARγ-ligand rosiglitazone was tested by performing concentration-dependent proliferation assays. Cells were incubated with decreasing concentrations of rosiglitazone and growth was measured after 2 days. HCT116 cells (IC_{50}=20μM) showed the highest sensitivity, followed by HT-29 cells (IC_{50}>50μM). Caco-2 and SW480 (IC_{50}>50μM) cells were resistant to PPARγ-ligand-dependent growth inhibition (n=4 experiments). To confirm PPARγ activation by rosiglitazone, colorectal cancer cells were incubated with increasing concentrations of rosiglitazone overnight and PPARγ promoter activity was measured by luciferase reporter assay. The PPARγ promoter showed the highest activity in HCT116 cells, consistent with the results obtained from proliferation experiments, followed by SW480 and Caco-2 cells. HT-29 cells were the least responsive with regard to promoter activity (n=4 experiments). Apart from the different sensitivity comparing the four cell lines, each cell line showed reduced proliferation with increasing concentrations of rosiglitazone and, except for HT-29, PPARγ activation (Fig. 26).
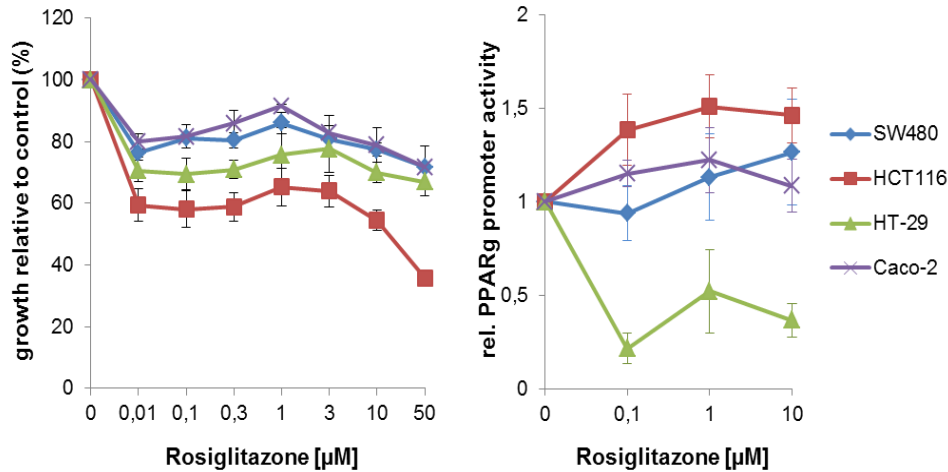
Figure 26 Influence of rosiglitazone on proliferation and PPARγ promoter activity in CRC cells. Left: Concentration response curve of rosiglitazone on SW480, HCT116, HT-29 and Caco-2 cells. Cells were incubated with increasing concentrations of rosiglitazone. Viability was measured after 48 h and O.D. values were calculated as % ± S.E. (n=3). Right: Cells were incubated with 0, 0.1, 1 and 10 µM rosiglitazone and PPARγ promoter activity was measured after 24 h (n=4).

These results show that presence of the Ras-inhibitor Caveolin-1 and activation of PPARγ can decrease the growth of colorectal cancer cells, which corroborates the *in vivo* results obtained from the *Apc^min/+* mouse model.

3.3 KRAS//PPARγ-KO mouse model

As observed in the *Apc^min/+* mouse model, PPARγ activity gets lost and Ras-signature is activated during tumorigenesis. To further investigate the influence of these two players, mice expressing active, G12V mutated *KRAS* and lacking PPARγ in the epithelium were interbred.

3.3.1 Confirmation of PPARγ knockout in mice

For generation of PPARγ-knockout mice, mice with floxed *Pparγ* gene (PPARγ-FL/FL) and mice expressing the Cre recombinase, which is under control of the murine villin promoter, were crossed. In the PPARγ-FL/FL-mice, a *loxP* site is inserted in front and behind exon 1 and 2 of the *Pparγ* gene [63]. These sites are recognized by the Cre recombinase, which is mainly expressed in the small and the large intestine through the villin promoter. The recombinase recognizes the *loxP* sites and excises PPARγ.

PCR on the cDNA of mouse tissue (stomach, liver, colon, ileum) from the different genotypes FL/FL//CRE_positive, FL/FL//CRE_negative and FL/+//CRE_positive showed that the Cre recombinase cuts out PPARγ in the villin expressing tissues (stomach, colon and ileum) and to a lesser extent in liver tissue. Furthermore, in homozygous mice (FL/FL), no wildtype PPARγ was

detectable, whereas heterozygous mice (FL/+) showed both wildtype and mutant PPARγ (Fig. 27).
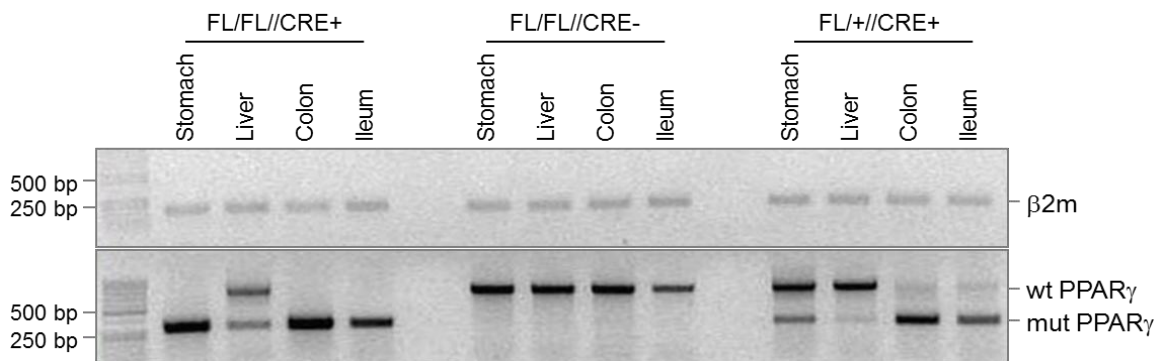

Figure 27 Verification of wildtype and mutant PPARγ in homo (FL/FL) or heterozygous (FL/+) mice with (+) or without (-) Cre recombinase. Upper panel: Expression of β2-microglobulin. Lower panel: Expression of wt PPARγ (700 bp) and/or mut PPARγ (300 bp). FL/FL=homozygous, FL/+=heterozygous, CRE+ =Cre positive, CRE- =Cre negative

3.3.2   Confirmation of active K-Ras in *KRAS* mutated mice

Mice harboring the activating *KRAS* G12V mutation which is under control of the villin promoter were used. GST-pull-down assay was applied to detect active K-Ras compared to total K-Ras in this mouse model. Pulldown revealed highest level of active K-Ras in the ileum and the colon tissue, whereas the stomach showed no active K-Ras. SW480 cells were taken as positive control (Fig. 28).
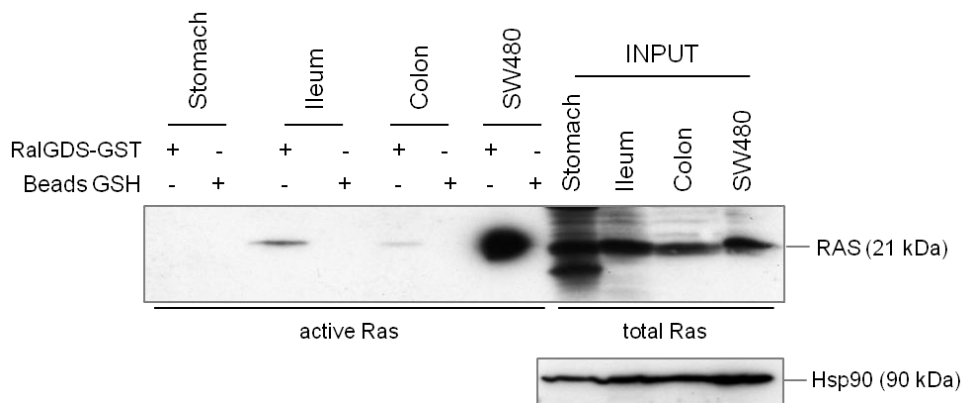

Figure 28 Detection of active Ras in a *KRAS* G12V mutated mouse. Western Blot of Ras Pulldown detecting active K-Ras in stomach, ileum and colon of a *KRAS* G12V mutated mouse compared to total Ras and Hsp90. Pulldown detects a higher active K-Ras level in ileum compared to colon tissue. No active Ras was detectable in stomach tissue. SW480 cells were used as a positive control.

3.3.3 Characterization of *KRAS* G12V and PPARγ-KO mice

KRAS G12V-mutant mice and PPARγ-knockout mice were characterized and compared to wildtype mice. Knockdown of PPARγ in PPARγ-KO mice was confirmed. As expected, *KRAS* G12V-mutated and PPARγ-knockout mice showed higher expression of phosphorylated and activated ERK. C-Raf was unchanged in all three genotypes. Furthermore, the tumor suppressor PTEN was inactivated as evident by decreased (activating) phosphorylation. Inhibition of PDK1 phosphorylation leads to inhibition of PDK1 in *KRAS* G12V mice, which is in accordance with dephosphorylation and therefore inactivation of Akt. Knockout of PPARγ seems to have no effect on expression of these proteins. Furthermore, the APC-activator GSK3β was highly phosphorylated at Ser9 and was therefore inhibited in both mutant mice (Fig. 29).
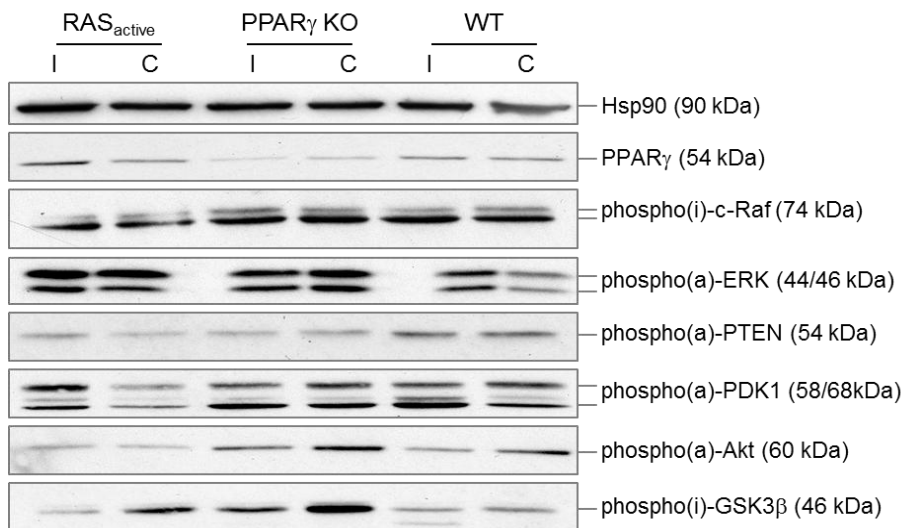
Figure 29 Western Blot of PPARγ, phospho-c-Raf, phospho-ERK, phospho-PTEN, phospho-PDK1, phospho-AKT, phospho-GSK3β compared to Hsp90 in ileum and colon of *KRAS* G12V-, PPARγKO-and wildtype-mice. Phosphorylation is either activating (a) or inactivating (i).

3.4 Ras-activity in colorectal cancer cell lines

As shown before in the *Apc^{min/+}* mouse model, analysis of the tumors revealed high activity of the Ras-pathway. To investigate the influence of active Ras on PPARγ, the colorectal cancer cell lines were first tested for their active K-Ras status by GST-pulldown assay. As expected, SW480 cells (*KRAS* G12V) showed highest endogenous levels of active K-Ras, followed by HCT116 cells (*KRAS* G13D). Active K-Ras was not detectable in HT-29 (*BRAF* V600E) and Caco-2 cells (*RAS* WT) (Fig. 30).

Figure 30 Western Blot of Ras-pulldown in colorectal cancer cell lines. SW480, HCT116, HT-29 and Caco-2 cells were subjected to active Ras-pulldown and analyzed by Western Blot, showing highest active K-Ras levels in SW480 followed by HCT116 cells. HT-29 and Caco-2 cells were used as a negative control. Total Ras (input) and Hsp90 are also shown.
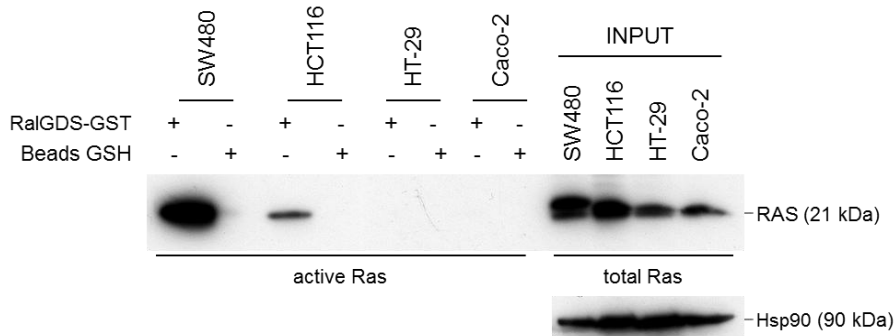
According to these results, SW480 and HCT116 cells were chosen as an *in vitro* model for simulating active K-Ras mice.

Cells were additionally sequenced to detect the *KRAS* mutation and confirmed the mutations taken from the literature. All cell lines showed basic phosphorylation/activity of ERK1/2, highest in HCT116 and HT-29 and lowest in Caco-2 cells. Cells were then starved overnight, incubated for 30 min with 1 μM erlotinib, an EGFR inhibitor, and 1 μM U0126, a MEK inhibitor and were then stimulated with 15 μM EGF for 10 min to activate the Ras-signaling pathway. SW480 cells showed reduction of phosphorylated ERK1/2 only for U0126, due to the *KRAS* G12V mutation. In HCT116 cells, both inhibitors were effective, which may be due to the weaker *KRAS* mutation G13D, where only one allele is affected (Fig. 31). HT-29 showed no reduction of phosphorylation in both cases, because of its mutated *BRAF* which is downstream of EGFR and MEK and is therefore not affected by this inhibition. In Caco-2, erlotinib efficiently repressed the phosphorylation of ERK1/2. On the contrary, U0126 had no effect on ERK1/2 phosphorylation, which may be due to the *RAS* WT status (Figure not shown).
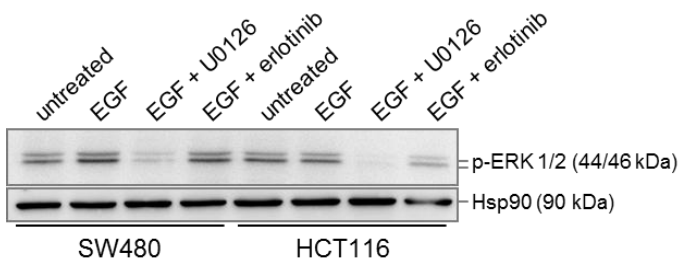

Figure 31 Decreased Ras-signaling by MEK (U0126) and EGFR (erlotinib) inhibition. Western Blot of SW480 and HCT116 cells treated with either U0126 or erlotinib, followed by stimulation of the Ras-signaling pathway using EGF. Expression of active phosphorylated ERK and Hsp90 as control is shown.

3.4.1 Inhibition of Ras/MEK promotes import of PPARγ to the nucleus

As already published, MEK is known to be a nuclear export shuttle for PPARγ [34]. To assess the influence of active Ras-signaling on PPARγ localization, cells were serum-deprived overnight and incubated for 0-8 hours with 1 µM U0126. In SW480 and HCT116 cells, PPARγ was released to the nucleus after MEK-inhibition, which was again more effective for HCT116 cells. This observation was confirmed by immunofluorescence staining for PPARγ in Caco-2 cells (Fig. 32).
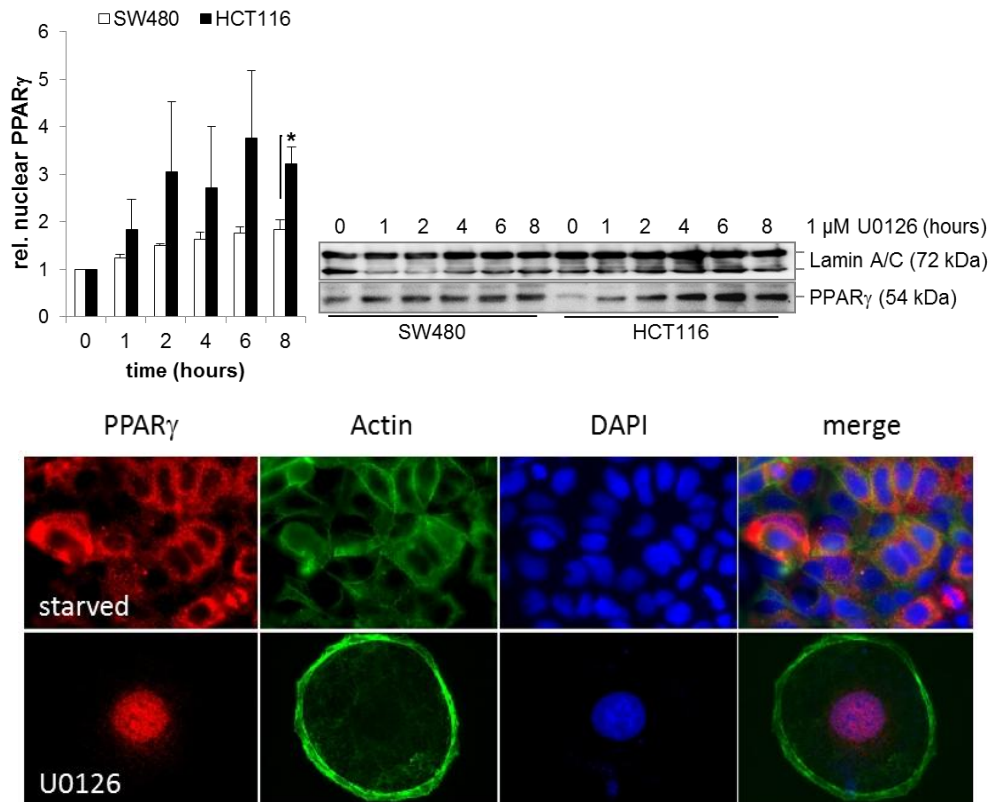
Figure 32 MEK-inhibition promotes PPARγ's nuclear import. Upper panel: Representative Western Blot of nuclear extract from SW480 and HCT116 cells treated with 1 µM U0126 for 0-8 h; O.D. values from four different experiments were normalized to Lamin A/C and calculated as –fold ± S.E. (n=4, *t-test $p < 0.05$ for 8 h SW480 *versus* HCT116 cells). Lower panel: IF from Caco-2 cells. Cells were either starved or starved+U0126 overnight; red-PPARγ, green-phalloidin (actin filaments), blue-DAPI (nuclei)

3.4.2 Combination of Ras-inhibition and PPARγ-activation inhibits proliferation of CRC cells *in vitro*

As shown before, PPARγ activation inhibits proliferation. Furthermore, MEK inhibition promotes translocation of PPARγ into the nucleus and reduces proliferation. To test, whether combination of Ras-inhibition and PPARγ activation potentiates proliferation inhibition, cells were treated with 100 µM rosiglitazone either alone or in combination with U0126 or erlotinib.

Proliferation was measured after 0-5 days by MTT assay. Proliferation of SW480 cells did not change with rosiglitazone and erlotinib either alone or in combination. Proliferation was slightly inhibited by U0126, but there was no additional effect by combination treatment, and inhibition did not reach statistical significance. HCT116 cells showed a decrease in proliferation by up to 50 % at day 3 with rosiglitazone (n=4, *t-test p<0.05 for day 1, 3 and 5, untreated *versus* rosiglitazone), and slight inhibition with erlotinib (by 30 % at day 3) and U0126 (by 40 % at day 3). By combining rosiglitazone with either erlotinib or U0126, growth was further inhibited compared to single treatment (n=4, *t-test p<0.05, by 10 % for rosiglitazone *versus* rosi+erlotinib and by 30 % erlotinib *versus* rosi+erlotinib at day 4 and 5, and by 25 % for U0126 versus U0126+rosi at day 5) (Fig. 33).
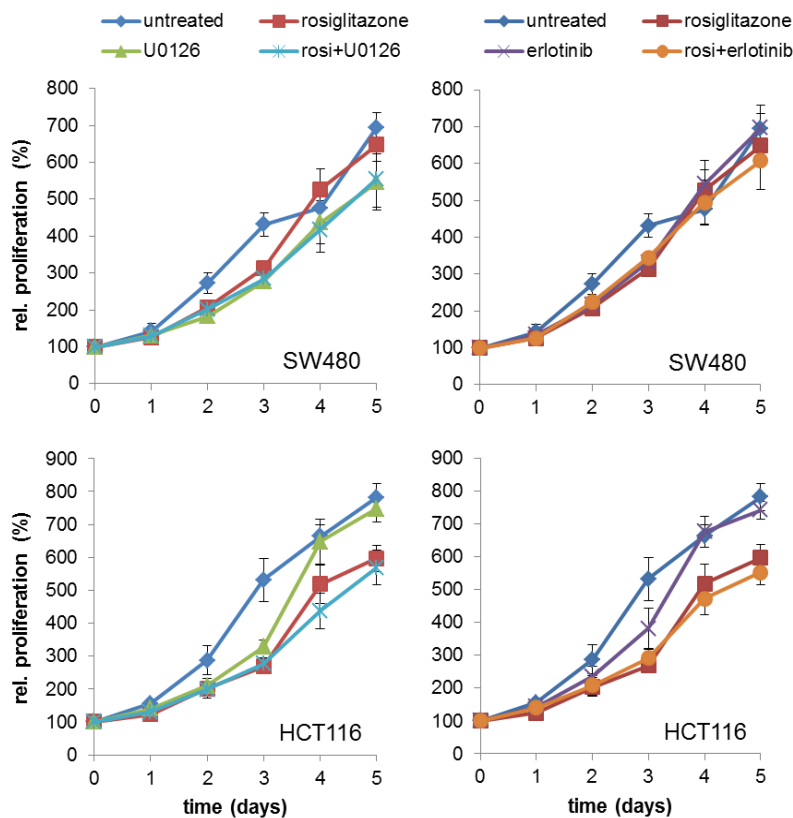
Figure 33 The Ras-inhibitors U0126 and erlotinib as well as the PPARγ activator rosiglitazone inhibit proliferation of CRC cells. SW480 (top) and HCT116 (bottom) cells were incubated with 100 μM rosiglitazone either alone or in combination with 1 μM U0126 (left) or 1 μM erlotinib (right). Proliferation was measured after 0, 1, 2, 3, 4 and 5 days using MTT. O.D. values were calculated as % ± S.E. (n=3).

To determine whether this proliferation inhibition takes place *via* PPARγ activation, cells were treated as before and PPARγ promoter activity was measured.
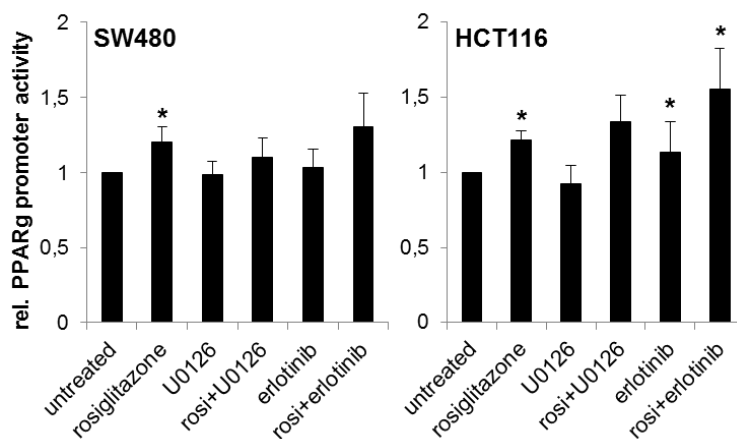
Figure 34 Effect of the Ras-inhibitors U0126 and erlotinib on PPARγ promoter activity in CRC cells. SW480 (left) and HCT116 (right) cells were incubated with 100 µM rosiglitazone either alone or in combination with 1 µM U0126 or 1 µM erlotinib. PPARγ promoter activity was measured after 24 h (*t-test p<0.05 treated *versus* untreated ± S.E. n=3).

PPARγ promoter activity was enhanced by rosiglitazone treatment in both cell lines (*t-test p<0.05, n=4). PPARγ activity was further enhanced by erlotinib treatment in HCT116 cells. No prominent effect was observed with U0126 and erlotinib alone in SW480 and U0126 in HCT116 cells. By combining rosiglitazone with U0126 or erlotinib, PPARγ activity was further enhanced in HCT116 cells by 10 % (U0126) and 30 % (erlotinib). In SW480 cells, the combination was less effective. The combination of rosiglitazone with erlotinib enhanced PPARγ activity by 10 % in SW480 cells (Fig. 34).

These data showed that proliferation of colorectal cancer cells can be inhibited by PPARγ-activation either by activation of PPARγ itself (by rosiglitazone) or by inhibition of the Ras-signaling pathway (by U0126 or erlotinib) which promotes PPARγ's import to the nucleus.

In summary, mice lacking PPARγ and expressing mutated *KRAS* tend to develop a more severe phenotype than littermates with *KRAS* mutation alone. PPARγ knockout mice showed more polyps, more extended lesions and more inflammation compared to *KRAS*-only mice (detailed microscopic analysis was done by P. Weidner-doctoral thesis, Universitätsklinikum Mannheim). Furthermore, *in vitro* analysis showed that inhibition of Ras-signaling results in reduced proliferation and enhanced PPARγ activity.

3.5 The Ras-inhibitor Dok1 is a new interaction partner for PPARγ

3.5.1 Interaction of Dok1 and PPARγ

The Ras-inhibitor Dok1 was found to be upregulated in the *Apc^(min/+)//Cav1*-KO mouse model by rosiglitazone treatment and is therefore a new target gene for PPARγ. Originally, immunoprecipitation of Caveolin-1 in MKN45 gastric cancer cells followed by MALDI-MS led to the identification of an approximately 37 kDa protein corresponding to the human docking protein (Dok1). This interaction was also confirmed by CoIP [57]. To test whether there is also an interaction between Dok1 and PPARγ in human colorectal cancer cell lines, CoIP was performed using PPARγ-antibody. IB revealed interaction of PPARγ with MEK (positive control as published by Burgermeister *et al.*[37]) and an N-terminal Dok1 antibody showed an approximately 37 kDa band in HCT116 cells (Fig. 35).
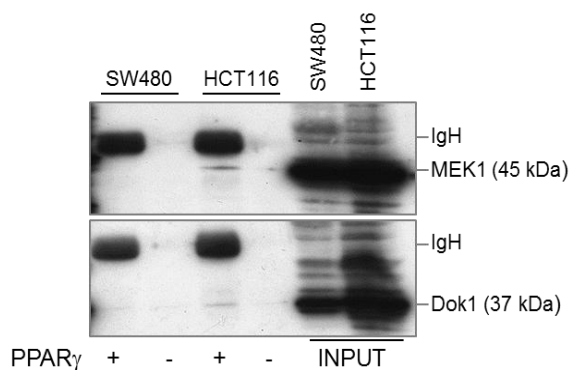
Figure 35 Interaction of PPARγ and Dok1 in SW480 and HCT116 cells. PPARγ antibody was used for immunoprecipitation. The interacting proteins MEK1 and Dok1 were detected by WB.

To further confirm the results of the CoIP, proximity ligation assay (PLA) was performed. This assay uses secondary antibodies which are labeled with oligonucleotides ("PLA probes") and generate a signal when the two probes, and therefore the two proteins of interest, are in close proximity. To this end, Hek293 cells were either untreated or treated with 1 µM rosiglitazone for 1 hour and PLA assay was performed using N-terminal Dok1 (A3) and PPARγ antibody. As a result, red spots indicated interaction of these two proteins. Interaction was slightly increased with rosiglitazone-treatment and seemed to be translocated to the nucleus (Fig. 36). The C-terminal Dok1 (M19) antibody was not as efficient in PLA assay possibly indicating the interaction of PPARγ with the N-terminal part of Dok1.
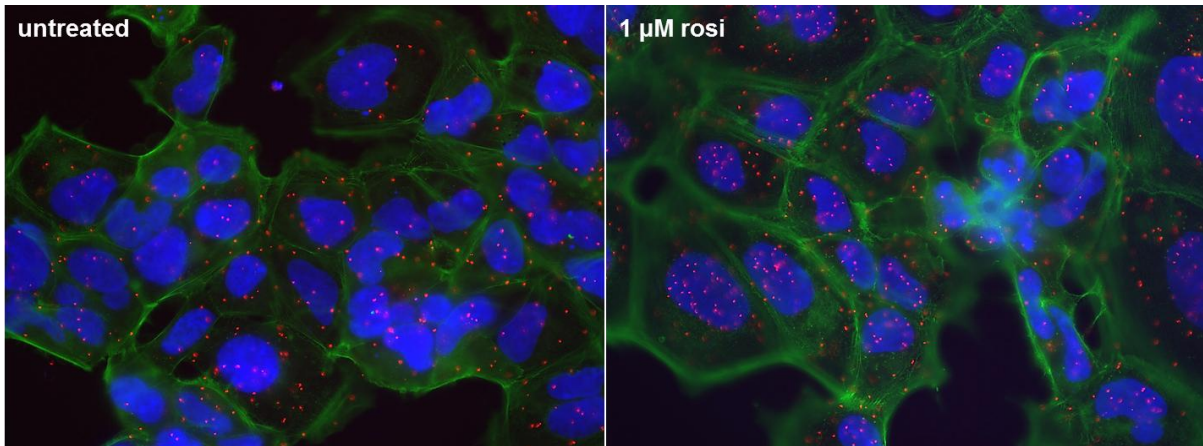
Figure 36 Representative picture of the proximity ligation assay of Dok1 and PPARγ in Hek293 cells. Cells are either untreated (left) or treated with 1 µM rosiglitazone for 1 h (right). Red spots indicate interaction of the two proteins tested. DAPI (blue) - nuclei, phalloidin (green) - actin filaments; Magnification x 630

3.5.2 Expression of Dok1 in human colon cancer cells

First, four human cell lines were evaluated for their Dok1 expression. Two different Dok1 antibodies were used. The first Dok1 (A3) antibody recognized the N-terminal half of the full-length Dok1p62 protein, comprising the PH and the PTB domain. The second Dok1 (M19) antibody recognized the C-terminal end of the protein. It is known from the literature that Dok1 exists in three different isoforms. The full-length Dok1p62 isoform consists of a pleckstrin homology domain (PH), which is important for membrane association, a phosphotyrosine binding domain (PTB) that allows interaction with other proteins, and a phoshotyrosine-rich C-terminal part including a nuclear export sequence (NES) [64]. The Dok1p44 isoform was found to lack the PH domain as a result of an alternative translation start and has therefore a perinuclear localization [65]. Furthermore, another isoform Dok1p22 exists due to alternative splicing which leads to truncation of the C-Terminus and thus of the PTB domain. Apart from the full-length Dok1p62 isoform, Dok1p22 additionally contains a proline-rich motif that might be necessary for binding to SH3 domains of other proteins [66]. Another Isoform with a predicted size of 33 kDa was found in chronic lymphocytic leukemia (CLL). Due to a frameshift mutation, Dok1 lacks the C-terminal end and therefore the NES domain responsible for nuclear localization [67] (Fig. 37).
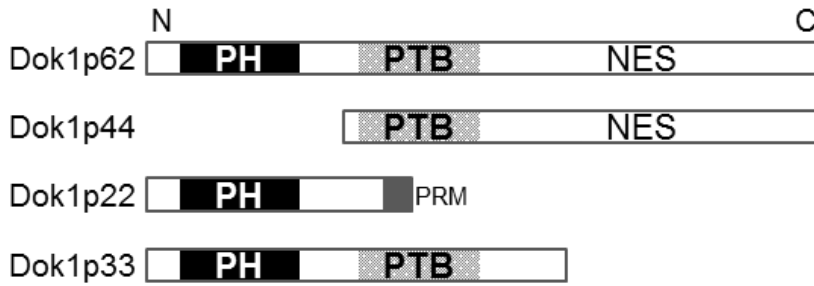
Figure 37 Four of the different Dok1 Isoforms. Legend: PH - pleckstrin homology domain, PTB - phosphotyrosine binding domain, NES - nuclear export sequence, PRM - proline rich motif

Human colorectal cancer cell lines were then analyzed for their expression pattern of Dok1 variants. Primers targeting the C- and the N-terminal part of Dok1 followed by RT-qPCR analyses revealed that Dok1 isoforms containing the C-Terminus and therefore the NES domain were present in higher amounts than isoforms containing the N-terminal PH domain. This result may indicate that, besides the full length Dok1p62 isoform, Dok1p44 is expressed.

Protein expression showed similar results. Apart from the predicted sizes 62, 44 and 22 kDa, a prominent band at 37 kDa was present using an antibody targeting the N-terminal half of the protein. SW480 and HCT116 cells showed highest Dok1 expression compared to HT-29 and Caco-2 cells at the mRNA level as well as on the protein level (Fig. 38).
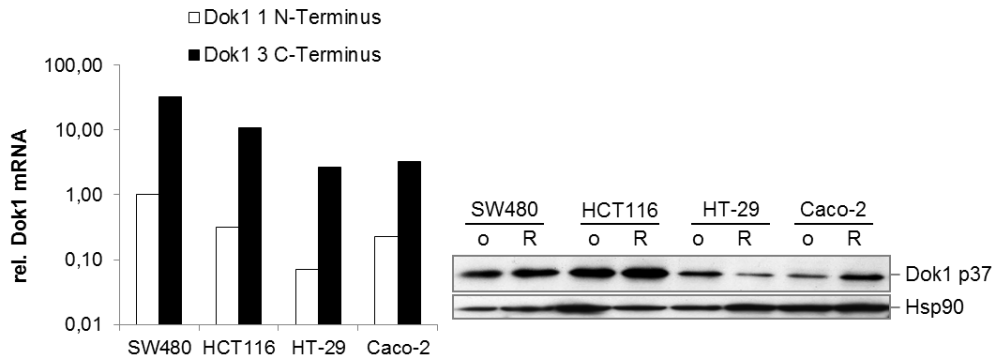
Figure 38 Expression of Dok1 in four colorectal cancer cell lines. Left: *DOK1* mRNA determined by RT-qPCR for SW480, HCT116, HT-29 and Caco-2 human CRC cells. CT-values were normalized to β2-microglobulin and calculated as –fold ± S.E. Right: Western Blot detecting Dok1 (N-Terminus) in CRC cells compared to Hsp90. Cells were either untreated (o) or treated with 1 µM rosiglitazone overnight (R).

Cells were then analyzed for Dok1 expression comparing antibodies targeting the N-terminal part (A3) or the C-terminal part (M19). Dok1p62 was slightly expressed in Hek293T cells. Dok1p44 was detected in all three cell lines, most prominent in Hek293T, with higher

intensity using the C-terminal antibody. A 37 kDa band was detected using the N-terminal antibody, maybe due to a lack of the C-Terminus as described for Dok1p33 in CLL [67] (Fig. 39).
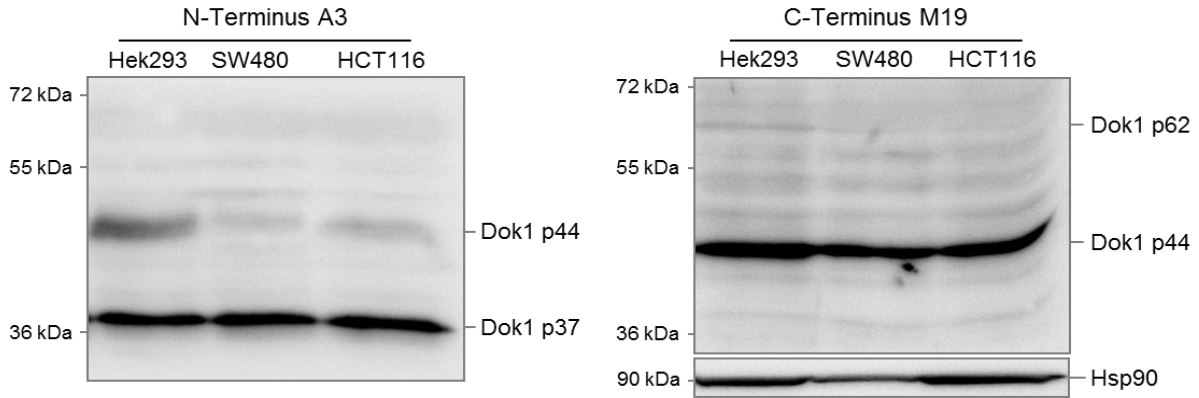
Figure 39 Presence of Dok1 isoforms in different human cell lines. Western Blot detecting the N-terminal end (left panel) or the C-terminal end (right panel) of Dok1 protein compared to Hsp90 in Hek293T, SW480 and HCT116 cells.

3.5.3 Molecular cloning of Dok1p62, Dok1p44 and Dok1p33 and mutagenesis of Dok1p62

As observed by Western Blot, the full-length isoform Dok1p62 was rarely expressed in the cell lines tested. To study the function of Dok1p62 and of the truncated isoforms Dok1p44 as well as Dok1p33 in colorectal cancer cells, Dok1 isoforms were cloned for overexpression.

Furthermore, to study the function of the different domains, Dok1p62 was mutated in its nuclear export sequence 3 (NES 3) to keep Dok1 in the nucleus. Besides the existing NES 1 and 2, NES 3 was shown to be the most important one for nuclear export of Dok1 [64]. Two arginine (R) residues (207-208 and 222-223) in the PTB domain were mutated to alanine (A), to inhibit interaction with other proteins like the EGF receptor [68] (Fig. 40).
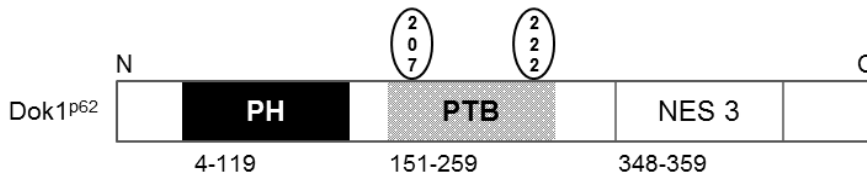
Figure 40 Mutations in Dok1p62. Dok1p62 was mutated in its PTB and NES 3 domain.

3.5.4 Dok1p62 wt and mutants inhibit Ras-signaling but fail to reduce proliferation in colorectal cancer cells

The cloned Dok1 products were tested for their expression on the RNA and protein level in Hek293T, HCT116 and SW480 cells. Expression was present in all three cell lines.

Furthermore, functionality of the Dok1p62 wildtype or mutants was determined by measuring ERK activity using ERK-pathway dependent activation of a SRE (serum response element) luciferase reporter gene as a surrogate readout. Therefore, cells were transiently transfected with Dok1p62 wildtype (WT), NES 3 (NES) or PTB (RR) mutant in addition to the SRE-luciferase construct. Cells were then starved or treated with 15 µM EGF overnight and luciferase activity of SRE was measured.

All three cell lines showed a decrease of SRE activation upon Dok1p62 transfection (n=3, *p<0.05 for pT *versus* Dok1) either in untreated or EGF-treated conditions, corroborating that the constructs are active and inhibit Ras-signaling. HCT116 cells with a *KRAS* G13D mutation revealed the best inhibition with Dok1, whereas SW480 cells with the stronger *KRAS* mutation G12V were more resistant. There was no difference in Ras-signaling inhibition between wildtype Dok1 and the NES or RR mutants (Fig. 41).

Figure 41 Impact of Dok1p62 wt and mutants on Ras-signaling. Hek293T, HCT116 and SW480 cells were transiently transfected with Dok1p62 wildtype (WT) and mutants in either the nuclear export sequence (NES) or the PTB domain (RR). Cells were then treated with 15 µM EGF overnight. SRE activity was measured using Luciferase assay and normalized to protein concentration (n=3, *t-test p<0.05 all *versus* pT untreated).

Next, Dok1p62 wt and mutants were tested for their effect on proliferation *in vitro*. Hek293T, HCT116 and SW480 cells were transfected with Dok1p62 and the corresponding mutants. Proliferation was measured after 0, 1, 2, 5 and 6 days. Neither Dok1p62WT nor the NES or RR mutants were able to inhibit proliferation of cancer cells compared to the empty vector control (data not shown) indicating that Ras-inhibition was either not efficient enough or that Ras-inhibition shown for SRE was a short-time effect.

3.5.5 Dok1 sensitizes colorectal cancer cells to PPARγ-ligands

As shown by CoIP (Fig. 35) there might be a physical interaction between Dok1 and PPARγ. To measure the activity of PPARγ in dependence of Dok1, cells were transfected with Dok1p62WT, Dok1p62NES or Dok1p62RR. Transfected cells were incubated with 0, 1 or 3 μM rosiglitazone for 24 h and proliferation was measured.

Dok1p62 enhances the rosiglitazone-sensitivity in all three cell lines tested compared to the empty vector control (Fig. 42). In HCT116 cells proliferation was decreased by 15 % with Dok1p62NES compared to EV control. In SW480 cells, Dok1 was less effective so that sensitivity was only enhanced by 5 % with Dok1p62WT compared to pT and did not reach statistical significance. Hek293T also showed slightly enhanced sensitivity by up to 10 % in Dok1p62WT compared to EV control (*t-test p<0.05 *versus* pT for 3 μM rosiglitazone, n=5).
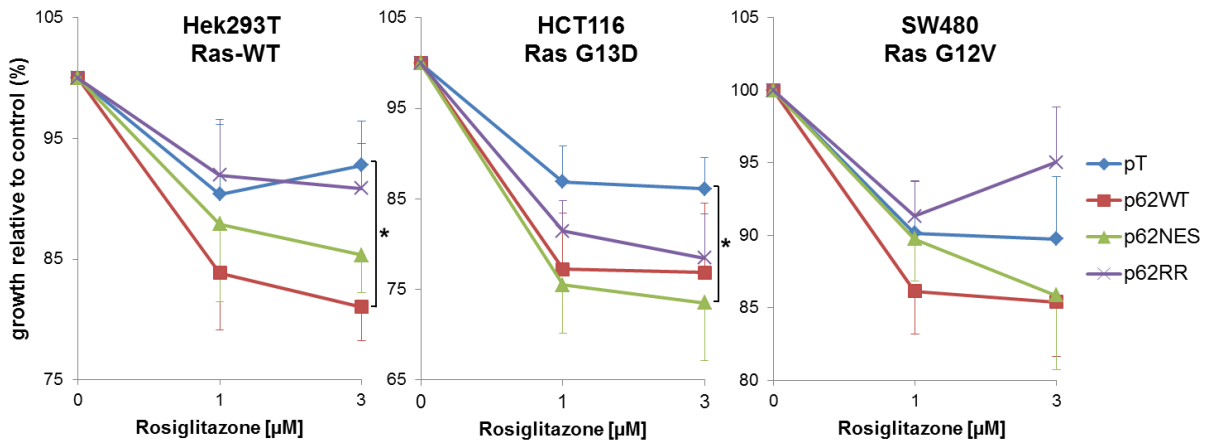
Figure 42 Influence of Dok1p62 wt and mutants on rosiglitazone-dependent proliferation. Rosiglitazone-dependent growth inhibition for Dok1 transfected Hek293T, HCT116 and SW480 cells; cells were transfected with pT, Dok1p62WT, Dok1p62NES or Dok1p62RR and incubated with increasing concentrations of rosiglitazone. Viability was measured after 48 h and O.D. values were calculated as % ± S.E. (n=3, *t-test p<0.05).

Cells were then examined for their PPARγ promoter activity. Cells were transfected with either Dok1p62WT or mutants and the PPRE-luciferase reporter plasmid, stimulated with 0, 0.1, 1 or 10 μM rosiglitazone overnight and PPARγ promoter activity was measured using luciferase assay. Activation of the PPARγ promoter was significantly enhanced in Dok1 transfected cells compared to empty vector control in HCT116 and Hek293T cells consistent with the results of the rosiglitazone sensitivity on the proliferation rate.
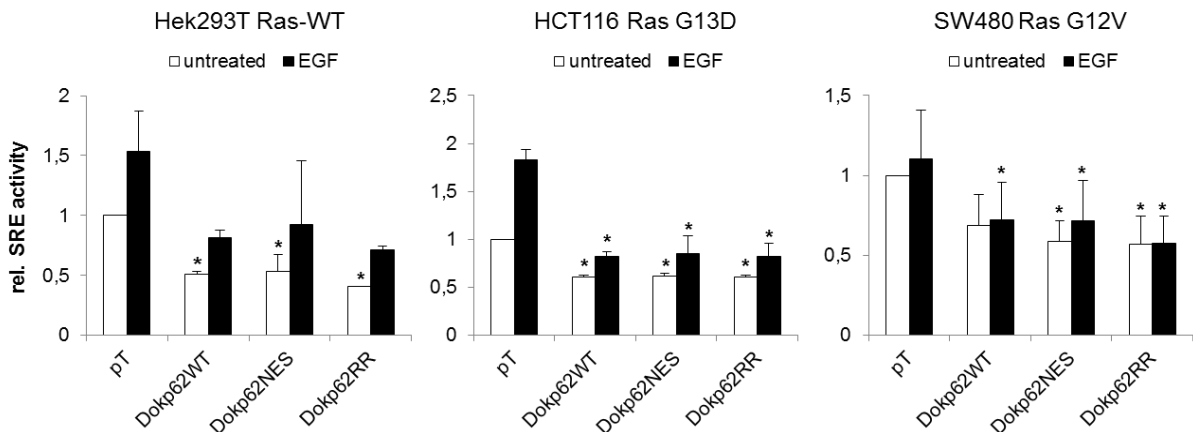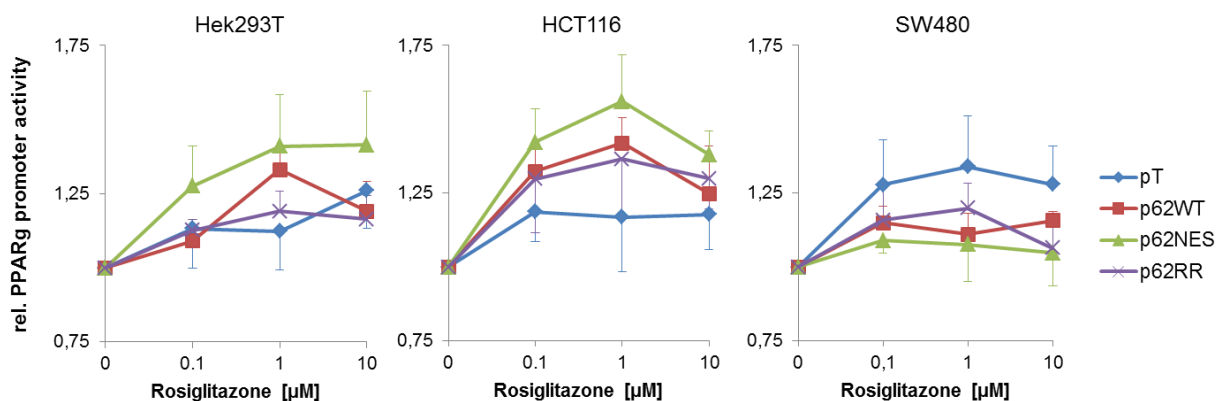
Figure 43 **Impact of Dok1p62 wt and mutants on PPARγ promoter activity.** Hek293T, HCT116 and SW480 cells were transiently transfected with Dok1p62 wildtype (WT) and the corresponding mutants in either the nuclear export sequence (NES) or the PTB domain (RR). Cells were then treated with 0, 0.1, 1 or 10 µM rosiglitazone overnight. PPRE activity was measured using Luciferase assay and normalized to protein concentration (n=3).

PPARγ promoter activity was significantly enhanced with Dok1p62WT, Dok1p62NES and Dok1p62RR in HCT116 by up to 33 % at 1 µM rosiglitazone compared to EV control (*t-test p=0.041 pT *versus* Dok1p62NES for 1 µM rosi). In Hek293T cells, activity was enhanced by 25 % in Dok1p62NES- and by 20 % in Dok1p62WT-transfected cells at 1 µM rosiglitazone, but did not reach statistical significance. SW480 cells were resistant to the PPARγ ligand and Dok1p62 transfection even reduced the PPARγ promoter activity (Fig. 43).

These results show that Dok1 can increase the PPARγ promoter activity which results in slightly enhanced sensitivity for the PPARγ ligand on the level of growth inhibition.

3.5.6 Dok1 promotes nuclear import of PPARγ

To test whether Dok1 changes the localization of PPARγ, cells were transiently transfected with pT, Dok1p62WT, NES or RR and subjected to subcellular fractionation. WB analyses of the nuclear fraction revealed that Dok1 increased the amount of nuclear PPARγ. Especially the NES and RR mutant facilitated the translocation of PPARγ to the nucleus by up to 200 % compared to EV control. Again, import of PPARγ to the nucleus was not increased in SW480 cells (Fig. 44).
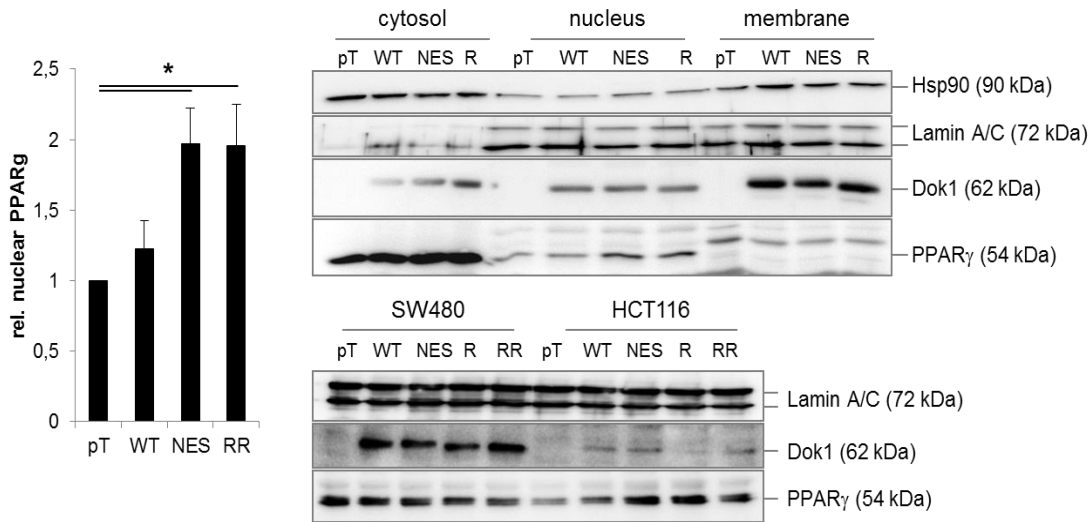
Figure 44 Dok1 promotes nuclear import of PPARγ. Right panel: representative WB of Hek293T cells transfected with pT, Dok1p62WT, NES and RR mutant. Cytosolic, nuclear and membrane fraction are shown. SW480 and HCT116 cells were transfected with pT, Dok1p62WT, NES, R, and RR mutants. Nuclear fraction is shown. Left panel: Quantification of nuclear PPARγ. O.D. was measured from bands, normalized to Lamin A/C and calculated as –fold ± S.E. (n=3, Hek293T and HCT116 cells were summarized, *t-test p=0.002 pT *versus* NES and RR).

To further corroborate the findings of the subcellular fractionation, immunofluorescence microscopy was done. Hek293T cells were either transfected with Dok1p62WT, NES or RR mutant and cells were stained for Dok1 and PPARγ.

As shown in Figure 45, Dok1p62NES and the RR mutant, but not Dok1p62WT enhanced the translocation of Dok1 and PPARγ into the nucleus, confirming the results of the SCF. In case of the RR mutant, Dok1 and PPARγ had a perinuclear distribution, whereas the NES mutant evoked a predominant nuclear localization of PPARγ and Dok1 to the nucleus.
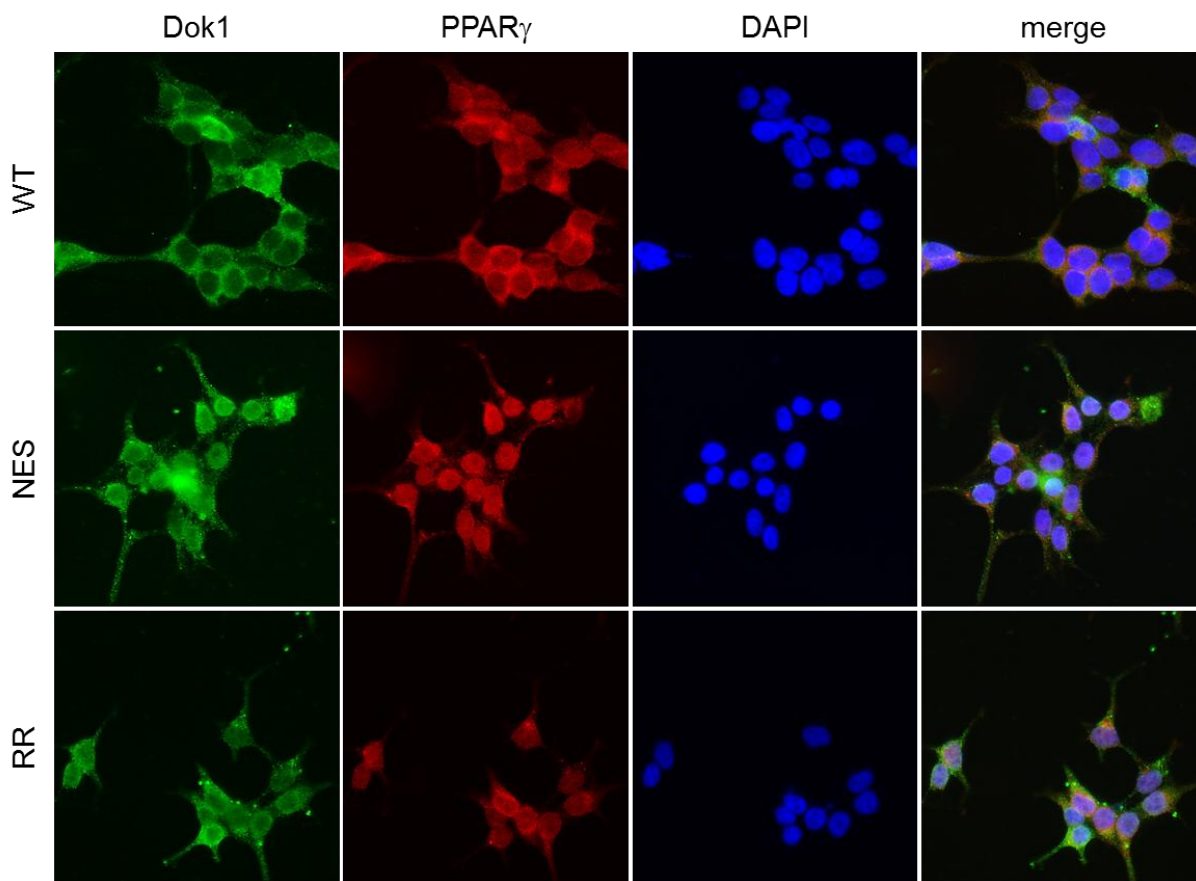
Figure 45 Immunofluorescence microscopy of Dok1 and PPARγ. Hek293T cells were transfected with Dok1p62WT, NES or RR mutant. NES and RR mutant show nuclear translocation of Dok1 and PPARγ. Green-Dok1, red-PPARγ, blue-nuclei; Magnification x 400

These results may explain how Dok1 enhances the sensitivity to rosiglitazone. Whether Dok1 acts as a nuclear import shuttle for PPARγ or whether PPARγ is released to the nucleus by Dok1-mediated inhibition of the Ras-signaling pathway (as shown for U0126 in Fig. 32) needs to be clarified in future studies. Dok1 could also promote the binding of PPARγ to its PPREs in the nucleus and thus enhance its transcriptional efficiency.

3.5.7 The Dok1 Isoforms p62 and p44, but not p33 promote PPARγ's activity

To compare the effects of the mutations with the truncated isoforms, cells were transiently transfected with Dok1p62 (full length), Dok1p44 (ΔpH) and Dok1p33 (ΔNES) and inhibition of Ras (SRE) and activation of PPARγ (PPRE) were measured by Luciferase assay.

To this end, cells were transiently cotransfected with Dok1p62, p44 or p33 and the SRE-luciferase construct. Cells were then starved or treated with 15 µM EGF overnight and luciferase activity of SRE was determined.

In Ras-WT Hek293T cells all three isoforms exerted a slight decrease of SRE activity compared to the empty vector control for EGF treated cells (n=5, *p<0.05 for pT *versus* p62 in EGF-treated cells). In HCT116 with a modest K-Ras activity due to the G13D mutation, Dok1p62 and, to a lesser extent, Dok1p33 were effective to inhibit Ras-signaling, whereas Dok1p44 was not (n=5, *p<0.05 for pT untreated or EGF-treated *versus* p62 and pT untreated *versus* p33). SW480 cells that express the *KRAS* G12V mutation with a strong Ras-activity did not react to EGF stimulation. Furthermore, transfection with Dok1 isoforms had no effect on Ras-inhibition in SW480 cells (Fig. 46).
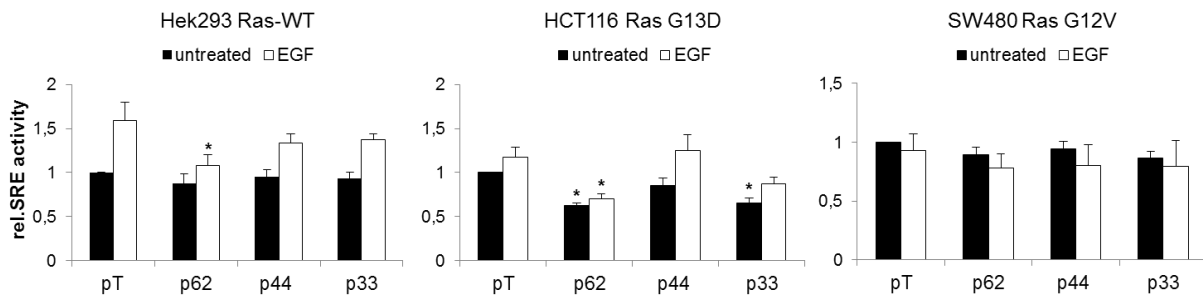
Figure 46 **Impact of Dok1 isoforms on Ras-signaling.** Hek293T, HCT116 and SW480 cells were transiently transfected with Dok1p62, Dok1p44 and Dok1p33. Cells were then treated with 15 µM EGF overnight. SRE activity was measured using Luciferase assay and normalized to protein concentration (n=3, *t-test p<0.05 all *versus* pT).

To further characterize the effect of the Dok1 isoforms on PPARγ activity, cells were transfected, incubated with increasing concentrations of rosiglitazone for 24 h and proliferation was measured.

Dok1p62 and Dok1p44 enhanced the rosiglitazone-sensitivity in Hek293T and HCT116 cells compared to the empty vector control (Fig. 47). Hek293T cells showed enhanced sensitivity by up to 10 % (*t-test p<0.05 p62, p44 *versus* p33 for 3 µM rosiglitazone, n=5). In HCT116 proliferation was decreased by up to 10 % with p44 and p62 (*t-test p<0.05 pT *versus* p44, p62 for 3 µM rosiglitazone, n=6). SW480 were again resistant to rosiglitazone-treatment and Dok1 overexpression.
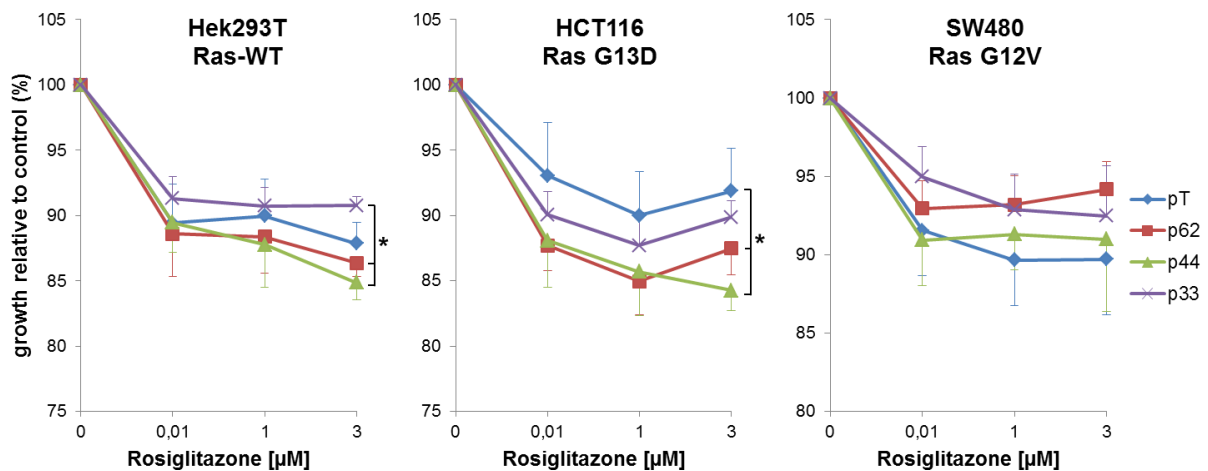
Figure 47 Effect of Dok1 isoforms on rosiglitazone-dependent proliferation. Rosiglitazone-dependent growth inhibition of Dok1-transfected Hek293T, HCT116 and SW480 cells; cells were transfected with pT, Dok1p62, p44 or p33 and incubated with increasing concentrations of rosiglitazone. Viability was measured after 24 h and O.D. values were calculated as % ± S.E. (n=6, *t-test p<0.05).

Cells were then further tested for their PPARγ promoter activity. Transfected cells were stimulated with 0, 0.1, 1 or 10 µM rosiglitazone overnight and PPARγ promoter activity was measured using luciferase assay. PPARγ promoter activity was enhanced by up to 30 % with Dok1 transfected cells compared to EV control in Hek293T cells (*t-test p<0.05 p33 *versus* pT for 0.1 µM rosiglitazone and p62, p44, p33 *versus* pT for 1 µM rosiglitazone, n=4). Surprisingly, increased PPARγ promoter activity in Dok1p33-transfected Hek293T cells did not result in enhanced sensitivity on the proliferation level.

In HCT116, Dok1p44 enhanced the PPARγ activity to 15 % compared to EV control. Compared to p62 and p44, p33 had no effect (*t-test p<0.05 p33 *versus* p62 and p44 for 0.1 µM rosiglitazone, n=4). SW480 cells were resistant to Dok1 transfection and rosiglitazone-treatment (Fig. 48).
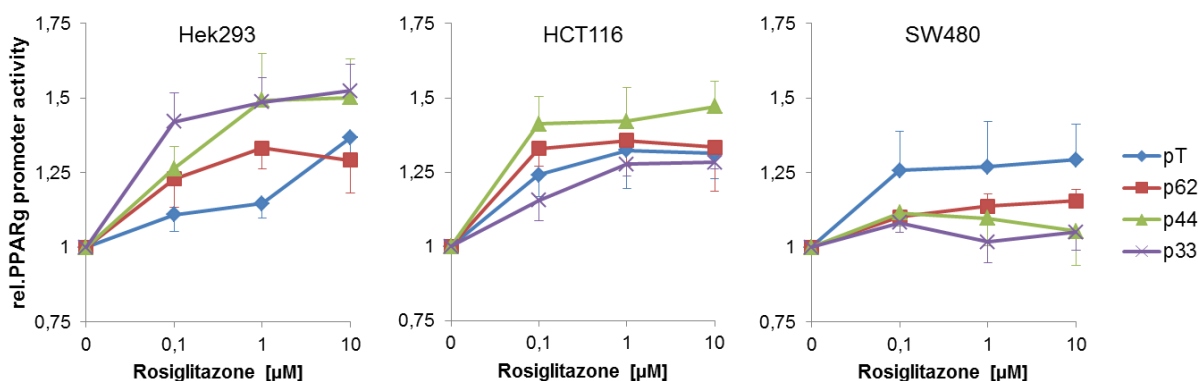
Figure 48 Impact of Dok1p62, Dok1p44 and Dok1p33 on PPARγ promoter activity. Hek293T, HCT116 and SW480 cells were transiently transfected with Dok1p62, Dok1p44 and Dok1p33. Cells were then treated with 0, 0.1, 1 or 10 μM rosiglitazone overnight. PPRE activity was measured using Luciferase assay and normalized to protein concentration (n=4).

In sum, N-terminal Dok1p33 (ΔNES) or C-terminal Dok1p44 (ΔPH) showed diverse effects either on SRE-inhibition or PPRE-activation. Dok1p33, that is supposed to be expressed in the nucleus, was less effective in enhancing sensitivity to rosiglitazone but more effective to inhibit Ras-signaling compared to Dok1p44 in HCT116 corroborating high importance of the PH domain in Ras-inhibition. On the other hand, Dok1p44 was most effective to enhance sensitivity to the PPARγ ligand. This might be due to the lack of membrane association supporting the hypothesis that Dok1 interacts with PPARγ in the cytosol to promote its nuclear import and points to an important role for the NES in PPARγ activation. In Ras-WT Hek293T cells, all three Dok1 isoforms showed slightly reduced Ras-signaling. PPARγ promoter activity was enhanced compared to EV control, resulting in slightly increased sensitivity for PPARγ ligands in p62 and p44 transfected cells. Enhanced PPRE and reduced SRE activity did not affect proliferation inhibition of Hek293T, which may be due to the Ras WT status. Cells with inactive Ras-signaling might therefore not show any reaction upon transfection of the Ras-inhibitor Dok1.

3.6 Dok1 expression in human colorectal cancer patients

As we could show that Dok1 inhibits Ras-signaling and promotes ligand sensitivity in CRC cell lines *in vitro*, we tested normal and tumor tissue of CRC patients for Dok1 expression. Dok1 expression was first analyzed on the mRNA level comparing normal tissue with tumor tissue of the same patient. In 5 out of 12 patients (42 %), Dok1 was downregulated in TU tissue, whereas in 7 out of 12 patients (58 %) Dok1 was upregulated (Fig. 49). There was also a different Dok1 expression comparing NT or TU among the CRC patients.
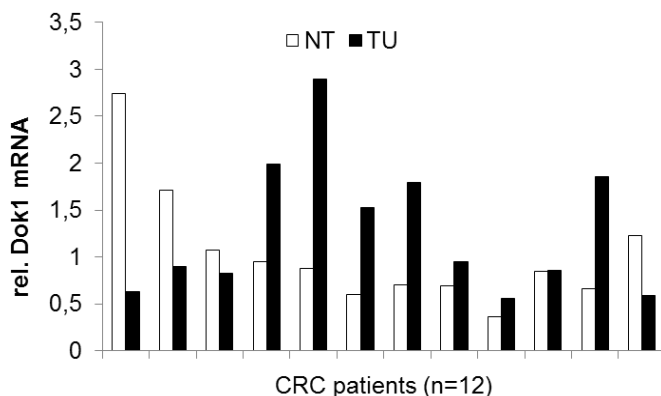
Figure 49 Relative *DOK1* mRNA expression in human CRC patients comparing NT and TU. Ct-values were normalised to β2-microglobulin and calculated as –fold.

DOK1 mRNA expression did not provide any information about the possible function in tumor development. Besides that, there was no information available about the patients or the progression of the tumor that could be correlated to Dok1 expression.

To study the expression of Dok1 in tumor samples of colorectal cancer patients in correlation to clinicopathological data, IHC staining for Dok1 was done using tissue microarrays (TMA). These arrays contained samples from colorectal cancer patients (n=68) and normal colon tissue (n=8) and were stained using the Dok1 antibody against the N-terminal half (A3) of the protein. Intensity of nuclear Dok1 in the epithelial compartments was estimated and was associated with the patient data. Intensity was defined as follows: 0=no staining, 1=very weak staining, 2=moderate staining, 3=strong staining. The two tissue arrays were analyzed separately (Fig. 50).
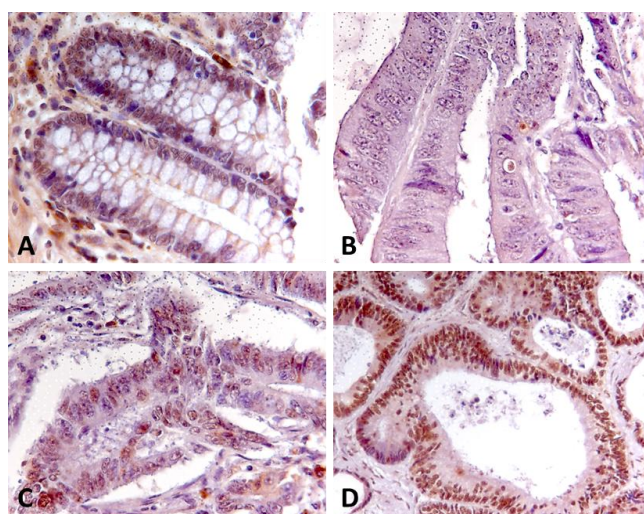
Figure 50 Dok1 nuclear staining in normal and tumor tissue. A-NT with strong staining, B-TU with no staining, C-TU with moderate staining, D-TU with strong staining (representative tissues are shown). Magnification x 400

Dok1 expression was significantly reduced to 40 % (*t-test p=0.0013) in colorectal cancer samples compared to normal colon tissue. Furthermore, Dok1 expression was decreased by up to 75 % with increasing grade "G" (*t-test p<0.05 NT *versus* G2, G3). Expression was also reduced by up to 70 % with increasing stage "T" (*t-test p<0.05 NT *versus* T2, T3, T4) and by up to 65 % with increasing nodal "N" status (*t-test p<0.05 NT *versus* N0, N1, N2/N4), showing that Dok1 expression is lost during tumor progression (Fig. 51). Because of the low case number, no conclusion could be made for the metastatic "M" status.
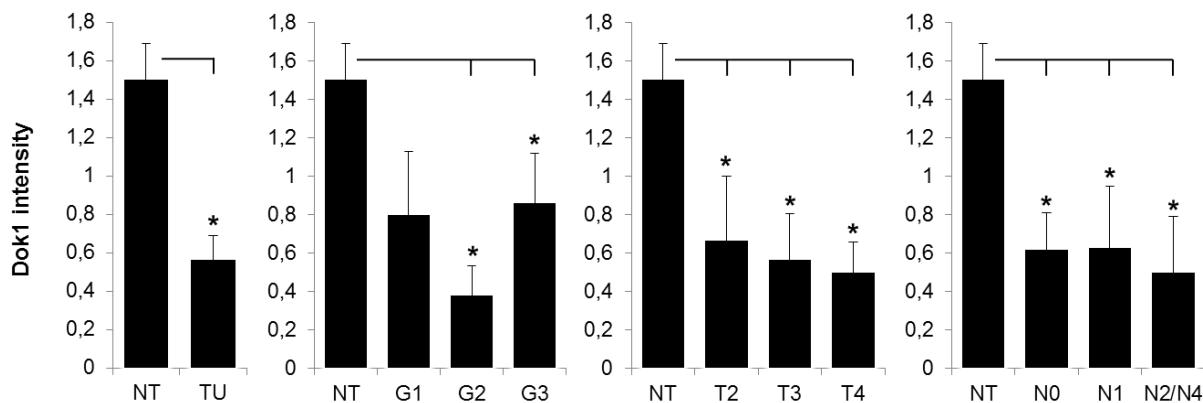
Figure 51 Dok1 expression in normal (NT) and tumor (TU) tissue according to grade, stage and nodal status (TMA I). Normal tissue (n=8) and tumor tissue (n=40) was analyzed according to Dok1 expression (score 0-3) and correlated to grade, stage and nodal status.

The second tissue array did not contain normal tissue. Nevertheless, a decrease in Dok1 expression with increasing grade "G" to 60 % comparing G1 with G3 was observed as well. With increasing stage "T" there was also a decreased Dok1 expression to 50 % (*t-test p<0.05, T2, T3 *versus* T4) and increasing nodal "N" status also resulted in decreased Dok1 expression by approximately 40 % (*t-test p<0.05, N0 *versus* N1/N2), confirming the results of the first tissue array. Further information showed that there was also decrease in Dok1 expression by 40 % with increasing "L" (tumoral invasion into lymphatic vessels) status (Fig. 52).
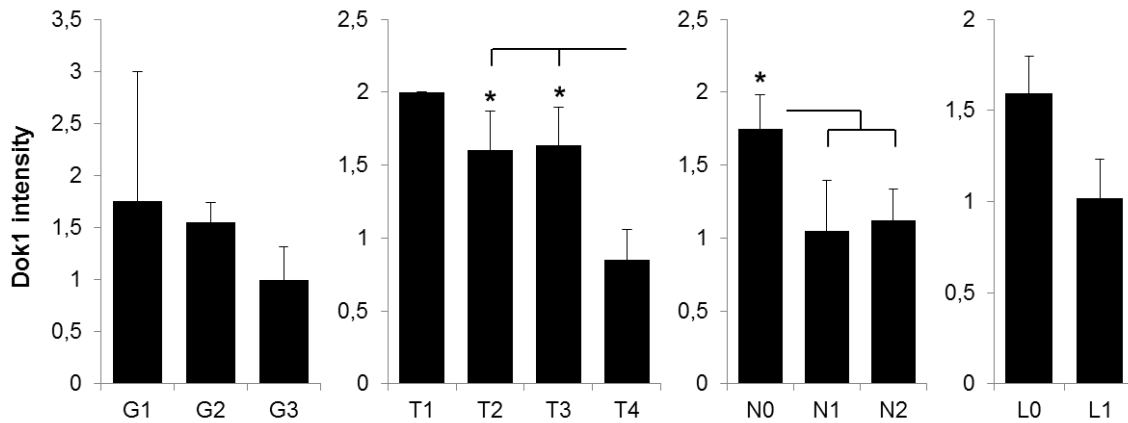
Figure 52 Expression of Dok1 in tumor tissue according to grade, stage and nodal status (TMA II). Tumor tissue (n=28) was analyzed according to Dok1 expression (score 0-3) and correlated to grade, stage, nodal status and invasion of the tumor into lymphatic vessels.

Correlation of Dok1 expression with localization and size of the tumor showed that Dok1 expression was reduced by 40 % in tumors of the cecum and also by 50 % in tumors of the rectum compared to colon tumors (*t-test $p<0.05$), probably also due to higher Dok1 expression in the colon tissue. Bigger tumors (6.0-10.0 cm) showed significantly reduced Dok1 expression by 40 % (*t-test $p=0.04$) compared to smaller tumors (4.0-5.0 cm) (Fig. 53).
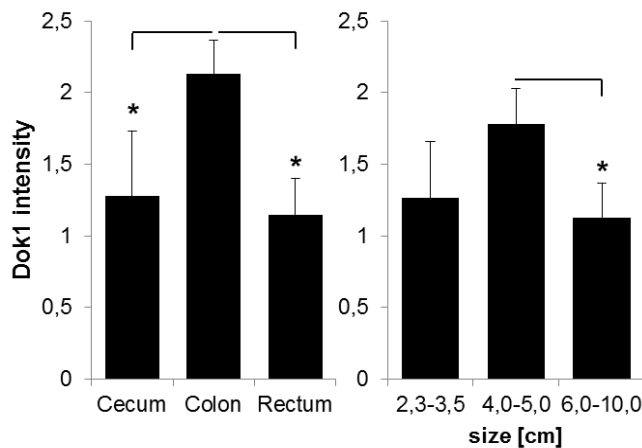
Figure 53 Expression of Dok1 in tumor tissue according to localization and size of the tumor (TMA II). Tumor tissue (n=28) was analyzed according to Dok1 expression (score 0-3) and correlated to localization and size of the tumor.

The results of the TMAs showed that Dok1 is lost during tumor progression and might thus be a possible tumor suppressor in CRC.

4. Discussion

The major aim of this thesis was to elucidate the role of the tumor suppressor Caveolin-1 in colorectal carcinogenesis *in vivo*. $Apc^{min/+}$ mice which were deficient for Cav1 expression were more susceptible to tumor development in the distal colon. Further investigation revealed a correlation of the tumor initiators APC/WNT and Ras with the tumor inhibitors Cav1 and PPARγ. Activation of Ras-signaling correlated with nuclear export of PPARγ and treatment of mice with the PPARγ agonist rosiglitazone alleviated tumor growth, independently of Cav1 expression. As a result, the Ras-inhibitor docking protein 1 (Dok1) was upregulated by rosiglitazone-therapy *in vivo* and is thus a candidate PPARγ target gene. Dok1 was further found to be a novel interaction partner for PPARγ and promotes ligand sensitivity and nuclear import of PPARγ *in vitro*. Moreover, Dok1 was reduced in CRC patients correlating with the severity of the disease.

Thus, a negative feedback loop might exist, where PPARγ activation upregulates the Ras-inhibitors Dok1 and Cav1 which then in turn inhibit the Ras-signaling pathway. The abrogation of Ras-signaling might further enhance PPARγ's nuclear import and activation, which leads to reduced proliferation. Therefore, PPARγ might be a putative new target for treatment of CRC, to circumvent active Ras-signaling resulting from mutations (Fig. 54).

As shown by Vogelstein [17] and Davies [2], the development of colorectal cancer is a process of different genetic alterations, that accumulate during tumorigenesis. Loss of APC and activation of K-Ras are early events of this process.

The $Apc^{min/+}$ mouse is one of the most prominent models to study FAP *in vivo*, nevertheless, adenomas are restricted to the small intestine and do not progress to invasive carcinoma. Due to anemia, $Apc^{min/+}$ mice die after 4-5 months. As mentioned in the introduction, the phenotype of $Apc^{min/+}$ C57BL6 mice changes upon inbreeding of different genetic backgrounds due to the action of modifier of min (MOM) loci. [51, 52] Crossing of $Apc^{min/+}$ mice with tumor-suppressor deficient mice results in enhanced tumor growth in the distal colon as shown for mice lacking *Smad3* [69] and *Tgfrβ* [70]. Likewise, interbreeding of $Apc^{min/+}$ mice to other mice harboring active oncogenes like e.g. mutated *Ras* [71, 72] also promotes tumor growth. According to this evidence, crossing of C57BL/6J $Apc^{min/+}$ mice with B6129SF2/J mice deficient in Cav1, another tumor suppressor, resulted in accelerated tumor growth in the distal colon.

Caveolin-1 was often characterized as a tumor suppressor gene because it inhibits the signaling activity of oncogenes like v-Abl or H-Ras. It was further found to inhibit MAP-kinase-signaling, an important pathway in tumor development [43], through direct interaction with the EGF-receptor [73]. Caveolin-1 was described to be downregulated in colon [45] or gastric

cancer [44]. Moreover, Caveolin-1 deficient mice as such showed defects in the lung, insulin signaling and cardiovascular function, so that loss of Cav1 alone is not sufficient to drive cancer. Nevertheless, Cav1-deficiency resulted in accelerated tumorigenesis combined with a second genetic alteration, like e.g. loss of the tumor suppressor Ink4a, or by treatment with a carcinogen [74]. These observations might also be true for the $Apc^{min/+}$ mice used in this thesis, where Cav1-deficiency resulted in higher incidence of colon tumors. The possible role of Cav1 as a tumor suppressor is underlined by its genetic locus on chromosome 7. This fragile region *(FRA7G)* is often linked to loss of heterozygosity (LOH) in tumors [43].

However, tumor development was not limited to Cav1-deficient mice but also occurred in $Apc^{min/+}$ mice which expressed wildtype *Cav1*. As demonstrated by other groups, $Apc^{min/+}$ mice show an altered tumorigenic phenotype due to interbreeding with other mouse strains of different backgrounds, which might be explained by the modifier of min (MOM) effect already mentioned in the introduction [51]. In 2011, Lisanti *et al.* showed that loss of Caveolin-1 in $Apc^{min/+}$ mice on a pure C57BL/6J background resulted in an increased polyp number, but no difference between the three varying *Cav1* genotypes was observable, indicating the presence of MOMs next to the *Cav1* region [56].

This observation might be an explanation for the occurrence of tumors in $Apc^{min/+}$ mice expressing Cav1 as well. To clarify this possibility, further analysis is needed. Nevertheless, the loss of Caveolin-1 on both alleles ($Cav1^{-/-}$) seemed to accelerate tumor growth in $Apc^{min/+}$ mice, resulting in a reduced life span and higher tumor incidence in the colon. In line with Cav1-loss in human tumors, mice in this study also showed reduced Cav1 expression in tumor tissue compared to normal tissue. In line with these results, higher *Wnt6* (APC-signaling) and *Cyclind1* (cell cycle progression) mRNA expression was observed with decreasing *Cav1* expression, which might explain the earlier appearance of colon tumors in $Apc^{min/+}//Cav1^{-/-}$ mice as well.

Another study showed that wildtype *APC* upregulated Cav1 expression in human colon cancer cells, which is mediated by FOXO1a. On the other hand, APC decreases the expression of c-Myc, which is known to repress Cav1 [75]. Since the mutation of *APC* is an early event of carcinogenesis, Cav1 acts as a tumor suppressor in the early tumorigenesis, which was also shown by Burgermeister *et al.* in 2007 [44]. The $Apc^{min/+}$ mice in this study showed increased levels of *c-Myc* as well, which might explain the loss of Cav1 in tumor tissue compared to normal tissue. Thus, loss of the APC indirectly leads to downregulation of Caveolin-1. Loss of Cav1 might therefore also be an important event in tumor initiation, and could explain the earlier onset of tumorigenesis in $Cav1^{-/-}$ mice in this study.

Furthermore, Cav1 is known as an inhibitor of the Ras-signaling pathway through interaction with the EGF-receptor [73]. In colon cancer, the *RAS* oncogenes are mutated in about 50 % of all cases, leading to constitutively active Ras-signaling and aberrant proliferation of the

cells [31]. In the *Apc^min/+//Cav1*-KO mouse model, active Ras-signaling was found in tumor tissue. Nevertheless, sequencing revealed no mutation in the *Kras* gene sequence. Again, complete loss of Cav1 followed by reduced Ras-inhibition could explain the earlier onset of tumorigenesis compared to wildtype *Cav1*.

In accordance to enhanced Ras-signaling, the PPARγ gene signature was decreased as revealed upon microarray analysis of colorectal tumor tissue, which was independent of the *Cav1* genotype. It is known from the literature that PPARγ is phosphorylated at serine84/112 (g1/g2) by active MAP-kinases. Furthermore, active Ras-signaling results in nuclear export of PPARγ by direct interaction with MEK. Both mechanisms lead to inhibition of PPARγ and result in decreased differentiation and enhanced apoptosis [37]. In the *Apc^min/+//Cav1*-KO mouse model, neither *Pparγ* mRNA nor PPARγ protein were reduced in the tumor tissue. Nevertheless, PPARγ target gene expression was found to be diminished and IHC staining revealed a shift from nuclear PPARγ in normal colon tissue to cytosolic PPARγ in tumor tissue. According to the *in vitro* studies, this nuclear export might also be due to active Ras-signaling *in vivo*. We showed previously, that nuclear import of PPARγ is facilitated by the endogenous Ras-inhibitors Cav1 and Dok1 and increases PPARγ's transcriptional activity [57]. Further *in vitro* results showed nuclear import of PPARγ by MEK inhibition in two CRC cell lines. *In vivo*, nuclear export of PPARγ in the tumor was independent of the *Cav1* genotype. As PPARγ is not lost as a protein, but exported from the nucleus, it is still a possible target for anti-cancer therapy.

Activation of PPARγ by rosiglitazone-diet in mice, where tumor development was already initiated, reduced tumor incidence and size. Furthermore, PPARγ target genes including *Cav1* and *Dok1* were reactivated, *Kras* and *Cyclind1*, important for cell cycle progression, were reduced. PPARγ activation hence resulted in reduced proliferation, which was corroborated by proliferation assays for CRC cell lines *in vitro*. As PPARγ is highly expressed in the colon and influences inflammation, PPARγ ligands were frequently tested to reduce colon cancer development [38]. In line with the results from this thesis, other authors showed that PPARγ activation reduces growth of colon cancer cells *in vitro* [76] and in *Apc^min/+* mice [77]. Furthermore, loss of PPARγ promotes tumor growth in *Apc^min/+* mice [78]. On the contrary, PPARγ activation was also described to enhance tumor growth in C57BL/6J *Apc^min/+* mice [79] and also in wildtype mice [80] *in vivo.* Another interesting study revealed that polyp formation in *Apc^min/+* mice decreases with increasing dosage of the PPARγ ligand pioglitazone [81]. In this thesis, treatment of *Apc^min/+* mice for 4 months with rosiglitazone reduced colon tumor formation. Moreover, wildtype mice did not show any abnormalities in the large and small intestine even upon long-term exposure to a moderate pharmacological dose (25mg/kg*day) of rosiglitazone for several months. The effect of PPARγ activation might therefore depend

on duration, dosage and type of therapy. Moreover, the genetic background may as well influence therapeutic outcome. Again, presence or absence of Cav1 did not influence therapeutic effects of rosiglitazone in our study, maybe due to already reduced Cav1 expression in the tumor tissue in all three genotypes.

In sum, codeficiency of APC and Cav1 resulted in enhanced Ras-signaling, reduced PPARγ signature and accelerated tumor growth. Ras and PPARγ inhibit each other, Ras through nuclear export or phosphorylation of PPARγ, and PPARγ through activation of endogenous Ras-inhibitors. These results provide new options for CRC treatment, where activating mutations in the Ras-signaling pathway are important factors responsible for treatment failure of therapies targeting the EGFR in CRC patients. PPARγ-mediated Ras-inhibition could therefore circumvent the problem of EGFR therapy resistance.

To analyze whether loss of PPARγ further promotes tumorigenesis in K-Ras-activated tissue *in vivo*, a new mouse model was established comprising PPARγ knockdown and *KRAS* mutation in the small and the large intestine independently of APC. In this thesis, the mouse model was generated and validated. Active K-Ras was detected in the ileum and, to a lesser extent, in the colon and was confirmed to be limited to the intestinal tract. Furthermore, proteins involved in Ras-signaling were found to be altered as were PPARγ target genes. As a result, PPARγ loss exacerbated tumorigenesis in *KRAS* G12V mutated mice compared to PPARγ wildtype mice in the small intestine but not in the colon. This observation might be explained by the higher expression of active K-Ras in the ileum as compared to the colon. This assumption was corroborated by Ras GTPase pulldown. As already mentioned, the *RAS* genes, especially *KRAS*, are often mutated and activated in human tumorigenesis and are therefore interesting targets investigated in cancer mouse models. Activation of K-Ras by G12D mutation in the whole animal predominantly resulted in lung cancer development, but also occurrence of thymic lymphoma, skin papilloma and aberrant crypt foci (ACF) of the colon was observed. These ACFs are clusters of abnormal crypts that show an irregular shape of the lumen as well as a thickening of the epithelium and are often found in CRC patients [82]. One possible explanation for the different distribution of the lesions is that some cells of e.g. the lung are more sensitive to the pro-proliferative property of K-Ras*,* and active K-Ras might also have different effects in diverse cell types. Interestingly, appearance of ACFs indicates that K-Ras plays a role in the early events of carcinogenesis. Another mouse model limited the expression of K-Ras (V12G) to the intestinal epithelium, to study the effect of K-Ras overexpression in the small and large intestine. This mutation resulted in intestinal lesions in more than 80 % of the mice with ACFs and even invasive adenocarcinomas without altering the APC expression. [58] Two types of ACFs, dyplastic and non-dysplastic, were analyzed in a study from 1994 regarding their *APC* and *KRAS* status. While *APC*

mutations were detected in dysplastic ACFs, which are more prone to progress to adenoma, *KRAS* mutations were found in non-dysplastic lesions. This study suggests that if *RAS* mutations occur first, the resulting non-dysplastic ACFs will rarely progress to adenoma. On the other hand, if *APC* is mutated, dysplastic ACFs with high potential for progression are formed with subsequent alterations in *RAS* [83]. This observation reflects the two mouse models used in this thesis, with *Apc* mutation and progression to adenoma, and K-Ras overexpression with a more alleviated phenotype. Nevertheless, loss of PPARγ resulted in a more severe phenotype in the ileum than active K-Ras alone and corroborates the findings from the *Apc^{min/+}//Cav1*-KO model. PPARγ presence activates Ras-inhibitory proteins like Dok1 and Cav1 and therefore diminishes Ras-induced abnormal proliferation. Moreover, PPARγ reduces inflammation in the colon, a risk factor and putative early event in colorectal tumorigenesis [7]. This study suggests that absence of PPARγ leads to aberrant cellular proliferation in the intestinal epithelium with active K-Ras. According to this, K-Ras activation in combination with the tumor suppressor INK4a/ARF results in enhanced tumor growth with a serrated phenotype similar to human CRC patients. The authors suggest that APC is not necessary to drive cancer, but can also be initiated by the Ras-Raf-MEK-signaling [24].

In the PPARγ-KO mice used in this study, the APC-activator GSK-3β is inactivated. The GSK-3β-APC-complex is known to reduce ß-catenin which activates pro-proliferative genes. Therefore, APC might be downregulated by loss of PPARγ and could enhance the tumor growth compared to PPARγ-expressing mice. It was shown before that PPARγ activation reduces colon cancer by decreasing nuclear β-catenin levels in *Apc*-wt mice and that PPARγ might be a possible tumor suppressor during tumor initiation by regulating β-catenin [84]. If loss of PPARγ accelerates tumor growth in *Kras* mutated mice *via* activation and stabilization of the APC-GSK-3β-β-catenin destruction complex followed by reduction of ß-catenin needs to be clarified.

In vitro, colorectal cancer cell lines harboring *KRAS* mutations were treated with Ras-inhibitors and PPARγ ligands alone or in combination. Combined therapy further reduced proliferation of CRC cells as compared to the single treatments. *In vivo* and *in vitro* results might provide a future option for a therapeutic approach by combining Ras-inhibitors with PPARγ ligands to further suppress tumorigenesis. Moreover, inhibition of Ras-signaling by PPARγ activation might be a putative new treatment for CRC patients to inhibit active Ras-signaling by circumventing the *RAS*-mutation and exploiting feedback loops downstream of the mutated components of the Ras-pathway. Future studies are needed to prove whether treatment of *Kras* mutated mice with the PPARγ ligand rosiglitazone is a new strategy to inhibit Ras-mediated tumorigenesis *in vivo*.

As mentioned in the introduction, *KRAS* mutations are often correlated with intrinsic unresponsiveness to therapies targeting the EGFR in CRC patients. Therefore, alternative treatments are needed. Originally, Dok1 was identified by us as a 37 kDa associated protein of Cav1 in MKN45 gastric cancer cells [57]. Mice treated with PPARγ ligands further revealed Dok1 as a possible target gene of PPARγ, which naturally inhibits Ras-signaling. Co-immunoprecipitation and proximity ligation assay corroborated physical interaction of Dok1 and PPARγ.

In 1997, Dok1 was first described as a 62 kDa, tyrosine-phosphorylated protein that binds the p120 Ras GTPase activating protein (RasGAP) [85, 86]. Furthermore, Dok1 was characterized as a tumor suppressor in lung cancer [87] and epithelial ovarian cancer [88]. Dok1p62, a member of the Dok (downstream of tyrosine kinases) family, contains different domains: the N-terminal PH (pleckstrin homology) domain, the PTB (phosphotyrosine binding) domain and a C-terminal domain containing tyrosine phosphorylation sites and proline-rich sequences. The PH domain is necessary for phospholipid binding and membrane targeting. The PTB domain of Dok1 is required for protein-protein interaction e.g. for the interaction with the active, tyrosine phosphorylated EGF-receptor (EGFR) [68]. Another important sequence is the C-terminal nuclear export sequence (NES), and it was shown that Dok1, besides its cytoplasmic localization, transits to the nucleus as a response to the current conditions of stimulation (e.g. starvation, adhesion, suspension, presence of growth factors). It was reported that nuclear Dok1 is not able to inhibit cellular proliferation due to active Ras-signaling *via* the EGF-receptor in the plasma membrane, because it is localized on the "wrong" cell compartment [64]. However, the role of nuclear Dok1 remained unknown and was explored in this thesis. Dok1 inhibits MAPKs, cellular proliferation and cell transformation, positively influences cell adhesion and migration and was shown to suppress lung cancer [64, 87].

To test the influence of the individual domains on proliferation and drug response in CRC cells, the NES and the PTB (RR) domain were mutated in full-length Dok1p62. Unlike observations made by others, neither Dok1p62WT nor Dok1p62NES or Dok1p62RR changed the basal proliferation rate of CRC cells and non-cancer Hek293T cells compared to EV transfected cells. A study from 2006 reported that proliferation is decreased by Dok1 in Hek293 cells. This effect is reversed by introduction of a NES mutation. Because of the nuclear localization, NES mutants are not able to inhibit EGFR at the plasma membrane and inhibition of proliferation is abrogated compared to wildtype Dok1p62 [64]. Maybe this discrepancy is due to the possibility that EGFR can be internalized and recycled or degraded *via* the endolysosomal system and even translocate to the nucleus depending on the cell type and condition. In this thesis, transiently transfected cells were used, whereas the study from 2006, Niu *et al.*[64] applied stable transfected clones. Nonetheless, Dok1p62 mutants

were still able to inhibit Ras-signaling in Hek293T and HCT116 cells as demonstrated by reduced ERK phosphorylation and c-Fos promoter activation. This effect might be due to Dok1 overexpression, which did not limit expression to the nucleus but also distributed Dok1 to the other cell compartments cytosol and insoluble membrane fractions as shown by subcellular fractionation. Ras-inhibition, however, was not efficient enough to diminish proliferation in CRC cells. Importantly, mutant Dok1p62NES, which is located preferably in the nucleus, and the PTB mutant, which is not able to bind to the EGFR in the membrane, augmented translocation of Dok1 and PPARγ into the nucleus. This translocation was accompanied by enhanced ligand-dependent PPARγ transcriptional activity. We therefore hypothesized that Dok1 might be a potent nuclear import shuttle for PPARγ. It was shown for MEK that PPARγ is exported from the nucleus by the MEK-PPARγ-complex [37]. Since we were able to demonstrate a physical interaction of PPARγ and Dok1, this might be true for nuclear import as well. In addition, inhibition of Ras-signaling could decrease the formation of the MEK-PPARγ complex and thus promote PPARγ's nuclear import. Future studies have to reveal how nuclear import of PPARγ is mediated by Dok1 and which domains or phosphorylation sites are necessary for Dok1 and PPARγ interaction. Furthermore, Dok1 can activate PPARγ indirectly by inhibition of its Ras-dependent phosphorylation. This link between Dok1 and PPARγ was shown in the white adipose tissue of mice. Mice lacking Dok1 showed increased Ras-signaling followed by phosphorylation by ERK1/2 and inactivation of PPARγ [89].

At least, three different isoforms of Dok1 have been described: p62[Dok1], p19-22[Dok1] and p44[Dok1]. The p62 isoform comprises the full-length protein. The p44 isoform lacks the PH domain and the p19-p22 isoform the PTB domain and the C-Terminus [57]. In CRC cell lines only the Dok1p44 protein was found using a C-terminal antibody. Besides that, a prominent band at 37 kDa was detected with an antibody raised against the N-Terminus of Dok1, but not with an antibody raised against the C-Terminus. This indicates that a truncated p37 isoform is present which lacks the C-Terminus and therefore the NES domain, thus explaining its favored nuclear localization. This isoform might be similar to one isoform found in chronic lymphocytic leukemia (CLL). The authors found the *DOK1* gene to be mutated and therefore truncated at the C-terminal end so that the NES is absent. This led to an approximately 33-35 kDa nuclear protein which was unable to inhibit MAPKs unlike the cytoplasmic Dok1p62 [67]. Although there was no mutation detected in CRC cells, other protein modifications might lead to truncation of Dok1p62 followed by impaired ability to inhibit Ras-signaling. Another isoform of Dok1, Dok1p44, is a result of alternative translation initiation due to acetylation at the N-Terminus. As a result of the missing PH domain, Dok1p44 is distributed perinuclear [65]. In this study, the isoforms Dok1p62, p44 and p33 were cloned,

expressed and analyzed regarding their function on proliferation, PPARγ activation and localization in CRC cell lines.

According to the literature, Dok1p44, lacking the PH domain, should not be able to inhibit Ras-signaling because it is not recruited to the membrane to inhibit Ras/MAPK [90]. The Dok1p33 isoform is lacking the nuclear export sequence (NES), was found to be mainly distributed to the nucleus and is therefore unable to inhibit MAPKs at the membrane as well. According to these assumptions, transient transfection of Dok1p62, p44 and p33 in CRC cells as well as in Hek293T did not result in a reduced proliferation rate.

Furthermore, it was shown by others that Dok1 is able to homodimerize with other Dok family members, with itself and even with overexpressed Dok *via* residue Tyrosine 146, which is located between the PH and the PTB domain. This Tyrosine 146 interacts with the PTB domain and it was shown that dimerization of Dok is important for its function [91, 92]. All of the cells used in this thesis expressed endogenous Dok1 and the interacting residue Tyrosine 146 is present in all three Dok1 isoforms. The overexpressing Dok1 mutants and isoforms might therefore homodimerize with each other or the endogenous Dok1. Thus, this interaction might support or even inhibit Dok1's function apart from its mutations or isoforms.

In sum, Dok1 was able to promote PPARγ's activity. This was dependent on the cell type and the *RAS*-status of the cells. In HCT116 and Hek293T cells, which had low Ras-activity or wildtype Ras, Dok1 had positive effects on PPARγ activity and enhanced its sensitivity to ligand stimulation. On the contrary, in SW480 cells, with both *KRAS* alleles mutated, Dok1 exerted no effects. It was shown for scaffold proteins (i.e. proteins that bind different members of signaling pathways) that too high or too low concentrations have the same effect, meaning that the optimal concentration of proteins lies in between [93]. In some cells, overexpression of Dok1 might promote PPARγ's activity. HCT116 cells are expressing high levels of the scaffold protein and the Ras-inhibitor Caveolin-1. Cav1 was found by us to interact with both Dok1 and PPARγ to build a trimolecular complex [57]. Cav1 might therefore bind high levels of Dok1 at the membrane and promote PPARγ's interaction with Dok1 and its transfer to the nucleus in HCT116 cells. In SW480 cells, the absence of Cav1 might instead trap the PPARγ-Dok1-complex at its proposed membranal localization. Interaction of Dok1 and PPARγ could then have the opposing effect, which is to keep PPARγ at the membrane/cytosol and inhibit its activity. Further studies have to reveal if Cav1 really has this high importance for the interaction of Dok1 with PPARγ.

As PPARγ activity did not necessarily result in growth inhibition (as seen in Hek293T cells) there might be other possible roles for PPARγ in additional cellular processes like e.g. senescence or differentiation. If Dok1 promotes PPARγ *via* direct interaction and nuclear import or if this effect is due to Dok1's ability to inhibit Ras-signaling needs to be clarified.

Discussion

Not much is known about the function of Dok1 in colorectal cancer patients. To this end, tissue microarrays of CRC patients and normal colon tissue were analyzed regarding their Dok1 expression. Advanced tumor staging correlated with decreased Dok1 expression, indicating that Dok1 is a possible tumor suppressor in CRC. According to the literature, gene expression of Dok1 was lost by hypermethylation in tumors like head and neck cancer, lung cancer and Burkitt's lymphoma [94]. Dok1 was further characterized as a tumor suppressor in epithelial ovarian cancer (EOC). On the contrary, *DOK1* was found to be hypermethylated, but this DNA-modification does not correlate with its suppression. Interestingly, Dok1 overexpression in tumor tissue results in an increased progression-free survival of patients and enhances sensitivity to cisplatin treatment in EOC cells *in vitro.* [88] This *in vivo* result is similar to the observation that Dok1 sensitized CRC cells to PPARγ ligand treatment *in vitro* and revealed a possible role for Dok1 as sensitizer for therapy and possible response prediction marker. Whether *DOK1* is hypermethylated in colon cancer and if Dok1 expression might be a useful marker to determine therapeutic outcome needs to be determined.

Taken together, these results showed that the tumor suppressor Dok1 is a suitable inhibitor of Ras-signaling even in *KRAS* mutated cell lines and a potential sensitizer for PPARγ therapy. It has to be determined if Dok1 might also be a possible new marker for therapy response in CRC patients.

In sum, this thesis characterized the signaling crosstalk of PPARγ and the Ras-pathway *in vivo* and their possible role in colon tumorigenesis. The *Apc^{min/+}* mouse model revealed a LOF of PPARγ in correlation with a GOF of Ras-signature in tumor tissue. This pattern was reversed by PPARγ activation, which decreased Ras-signaling and inhibited tumorigenesis. The important role of PPARγ in K-Ras-mediated tumorigenesis was corroborated by the *KRAS* G12V/PPARγ-deficient mouse model that displayed a more severe phenotype than *KRAS* G12V transgenic mice with functional wildtype PPARγ. Ras-mediated repression of PPARγ either through its phosphorylation or its nuclear export promotes CRC tumorigenesis. On the other hand, PPARγ was able to inhibit active signaling in *KRAS*-mutated human CRC cells through activation of endogenous Ras-inhibitors Dok1 and Cav1. These tumor suppressors were found to be decreased in colon cancer, but when present they are able to sensitize the cells for PPARγ ligands [57] or cisplatin [88]. Activation of PPARγ might therefore be a putative new approach to treat CRC patients that do not respond to anti-EGFR therapy (e.g. cetuximab) due to activating *RAS*-mutations (Fig. 54).

Figure 54 Correlation between the Ras/WNT- and the Cav1/PPARγ-signaling in CRC copied from Friedrich *et al.* [59]. Legend: Blue-tumor inhibitors; Red-tumor promoters; Blue arrows-activation; Red arrows-inhibition; Black arrows-translocation of proteins. Cav1 and APC wt decrease the cellular proliferation by inhibiting β-catenin's nuclear import and Ras in normal tissue. Deficiency of active Ras-signaling allows PPARγ to inhibit β-catenin and to activate anti-proliferative genes like *Dok1*, *Cav1* or *Pparγ* itself, which in turn inhibit Ras *via* a negative feedback loop. In tumor tissue, loss of Cav1 and/or APC through mutation lead to nuclear translocation of β-catenin followed by inhibition of PPARγ target genes and activation of pro-proliferative genes like *Cyclind1* and *Myc.* Moreover, loss of Cav1 enhances WNT- and Ras-signaling and accumulation of mutations in the Ras-pathway further enhances its activity. Active Ras-signaling promotes cytosolic sequestration of PPARγ *via* MEK1/2 and thus inhibits PPARγ's transcriptional activity in the nucleus. Inhibition of Ras-signaling by the EGFR/MEK-inhibitors erlotinib and U0126 combined with activation of PPARγ by rosiglitazone may be a new approach to treat CRC patients which do not respond to anti-EGFR therapy.

5. References

1.   Zavoral M, Suchanek S, Zavada F, et al. Colorectal cancer screening in Europe. World J Gastroenterol 2009;15:5907-15.

2.   Davies RJ, Miller R, Coleman N. Colorectal cancer screening: prospects for molecular stool analysis. Nat Rev Cancer 2005;5:199-209.

3.   Compton CC. Colorectal carcinoma: diagnostic, prognostic, and molecular features. Mod Pathol 2003;16:376-88.

4.   Edge SB, Compton CC. The American Joint Committee on Cancer: the 7th edition of the AJCC cancer staging manual and the future of TNM. Ann Surg Oncol 2010;17:1471-4.

5.   Chan AT, Giovannucci EL. Primary prevention of colorectal cancer. Gastroenterology 2010;138:2029-2043 e10.

6.   Derry MM, Raina K, Agarwal C, et al. Identifying molecular targets of lifestyle modifications in colon cancer prevention. Front Oncol 2013;3:119.

7.   Westbrook AM, Szakmary A, Schiestl RH. Mechanisms of intestinal inflammation and development of associated cancers: lessons learned from mouse models. Mutat Res 2010;705:40-59.

8.   Round JL, Mazmanian SK. The gut microbiota shapes intestinal immune responses during health and disease. Nat Rev Immunol 2009;9:313-23.

9.   Clayburgh DR, Shen L, Turner JR. A porous defense: the leaky epithelial barrier in intestinal disease. Lab Invest 2004;84:282-91.

10.   Heyer J, Yang K, Lipkin M, et al. Mouse models for colorectal cancer. Oncogene 1999;18:5325-33.

11.   Cunningham D, Atkin W, Lenz HJ, et al. Colorectal cancer. Lancet 2010;375:1030-47.

12.   Geigl JB, Obenauf AC, Schwarzbraun T, et al. Defining 'chromosomal instability'. Trends Genet 2008;24:64-9.

13.   Rao CV, Yamada HY. Genomic instability and colon carcinogenesis: from the perspective of genes. Front Oncol 2013;3:130.

14.   Lynch HT, Shaw MW, Magnuson CW, et al. Hereditary factors in cancer. Study of two large midwestern kindreds. Arch Intern Med 1966;117:206-12.

15.   Green SE, Bradburn DM, Varma JS, et al. Hereditary non-polyposis colorectal cancer. Int J Colorectal Dis 1998;13:3-12.

16.   Galiatsatos P, Foulkes WD. Familial adenomatous polyposis. Am J Gastroenterol 2006;101:385-98.

17.   Fearon ER, Vogelstein B. A genetic model for colorectal tumorigenesis. Cell 1990;61:759-67.

18.   Arends JW. Molecular interactions in the Vogelstein model of colorectal carcinoma. J Pathol 2000;190:412-6.

19.   Al-Sohaily S, Biankin A, Leong R, et al. Molecular pathways in colorectal cancer. J Gastroenterol Hepatol 2012.

20.   Pino MS, Chung DC. The chromosomal instability pathway in colon cancer. Gastroenterology 2010;138:2059-72.

21.   Kanthan R, Senger JL, Kanthan SC. Molecular events in primary and metastatic colorectal carcinoma: a review. Patholog Res Int 2012;2012:597497.

22.   Issa JP. Colon cancer: it's CIN or CIMP. Clin Cancer Res 2008;14:5939-40.

23.   Noffsinger AE. Serrated polyps and colorectal cancer: new pathway to malignancy. Annu Rev Pathol 2009;4:343-64.

24.   Bennecke M, Kriegl L, Bajbouj M, et al. Ink4a/Arf and oncogene-induced senescence prevent tumor progression during alternative colorectal tumorigenesis. Cancer Cell 2010;18:135-46.

25.   Prenen H, Tejpar S, Van Cutsem E. New strategies for treatment of KRAS mutant metastatic colorectal cancer. Clin Cancer Res 2010;16:2921-6.

26.   Mirzoeva OK, Das D, Heiser LM, et al. Basal subtype and MAPK/ERK kinase (MEK)-phosphoinositide 3-kinase feedback signaling determine susceptibility of breast cancer cells to MEK inhibition. Cancer Res 2009;69:565-72.

27.   Burgermeister E, Seger R. PPARgamma and MEK Interactions in Cancer. PPAR Res 2008;2008:309469.

28.   Pearson G, Robinson F, Beers Gibson T, et al. Mitogen-activated protein (MAP) kinase pathways: regulation and physiological functions. Endocr Rev 2001;22:153-83.

29.   Chuderland D, Seger R. Protein-protein interactions in the regulation of the extracellular signal-regulated kinase. Mol Biotechnol 2005;29:57-74.

30.   McCubrey JA, Steelman LS, Chappell WH, et al. Roles of the Raf/MEK/ERK pathway in cell growth, malignant transformation and drug resistance. Biochim Biophys Acta 2007;1773:1263-84.

31.   Janssen KP, Abal M, El Marjou F, et al. Mouse models of K-ras-initiated carcinogenesis. Biochim Biophys Acta 2005;1756:145-54.

32.   Arrington AK, Heinrich EL, Lee W, et al. Prognostic and Predictive Roles of KRAS Mutation in Colorectal Cancer. Int J Mol Sci 2012;13:12153-68.

33.   Zlobec I, Kovac M, Erzberger P, et al. Combined analysis of specific KRAS mutation, BRAF and microsatellite instability identifies prognostic subgroups of sporadic and hereditary colorectal cancer. Int J Cancer 2010;127:2569-75.

34.   Burgermeister E, Seger R. MAPK kinases as nucleo-cytoplasmic shuttles for PPARgamma. Cell Cycle 2007;6:1539-48.

35.   van Beekum O, Fleskens V, Kalkhoven E. Posttranslational modifications of PPAR-gamma: fine-tuning the metabolic master regulator. Obesity (Silver Spring) 2009;17:213-9.

36.   Murphy GJ, Holder JC. PPAR-gamma agonists: therapeutic role in diabetes, inflammation and cancer. Trends Pharmacol Sci 2000;21:469-74.

37.   Burgermeister E, Chuderland D, Hanoch T, et al. Interaction with MEK causes nuclear export and downregulation of peroxisome proliferator-activated receptor gamma. Mol Cell Biol 2007;27:803-17.

38.   Auwerx J. Nuclear receptors. I. PPAR gamma in the gastrointestinal tract: gain or pain? Am J Physiol Gastrointest Liver Physiol 2002;282:G581-5.

39.   Voutsadakis IA. Peroxisome proliferator-activated receptor gamma (PPARgamma) and colorectal carcinogenesis. J Cancer Res Clin Oncol 2007;133:917-28.

40.   Ogino S, Shima K, Baba Y, et al. Colorectal cancer expression of peroxisome proliferator-activated receptor gamma (PPARG, PPARgamma) is associated with good prognosis. Gastroenterology 2009;136:1242-50.

41.   Pancione M, Forte N, Sabatino L, et al. Reduced beta-catenin and peroxisome proliferator-activated receptor-gamma expression levels are associated with colorectal cancer metastatic progression: correlation with tumor-associated macrophages, cyclooxygenase 2, and patient outcome. Hum Pathol 2009;40:714-25.

42.   Lehrke M, Lazar MA. The many faces of PPARgamma. Cell 2005;123:993-9.

43.   Cohen AW, Hnasko R, Schubert W, et al. Role of caveolae and caveolins in health and disease. Physiol Rev 2004;84:1341-79.

44. Burgermeister E, Xing X, Rocken C, et al. Differential expression and function of caveolin-1 in human gastric cancer progression. Cancer Res 2007;67:8519-26.

45. Bender FC, Reymond MA, Bron C, et al. Caveolin-1 levels are down-regulated in human colon tumors, and ectopic expression of caveolin-1 in colon carcinoma cell lines reduces cell tumorigenicity. Cancer Res 2000;60:5870-8.

46. Rodel F, Capalbo G, Rodel C, et al. Caveolin-1 as a prognostic marker for local control after preoperative chemoradiation therapy in rectal cancer. Int J Radiat Oncol Biol Phys 2009;73:846-52.

47. Goetz JG, Lajoie P, Wiseman SM, et al. Caveolin-1 in tumor progression: the good, the bad and the ugly. Cancer Metastasis Rev 2008;27:715-35.

48. Polakis P. The adenomatous polyposis coli (APC) tumor suppressor. Biochim Biophys Acta 1997;1332:F127-47.

49. Hanson CA, Miller JR. Non-traditional roles for the Adenomatous Polyposis Coli (APC) tumor suppressor protein. Gene 2005;361:1-12.

50. Fearon ER. Molecular genetics of colorectal cancer. Annu Rev Pathol 2011;6:479-507.

51. McCart AE, Vickaryous NK, Silver A. Apc mice: models, modifiers and mutants. Pathol Res Pract 2008;204:479-90.

52. Taketo MM. Mouse models of gastrointestinal tumors. Cancer Sci 2006;97:355-61.

53. Karim BO, Huso DL. Mouse models for colorectal cancer. Am J Cancer Res 2013;3:240-50.

54. Kwong LN, Dove WF. APC and its modifiers in colon cancer. Adv Exp Med Biol 2009;656:85-106.

55. Cormier RT, Hong KH, Halberg RB, et al. Secretory phospholipase Pla2g2a confers resistance to intestinal tumorigenesis. Nat Genet 1997;17:88-91.

56. Crist RC, Roth JJ, Lisanti MP, et al. Identification of Mom12 and Mom13, two novel modifier loci of Apc (Min) -mediated intestinal tumorigenesis. Cell Cycle 2011;10:1092-9.

57. Burgermeister E, Friedrich T, Hitkova I, et al. The Ras Inhibitors Caveolin-1 and Docking Protein 1 Activate Peroxisome Proliferator-Activated Receptor {gamma} through Spatial Relocalization at Helix 7 of Its Ligand-Binding Domain. Mol Cell Biol 2011;31:3497-510.

58. Janssen KP, el-Marjou F, Pinto D, et al. Targeted expression of oncogenic K-ras in intestinal epithelium causes spontaneous tumorigenesis in mice. Gastroenterology 2002;123:492-504.

59. Friedrich T, Richter B, Gaiser T, et al. Deficiency of caveolin-1 in Apcmin/+ mice promotes colorectal tumorigenesis. Carcinogenesis 2013.

60. Schlemper RJ, Riddell RH, Kato Y, et al. The Vienna classification of gastrointestinal epithelial neoplasia. Gut 2000;47:251-5.

61. Yeh JJ, Routh ED, Rubinas T, et al. KRAS/BRAF mutation status and ERK1/2 activation as biomarkers for MEK1/2 inhibitor therapy in colorectal cancer. Mol Cancer Ther 2009;8:834-43.

62. Brandi G, Tavolari S, De Rosa F, et al. Antitumoral efficacy of the protease inhibitor gabexate mesilate in colon cancer cells harbouring KRAS, BRAF and PIK3CA mutations. PLoS One 2012;7:e41347.

63. He W, Barak Y, Hevener A, et al. Adipose-specific peroxisome proliferator-activated receptor gamma knockout causes insulin resistance in fat and liver but not in muscle. Proc Natl Acad Sci U S A 2003;100:15712-7.

64.   Niu Y, Roy F, Saltel F, et al. A nuclear export signal and phosphorylation regulate Dok1 subcellular localization and functions. Mol Cell Biol 2006;26:4288-301.

65.   Kobayashi R, Patenia R, Ashizawa S, et al. Targeted mass spectrometric analysis of N-terminally truncated isoforms generated via alternative translation initiation. FEBS Lett 2009;583:2441-5.

66.   Hubert P, Ferreira V, Debre P, et al. Molecular cloning of a truncated p62Dok1 isoform, p22Dok(del). Eur J Immunogenet 2000;27:145-8.

67.   Lee S, Roy F, Galmarini CM, et al. Frameshift mutation in the Dok1 gene in chronic lymphocytic leukemia. Oncogene 2004;23:2287-97.

68.   Zhang Y, Yan Z, Farooq A, et al. Molecular basis of distinct interactions between Dok1 PTB domain and tyrosine-phosphorylated EGF receptor. J Mol Biol 2004;343:1147-55.

69.   Sodir NM, Chen X, Park R, et al. Smad3 deficiency promotes tumorigenesis in the distal colon of ApcMin/+ mice. Cancer Res 2006;66:8430-8.

70.   Zeng Q, Phukan S, Xu Y, et al. Tgfbr1 haploinsufficiency is a potent modifier of colorectal cancer development. Cancer Res 2009;69:678-86.

71.   D'Abaco GM, Whitehead RH, Burgess AW. Synergy between Apc min and an activated ras mutation is sufficient to induce colon carcinomas. Mol Cell Biol 1996;16:884-91.

72.   Luo F, Brooks DG, Ye H, et al. Mutated K-ras(Asp12) promotes tumourigenesis in Apc(Min) mice more in the large than the small intestines, with synergistic effects between K-ras and Wnt pathways. Int J Exp Pathol 2009;90:558-74.

73.   Couet J, Sargiacomo M, Lisanti MP. Interaction of a receptor tyrosine kinase, EGF-R, with caveolins. Caveolin binding negatively regulates tyrosine and serine/threonine kinase activities. J Biol Chem 1997;272:30429-38.

74.   Mercier I, Jasmin JF, Pavlides S, et al. Clinical and translational implications of the caveolin gene family: lessons from mouse models and human genetic disorders. Lab Invest 2009;89:614-23.

75.   Roy UK, Henkhaus RS, Ignatenko NA, et al. Wild-type APC regulates caveolin-1 expression in human colon adenocarcinoma cell lines via FOXO1a and C-myc. Mol Carcinog 2008;47:947-55.

76.   Sarraf P, Mueller E, Jones D, et al. Differentiation and reversal of malignant changes in colon cancer through PPARgamma. Nat Med 1998;4:1046-52.

77.   Yamaguchi K, Cekanova M, McEntee MF, et al. Peroxisome proliferator-activated receptor ligand MCC-555 suppresses intestinal polyps in ApcMin/+ mice via extracellular signal-regulated kinase and peroxisome proliferator-activated receptor-dependent pathways. Mol Cancer Ther 2008;7:2779-87.

78.   McAlpine CA, Barak Y, Matise I, et al. Intestinal-specific PPARgamma deficiency enhances tumorigenesis in ApcMin/+ mice. Int J Cancer 2006;119:2339-46.

79.   Lefebvre AM, Chen I, Desreumaux P, et al. Activation of the peroxisome proliferator-activated receptor gamma promotes the development of colon tumors in C57BL/6J-APCMin/+ mice. Nat Med 1998;4:1053-7.

80.   Yang K, Fan KH, Lamprecht SA, et al. Peroxisome proliferator-activated receptor gamma agonist troglitazone induces colon tumors in normal C57BL/6J mice and enhances colonic carcinogenesis in Apc1638 N/+ Mlh1+/- double mutant mice. Int J Cancer 2005;116:495-9.

81.   Niho N, Takahashi M, Shoji Y, et al. Dose-dependent suppression of hyperlipidemia and intestinal polyp formation in Min mice by pioglitazone, a PPAR gamma ligand. Cancer Sci 2003;94:960-4.

82.   Johnson L, Mercer K, Greenbaum D, et al. Somatic activation of the K-ras oncogene causes early onset lung cancer in mice. Nature 2001;410:1111-6.

83.   Jen J, Powell SM, Papadopoulos N, et al. Molecular determinants of dysplasia in colorectal lesions. Cancer Res 1994;54:5523-6.

84.   Girnun GD, Smith WM, Drori S, et al. APC-dependent suppression of colon carcinogenesis by PPARgamma. Proc Natl Acad Sci U S A 2002;99:13771-6.

85.   Yamanashi Y, Baltimore D. Identification of the Abl- and rasGAP-associated 62 kDa protein as a docking protein, Dok. Cell 1997;88:205-11.

86.   Carpino N, Wisniewski D, Strife A, et al. p62(dok): a constitutively tyrosine-phosphorylated, GAP-associated protein in chronic myelogenous leukemia progenitor cells. Cell 1997;88:197-204.

87.   Berger AH, Niki M, Morotti A, et al. Identification of DOK genes as lung tumor suppressors. Nat Genet 2010;42:216-23.

88.   Mercier PL, Bachvarova M, Plante M, et al. Characterization of DOK1, a candidate tumor suppressor gene, in epithelial ovarian cancer. Mol Oncol 2011;5:438-53.

89.   Hosooka T, Noguchi T, Kotani K, et al. Dok1 mediates high-fat diet-induced adipocyte hypertrophy and obesity through modulation of PPAR-gamma phosphorylation. Nat Med 2008;14:188-93.

90.   Zhao M, Schmitz AA, Qin Y, et al. Phosphoinositide 3-kinase-dependent membrane recruitment of p62(dok) is essential for its negative effect on mitogen-activated protein (MAP) kinase activation. J Exp Med 2001;194:265-74.

91.   Boulay I, Nemorin JG, Duplay P. Phosphotyrosine binding-mediated oligomerization of downstream of tyrosine kinase (Dok)-1 and Dok-2 is involved in CD2-induced Dok phosphorylation. J Immunol 2005;175:4483-9.

92.   Songyang Z, Yamanashi Y, Liu D, et al. Domain-dependent function of the rasGAP-binding protein p62Dok in cell signaling. J Biol Chem 2001;276:2459-65.

93.   Good MC, Zalatan JG, Lim WA. Scaffold proteins: hubs for controlling the flow of cellular information. Science 2011;332:680-6.

94.   Saulnier A, Vaissiere T, Yue J, et al. Inactivation of the putative suppressor gene DOK1 by promoter hypermethylation in primary human cancers. Int J Cancer 2012;130:2484-94.

6. Abbreviations

5-FU	5-Fluorouracil
AB	Antibody
ACF	Aberrant crypt foci
AJCC	American Joint Comittee on Cancer
APC	Adenomatous polyposis coli
ATCC	American Type Culture Collection
ATP	Adenosine triphosphate
BCA	Bicinchoninic acid
bp	Base pairs
BRAF	v-Raf murine sarcoma viral oncogene homolog B1
Caco-2	Human colorectal adenocarcinoma cell line
Cav-1	Caveolin-1
cDNA	Complementary desoxyribonucleic acid
CIMP	CpG island methylator phenotype
CIN	Chromosomal instability
CO_2	Carbon dioxide
CoIP	Coimmunoprecipitation
CpG	Cytosine-phosphate-Guanine
CRC	Colorectal cancer
Cre	Cre recombinase, enzyme
Ct	Cycle threshold
C-Terminus	Carboxy-Terminus
Cy3	Cyanine dye
DAB	3,3'-Diaminobenzidine
DAPI	4,6-Diamidino-2-phenylindol dihydrochlorid
DH5α	*Escherichia coli* strain
DNA	Desoxyribonucleic acid
dNTP	Desoxyribonucleosidetriphosphate
DTT	Dithiothreitol
ECL	Enhanced chemiluminescence

EGF	Epidermal growth factor
EGFR	Epidermal growth factor receptor
ERK	Extracellular signal-regulated kinase
EtOH	Ethanol
FAP	Familial adenomatous polyposis
FCS	Fetal calf serum
FL/FL	Floxed/floxed
FOLFIRI	Folinic acid, Fluorouracil, Irinotecan
FOLFOX	Folinic acid, Fluorouracil, Oxaliplatin
GDP	Guanosine diphosphate
GI	Gastrointestinal
GOF	Gain of function
GSEA	Gene set enrichment analysis
GTP	Guanosine triphosphate
H&E	Hematoxylin & Eosin
HCl	Hydrochloric acid
HCT116	Human colorectal carcinoma cell line
hEGF	Human epidermal growth factor
Hek293T	Human embryonic kidney, T-Antigen
HNPCC	Hereditary non-polyposis coli
HRP	Horseradish peroxidase
HT-29	Human colorectal adenocarcinoma cell line
IB	Immunoblotting
IBD	Inflammatory bowel disease
IHC	Immunohistochemistry
kb	Kilo base
kDa	Kilo Dalton
KO	Knockout
K-Ras	Kirsten rat sarcoma viral oncogene homolog
LOF	Loss of function
LOH	Loss of heterozygosity

Abbreviations

M	Molar
mA	Milliampere
MALDI-MS	Matrix Assisted Laser Desorption Ionization-Mass Spectrometry
MAPK	Mitogen activated protein kinase
MEK	Mitogen-activated protein kinase kinase
min	Multiple intestinal metaplasia
MMR	Mismatch repair
MOM	Modifier of min
mRNA	Messenger RNA
MSI	Microsatellite instability
MSS	Microsatellite stable
MTT	3-(4,5-Dimethylthiazol-2-yl)-2,5-diphenyltetrazolium bromide
mut	Mutant
NES	Nuclear export signal
NT	Normal tissue
N-Terminus	Amino-Terminus
PBS	Phosphate buffered saline
PCR	Polymerase chain reaction
PFA	Paraformaldehyde
PH	Pleckstrin homology
PLA	Proximity ligation assay
PPARγ	Peroxisome proliferator activated receptor gamma
PPRE	PPAR responsive element
pT	pTarget empty vector
PTB	Phosphotyrosine binding domain
PTEN	Phosphatase and tensin homolog
RAF	Rat fibrosarcoma, oncogene
RAS	Rat sarcoma, oncogene
RLU	Relative light units
RNA	Ribonucleic acid
Rosi	Rosiglitazone
rpm	Revolutions per time
RT	Room temperature
RT-qPCR	Real time-quantitative PCR

Abbreviations

RXR	Retinoic X receptor
SCF	Subcellular fractionation
SDS-PAGE	Sodium dodecyl sulfate-polyacrylamide gel electrophoresis
shRNA	Short hairpin RNA
siRNA	Small interfering RNA
SRE	Serum response element
SW480	Human colorectal adenocarcinoma cell line
SYBR	DNA intercalating cyanine dye
TAF-1	Transactivation function-1
TMA	Tissue microarray
TNM	Tumors-Nodes-Metastasis; staging system
TOP10	*Escherichia coli* strain
TRIS	Tris(hydroxymethyl)-aminomethan
TU	Tumor tissue
UICC	International Unit Against Cancer
V	Volt
v/v	Volume per volume
VEGF	Vascular endothelial growth factor
w/v	Weight per volume
WB	Western blot
WNT	Wingless-type MMTV integration site family
WT, wt	Wildtype
X-Gal	5-bromo-4-chloro-indolyl-β-D-galactopyranoside

7. Appendices

Cloning and mutagenesis of Dok1

DOK1 docking protein 1, 62kDa (downstream of tyrosine kinase 1) (human)

→Start Dok1p62, Dok1p33

```
             gaattcatggacgga gcagcggatg gaagggccgc ttttttgca
  61 gagtcagcgc tttgggacca agaggtggag gaagacctgg gccgtgctct acccggccag
 121 tccccacggc gtagcgcggc tcgagttctt tgaccataag gggtcgagct ctgggggtgg
 181 ccgagggagc tcgcgccgcc tggactgcaa agtgatccgt ctggctgagt gtgtgagtgt
 241 ggcccccgtc accgtggaga cccccccctga gcccggcgcc actgccttcc gcctggacac
 301 tgctcagcgc tcgcacctgc tggcggccga cgcgccgtcc agtgcagcct gggtgcagac
 361 gctgtgccga aacgcctttc cgaaaggcag ctggactctg cgcctaccg ataacccacc
```

→Start Dok1p44

```
 421 taagctttct gccctggaga tgctggagaa ctccttgtac agccctacct gggaaggatc
 481 ccaattctgg gtaacggtgc agaggactga ggccgccgag cgctgtggcc tgcatggctc
 541 ctacgtgctg agggtggagg ctgaaaggct gactctcctg accgtggggg cccagagtca
```

→R207A mutation site

```
 601 gatactggag ccactcctgt cctggcccta cactctgttg cgtcgctatg gccgggacaa
```

→R222A mutation site

```
 661 ggtcatgttc tctttcgagg ccggccgccg ctgcccctca ggccctggaa ccttcacctt
 721 ccagacggca cagggaaatg acatcttcca ggcagttgag actgccatcc accggcagaa
 781 ggcccaggga aaggccggac aggggcacga tgttctcaga gctgactccc atgaagggga
```

→Stop Dok1p32

```
 841 ggtggcagag gggaagttgc cttccccacc tggcccccaa gagctcctcg acagtccccc
 901 agccctgtat gctgagccct tagactccct gcgcattgct ccatgccctt cccaggactc
 961 cctatactca gaccccttgg acagcacgtc tgctcaggca ggagagggag tacaacggaa
```

→NES mutation site

```
1021 gaaacctctc tattgggact tgtatgagca tgcgcagcag cagttgctga aggccaagct
1081 gacagacccc aaagaggatc ccatctatga tgaacctgag ggcctggccc cagtccctcc
1141 ccagggcctt tatgatctgc ctcgggagcc caaggatgca tggtggtgcc aagctcgggt
1201 gaaggaggag ggctatgagc tcccctacaa ccctgccact gatgactacg ctgtgccacc
1261 ccctcggagc acaaagcccc tccttgctcc caagccccag ggcccagcct ccctgaacc
1321 tggtactgca actggcagtg gcatcaaaag ccacaactca gccctgtaca gccaggtcca
1381 gaagagcggg gcctcaggga ctgggactg tgggctctct agagtaggga ctgacaagac
```

→Stop Dok1p62, Dok1p44

```
1441 tggggtcaagtcagagggctctacctgagaattc
```
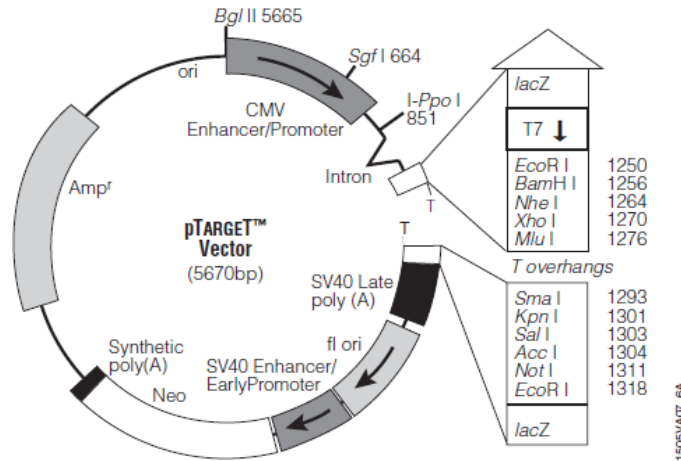
pTarget^{TM} expression vector (from Promega).

Dok1p62, p44 and p33 were inserted *via EcoRI* (<u>GAATTC</u>) digestion

Student's *t*-test

(from Bortz, Döring: Forschungsmethoden und Evaluation, 3. Auflage, 2005, Springer Medizin Verlag Heidelberg)

The Student's *t*-test was used to compare the means of two different populations like e.g. NT *versus* TU or untransfected *versus* transfected cells. Its basis is the definition of a null hypothesis, saying that the means of the different populations are equal. For significant differences, H$_0$ needs to be rejected ($\bar{x}_1, \bar{x}_2$: mean of the samples)

$$H_0: \bar{x}_1 = \bar{x}_2$$

The Student's *t*-test depends on the sample size n (degrees of freedom, $df = n_1 + n_2 - 2$) and on the standard error of the samples $\hat{\sigma}^2$ (variances). For use of the *t*-test in this thesis, one has to assume that the variances are equal for the two groups and that the values are normally distributed ($\hat{\sigma}_{(\bar{x}1-\bar{x}2)}$: standard error of the means). The *t*-value is calculated using the formula

$$t = \frac{\bar{x}_1 - \bar{x}_2}{\hat{\sigma}_{(\bar{x}1-\bar{x}2)}}$$

The significance can then be determined using the *t*-table and the df- and t-value. If the null hypothesis can be rejected, the differences between the two populations (x_1, x_2) did not occur by chance. The probability to incorrectly reject the null hypothesis should be less than 5 % (*p<0.05).

The statistical analysis was done using the *t*-test function of Microsoft Excel.

Acknowledgment

First I would like to thank Prof. Matthias Ebert, Prof. Roland Schmid and the head of the SFB824 (DFG) Prof. Markus Schwaiger for giving me the opportunity to perform this work at the 2nd Medical Department, Klinikum rechts der Isar of the TUM.

I would also like to thank my supervisors and examiners of this thesis PD Dr. rer. nat. Klaus-Peter Janssen and Prof. Jürgen Scheurle.

I especially want to thank my mentor and head of the laboratory Dr. rer. nat. Elke Burgermeister for the development of the scientific research concept, the excellent supervision and scientific discussions.

Furthermore, I would like to thank the pathologists PD Dr. med. Timo Gaiser (Universitätsmedizin Mannheim) and Prof. Christoph Röcken (Universität Kiel) for providing and examination of the CRC tissue samples.

I further want to thank the coworkers from my working groups in Munich and Mannheim for help and suggestions and for providing a friendly working atmosphere. I especially want to mention Ivana Hitkova, who managed the move to Mannheim with me. I also want to thank the medical students Birgit Richter, Philip Weidner and Christian Weber for their assistance in microscopic analysis of the mouse models as well as PD Dr. sc. hum. Christel Weiss (Universitätsmedizin Mannheim) for SAS analysis of the APC-mouse model.

I also would like to thank my family and friends for their support and encouragement over the years. They played an important role in the accomplishment of this thesis.

Curriculum Vitae

<u>Persönliche Daten</u>

Name:	Teresa Maria Friedrich
Geburtsdatum:	26.08.1983
Geburtsort:	Gräfelfing (München)

<u>Bildungsgang</u>

01/2010-08/2013   **Promotion** an der Chirurgischen Klinik und Poliklinik und der II. Medizinischen Klinik und Poliklinik, Klinikum rechts der Isar, Technische Universität München

Thema der Dissertation: „Ras-driven mouse models of colorectal cancer: Interaction of MAPKs with the nuclear receptor PPARγ"

12/2008-07/2009   **Praktikum** am Children's Medical Research Institute, Cell Transformation Unit, Westmead (Sydney), Australien

Thema der Arbeit : „Functions of p53 during genotoxic stress"

09/2008-10/2008   **Wissenschaftliche Mitarbeit** in der AG Prof. Dr. K. Jung, molekulare Mikrobiologie, LMU München

10/2007-07/2008   **Diplomarbeit** bei Prof. Dr. H. Jung, Bakterielle Physiologie und Biochemie, LMU München

Thema der Diplomarbeit: „Funktionen des Zwei-Komponenten-Systems CbrA/CbrB in *Pseudomonas putida KT2440*"

09/2006-10/2006   **Forschungspraktikum** bei Prof. Dr. H. Jung, Bakterielle Physiologie und Biochemie, LMU München

Thema der Arbeit: „Intramolekulare Crosslinking Analysen des Natrium/Prolin-Transporters PutP"

10/2003-06/2008   **Studium der Biologie** an der Ludwig-Maximilians-Universität München

Abschluss als **Diplom-Biologin**

Gesamtnote der Diplomprüfung: 1,3

Studienschwerpunkte: Mikrobiologie, Zellbiologie, Biochemie

1994-2003   **Allgemeine Hochschulreife**

Carl-Spitzweg-Gymnasium, Germering-Unterpfaffenhofen

Note: 2,2